Appendix A
Historical Notes

A.1 Piotr Leonidovitch Kapitza (1894–1984)

Kapitza together with his son Sergey Petrovitch Kapitza (born in 1928) conducted the first well-controlled experiment on a falling film [141]. Kapitza's theoretical contribution [140] to the subject contains some innovative and pioneering ideas, such as the averaging of the governing equations across the film thickness. The resulting averaged equations were later on developed with great success.

However, Kapitza is better known for his experiments on intense magnetic fields, helium liquefaction and the discovery of helium superfluidity (see Fig. A.1), for which he earned the Nobel Prize for Physics in 1978. His pioneering work on falling liquid films is actually minor in comparison to his contributions to low temperature physics, high-power electronics and plasma physics, not to mention his contributions to air liquefaction and fractionation technologies (his design of a high efficiency compressed gas turbo engine is still used in the large scale production of oxygen). Yet, how Kapitza got interested in the problem of falling films is an interesting story by itself [28].

Kapitza was born in 1894 at Kronstad, an island fortress near St. Petersburg. He graduated from Petrograd/St. Petersburg Polytechnic Institute in 1919. In 1916

Fig. A.1 P.L. Kapitza (*right*) and his assistant S.I. Filimonov conducting an experiment on helium superfluidity at the Institute for Physical Problems, Moscow, 1940. Reprinted with permission from Kapitza Memorial Museum, Kapitza Institute for Physical Problems, Moscow

S. Kalliadasis et al., *Falling Liquid Films*, Applied Mathematical Sciences 176,
DOI 10.1007/978-1-84882-367-9, © Springer-Verlag London Limited 2012

he married Nadezhda Kirillovna Chernosvitova. In the years 1919–1920 he lost his wife and two children. Their death was due to the terrible conditions following the revolution and the civil war, augmented by the so-called Spanish influenza. This dramatic period was overcome thanks to the encouragement of eminent colleagues and friends like A.F. Ioffe, A.N. Krylov and N.N. Semenov, who firmly believed in Kapitza's brilliance for science. As member of a scientific committee, Kapitza embarked on a trip to England in 1921, eventually ending up working on his PhD with the eminent E. Rutherford at the Cavendish Laboratory of Cambridge University. He completed his doctorate in 1923 and continued working with Rutherford for several years after that, and although the original plan was for him to stay only over the winter of 1921, he remained in Cambridge for 13 years. In 1927 he married Anna Alekseyevna Krylova, daughter of the earlier mentioned Krylov. The couple had two sons, Sergey (born in 1928) who became a physicist, and Andrei (born in 1931), who became a geoscientist. In 1929 Kapitza was elected to the Fellowship of the Royal Society.

During his time in England, Kapitza frequently returned to Russia to give seminars. From 1926 to 1934 he visited Russia nearly every summer and was always granted a return visa to come back to England, a very unusual practice at that time. In autumn 1934, on one of his trips back to Russia, his unusual status came to an end and his passport was seized at Stalin's order. The reasons of Kapitza's retention in Russia are unclear. According to Rutherford, "Kapitza in one of his expansive moods in Russia told the Soviet engineers that he himself would be able to alter the whole face of electrical engineering in his lifetime." The need of talented researchers in physical sciences to support the Soviet economy at that time supports Rutherford's testimony [28, p. 46]. Kapitza had to wait 32 years before permission was granted him to visit England again. In Moscow he was ordered to open a new laboratory and to found the Institute for Physical Problems, of which he was the first director and which since then has borne his name. Kapitza's equipment at the Royal Society Mond laboratory was purchased by the Soviet government with the help of Rutherford and then shipped to Russia. It is at that time that Kapitza conducted his work on low temperature physics and discovered the superfluidity of helium II (1937). In 1978 he was awarded the Nobel Prize in Physics "for his basic inventions and discoveries in the area of low-temperature physics" (unusual indeed, as these results had been obtained four decades earlier).

After the war, Kapitza refused to work under Beria (also head of the state police, the N.K.V.D., soon renamed M.V.D., after the war) on the Russian nuclear weapon project. Due to Beria's hostility, he was fired from the post of director at his Institute and he had no other choice but to retire to his dacha in Nikolina Gora (Nicholas Hill) near Moscow to the end of the Stalin era (1946–1953). It was not the first time that Kapitza had to face the all powerful N.K.V.D. Already in 1938, in the midst of one of the worst purges preceding Word War II, he wrote directly to Stalin and to Beria and obtained the release of his friend Landau, who was then accused of spying on behalf of Germany.

According to Landau's own testimony:

> "Kapitza went to the Kremlin and announced that he would have to leave his Institute if I wasn't released. It is hardly necessary to say that such an action in those years required no little courage, great humanity and crystal-clear honesty" [28, p. 67].[1]

Not without a good sense of humor, Kapitza rebaptized his small dacha "Izba for Physical Problems." It was there that Kapitza conducted amongst other pieces of work his pioneering experiments on falling film instabilities with the help of his son Sergey and, at times, of his other son, Andrei.

Here is what the father Kapitza wrote about their falling film house experiments in one of his letters dated 2 December 1949 and addressed to one of his friends and colleagues, Vladimir Engelhardt, molecular biologist and member of the Russian Academy of Sciences:

> "I then thought that in the position I found myself, the only possibility of continuing scientific research work was to take up biology. I thought there was no branch of physics where it would be possible to look for really new and significant phenomena. But I was wrong. Almost immediately after I was deprived of my Institute and its facilities for low temperatures and high magnetic fields, I came across an interesting question in hydrodynamics—the flow of a thin layer of a viscous liquid. Ever since the time of Poiseuille this was considered as a classical case of laminar flow, but I realized that there are a number of indications that this is not so. [...] It is rare to discover a new form of wave motion and I decided to look into it. With the modest means at my disposal in my dacha, and of course with the help of my son [Sergey], I succeeded in observing and studying this type of wave flow and in confirming my theory" [28, p. 388].

Would Kapitza have ever considered the problem of falling liquid films if he had not been compelled to stop working on low temperature physics? Probably not. In another letter addressed directly to Stalin, Kapitza complained about his work conditions at Nikolina Gora. Referring to his experiment on falling films, he wrote:

> "But the work goes slowly since I have to do everything myself, even making the necessary apparatus with my own hands, helped only by my family" [28, p. 386].

It is not an overstatement to say that Kapitza was an outstanding experimentalist. A favorite hobby was to dismantle watches and to repair them, manufacturing himself the spare parts.[2] Indeed, reading Kapitza's own description of his falling film experimental set-up, one wonders how he achieved such accuracy while assigned to residence in his country home. The fluid, water or alcohol, was injected at the top of a vertical glass tube of 2.5 cm in diameter and 20 to 25 cm in length. To ensure the axisymmetry of the observed waves, a great accuracy was necessary in manufacturing the surface of the tube and of the supply unit. In fact, an accuracy to within one micron was necessary in the design of the conical shape mandrel placed

[1] All quotations in Appendix A.1, are reprinted from "Kapitza in Cambridge and Moscow: life and letters of a Russian scientist," J.W. Boag, P.E. Rubinin and D. Shoenberg, North-Holland, pp. 67, 386 and 388, Copyright (1990).

[2] An anecdote underlines his interest on watchmaking: On a trip to Strasbourg in 1926, Kapitza asked the clockmaker in charge of the maintenance of the famous cathedral clock to show him the details of the clock mechanism.

at the top of the tube to maintain a regular distribution of the fluid. Kapitza designed a clever stroboscopic device to illuminate the free surface of the film and to detect the waves. A task that was not easy considering that the film thickness was no more than a few tenths of a millimeter. The vibrations of the motor rotating the stroboscope were transferred to the tube at a small but sufficient level to synchronize the wave dynamics of the film and the stroboscope so that standing permanent images of the traveling waves on the film surface were produced. Up to now, the quality of the experimental results obtained by Kapitza and his son has been rarely reached in other experiments and their data are still used as benchmarks for the numerical studies devoted to falling film flows.

A.2 Carlo Giuseppe Matteo Marangoni (1840–1925)

Marangoni's influence on interfacial phenomena in liquids through two seminal contributions [179, 180] is so great that his name is nearly always associated with this area of research. He was born in Pavia, Italy, and graduated from the University of Pavia ("Laurea in Mathematiche pure e applicate"—somewhat equivalent to a Masters thesis) in 1865, under the supervision of Professor Giovanni Cantoni, with a dissertation entitled "Sull' espansione delle goccie liquide" (On the spreading of liquid drops) [178]. He then moved to Florence where he eventually became a high school physics teacher at the high school "Liceo Classico Dante," where he taught for four decades (1869–1916) (see Fig. A.2). He died in Florence in 1925.

He dedicated much of his time to the development of the Department of Physics, especially the Laboratory of Physics. He was recognized by his colleagues and students as a consummate teacher but also as a skilled investigator and scientist,[3] patient and ingenious, always stimulating interest and curiosity.

Marangoni left many writings attesting to the high scientific quality of his works. The most significant ones are those on capillarity, drops, on certain optical illusions and various educational experiments. Though James Thompson [271] initially understood that the formation of "tears of wine" at the wall of a glass was promoted by the difference of surface tensions between water and alcohol, it was Marangoni who gave the first rigorous explanation of this phenomenon. He formulated a rather complete theory for flows driven by surface tension gradients due to variations in temperature or composition, an effect that now bears his name. Despite the explanation of the "tears of wine" he was a fervent teetotaler.

Marangoni also contributed to meteorology and invented an apparatus to observe clouds. Anecdotally, the formation of hail was for him an assiduous topic, for which he tried to give an explanation for many years. Though he did not manage to give a satisfactory theory, his numerous observations and ideas were shown to be useful for subsequent generations.

[3] During the time, a great part of scientific research was actually conducted in high school laboratories, which were often equipped better than university ones.

Fig. A.2 Carlo Marangoni at the Liceo Classico Dante in Florence, Italy [173]. This picture comes from a larger one showing a group of high school teachers and students celebrating final year high school graduation in 1909. The original photograph belongs to a private collection (Dr. Valleri). A photographic reproduction of the original photograph is deposited in the archive of Liceo Classico Dante. Photo courtesy of Prof. G. Loglio

Noteworthy is that he had the singular merit of being one of the very first (since 1882) to claim that the "future and the economic wealth of Italy was in its mountain water, and forests that protect water and fuel." Being an apostle of reforestation, he was also involved in agricultural economics.

Appendix B
On the Surface Tension Constitutive Relation and Newton's Law of Cooling

B.1 Surface Tension Relation

The linear approximation for the surface tension in (2.1) is the basic equation used to model the Marangoni effect and can be viewed as an equation of state for the interface. The rate $(d\sigma/dT_s)_{T_\infty}$ is the agent for this effect. Notice that although generally the surface tension decreases when the temperature increases (this is the case of "normal thermocapillarity," $\gamma > 0$), there are systems like some water–alcohol solutions and liquid crystals that display the opposite behavior or even exhibit a minimum for $\sigma = \sigma(T_s)$ ("anomalous thermocapillarity" [189], $\gamma < 0$ or both $\gamma > 0$ and $\gamma < 0$). For most of the monograph, when we examine the influence of the Marangoni effect, i.e., in Chaps. 3, 5 and 9 where we consider the case of a film heated uniformly from below, we restrict our attention to the normal thermocapillarity case, i.e., $\gamma > 0$.

B.2 Newton's Law of Cooling

Around 1700 Newton considered the convective cooling of a warm body by a cool gas and suggested that cooling would be such that the temperature T of the body changes according to $dT/dt \propto T - T_\infty$, where T_∞ is the temperature of the incoming fluid, but he never wrote the expression (2.2). However, from the first law of thermodynamics for a closed system and in the absence of work, $Q = dU/dt \propto dT/dt$, where Q is the heat transfer rate between the system and its surroundings and U its internal energy. Hence, $Q \propto T - T_\infty$, which can be rewritten in terms of the heat flux $q = Q/A$ with A the body's area as $q = \alpha(T - T_\infty)$.

Newton's law of cooling is not based on fundamental principles, as, e.g., Newton's law of viscosity, but it is phenomenological in that it is the relation that defines the heat transfer coefficient α. It is introduced for simplicity and mathematical convenience as it allows us to bypass the substantially more involved conjugated heat transfer problems in the air–liquid, liquid–solid and solid–air interfaces. (Although

S. Kalliadasis et al., *Falling Liquid Films*, Applied Mathematical Sciences 176,
DOI 10.1007/978-1-84882-367-9, © Springer-Verlag London Limited 2012

substantially more involved, by assuming continuity of temperatures and normal components of heat fluxes in any boundary, in principle one could solve for the motion and temperature distribution in all phases.)

In general, the factors influencing the heat transfer coefficient α will depend on the particular mode of heat transfer [162]:

(i) "Forced convection," e.g., flow over a flat plate. In this case α depends on the physical properties of the phase to which heat is being transported. (The properties are in general a function of temperature, but for gases and relatively small temperature differences, as is the case here, this dependence is weak.) α also depends on the physical state of this phase, i.e., a fast moving fluid will in general have better heat transfer characteristics than a slowly moving one.

In fact, α increases with the average velocity of the phase to which heat is transported, e.g., it is directly proportional to the average velocity raised to the $1/2$ power for flow over a flat plate. In our case the gas is dragged by the liquid, but due to the relatively slow motion of the liquid (in this monograph the Reynolds numbers are small to moderate) most likely forced convection in the gas has a minimal effect on heat transfer.

(ii) "Natural convection" caused by density changes, which is quite likely the case here for the gas in contact with both the liquid and the solid; however, in the formulation of the basic equations we adopt a one-fluid approach in which the motion of the gas does not influence the motion of the liquid (from H5 in Chap. 2).

α depends on the physical properties of the phase to which heat is being transported (again, for gases the properties have a weak dependence on temperature) and the temperature difference $T - T_0$ (e.g., it is directly proportional to $(T - T_0)^{1/4}$ for natural convection from a vertical or horizontal heated plane); hence it depends indirectly on the heat resistance of the phase under consideration or equivalently its thermal conductivity—large thermal conductivity of the phase under consideration will in general lead to a larger T and hence larger α.

These observations imply that the heat transfer characteristics of the liquid–gas interface will in general be different from those of the solid–gas one, leading to different heat transfer coefficients for the two interfaces. More precisely, since in general the temperature, say T_{liq}, of the liquid at the liquid–gas interface will be smaller than the temperature of the solid at the solid–gas interface and since the heat transfer coefficient grows with $T - T_0$, the liquid–gas coefficient will be smaller than the solid–gas one.

Further, since by nature a falling film evolves in both time and space, α would also depend on both time and position. For simplicity we shall assume that wavy regimes more or less homogenize the heat transfer process at the liquid–gas interface. In addition, changing the liquid flow rate will also influence the temperature difference in the liquid and hence the liquid–gas heat transfer coefficient. However, provided that the temperature difference in the liquid is small relative to the temperature difference $T_{\text{liq}} - T_\infty$ to begin with, the effect of liquid flow rate on the liquid–gas coefficient will be small. As an example, consider a situation where the temperature difference in the liquid is 2°C, $T_{\text{liq}} = 30$°C and $T_\infty = 0$°C. Assume

now that the flow rate is quadrupled, which from our discussion above suggests that for convection heat transfer in the liquid, the heat transfer coefficient in the liquid is doubled leading to a 50% reduction of the temperature difference in the liquid. That is, it results in a difference of 1°C, which in turn leads to a new $T_{\text{liq}} = 31°\text{C}$ (assuming that the liquid temperature at the solid–liquid interface is not affected). The heat transfer coefficient at the liquid–gas interface then changes only by a factor of $(31/30)^{1/4} \approx 1.008$, and hence it remains practically unaltered. A small temperature difference in the liquid can be achieved either with a high liquid conductivity and/or by increasing the flow rate, which for simplicity we shall assume is the case here. The liquid–gas heat transfer coefficient then becomes practically independent of the liquid and depends only on the physical properties of the gas.

Appendix C
Definitions and Derivations

C.1 Heat Flux Boundary Condition (HF)

The HF thermal boundary condition is obtained by solving the steady state energy equation (2.5) for the wall temperature $T_{\rm w}$ augmented with a heat generation term on its right hand side, $q_{\rm w}/h_{\rm w}$, representing the heat flux generated by the heater per unit wall thickness:

$$\lambda_{\rm w}\partial_{yy}T_{\rm w}+\frac{q_{\rm w}}{h_{\rm w}}=0, \tag{C.1}$$

where $\lambda_{\rm w}$ is the wall thermal conductivity. This is a Poisson equation in a region bounded by two surfaces: the top surface where we impose continuity of temperatures:

$$y=0: T_{\rm w}=T, \tag{C.2a}$$

with T the liquid temperature on the wall, and the bottom surface where Newton's law of cooling in (2.2) applies:

$$y=-h_{\rm w}: \lambda_{\rm w}\partial_y T_{\rm w}=\alpha_{\rm w}(T_{\rm w}-T_\infty), \tag{C.2b}$$

where $\alpha_{\rm w}$ is the heat transfer coefficient between the wall and the gas. The geometry is sketched in Fig. 2.2. At $y=-h_{\rm w}$, $\mathbf{n}=-\mathbf{j}$, with $\mathbf{j}$ the unit vector having the direction of the positive y-axis. Notice that the heat conduction term $\lambda_{\rm w}\partial_{xx}T_{\rm w}$ has been neglected in (C.1): Once we obtain the solution for $T_{\rm w}$ the wall thickness will be shrunk to zero as the wall is just a heat source while the liquid and the gas are just heat sinks, and hence streamwise heat conduction in the wall is negligible. This would not be the case, however, for nonuniform heating, $q_{\rm w}=q_{\rm w}(x)$, e.g., localized heating/point source, which would induce conduction in the streamwise direction so that the term $\lambda_{\rm w}\partial_{xx}T_{\rm w}$ in (C.1) should be retained.

The solution of (C.1) is readily obtained to be

$$T_{\rm w}=-\frac{q_{\rm w}}{2\lambda_{\rm w}h_{\rm w}}y^2+\mathsf{A}y+\mathsf{B}, \tag{C.3a}$$

S. Kalliadasis et al., *Falling Liquid Films*, Applied Mathematical Sciences 176,
DOI 10.1007/978-1-84882-367-9, © Springer-Verlag London Limited 2012

where the two integration constants A and B are determined from the boundary conditions (C.2a), (C.2b):

$$\mathsf{A} = \frac{-q_{\mathrm{w}}(1 + \frac{\alpha_{\mathrm{w}} h_{\mathrm{w}}}{2\lambda_{\mathrm{w}}}) + \alpha_{\mathrm{w}}(T - T_{\infty})}{\lambda_{\mathrm{w}} + \alpha_{\mathrm{w}} h_{\mathrm{w}}}, \tag{C.3b}$$

$$\mathsf{B} = T. \tag{C.3c}$$

Continuity of fluxes at the substrate demands

$$y = 0 : \lambda \partial_y T = \lambda_{\mathrm{w}} \partial_y T_{\mathrm{w}}. \tag{C.4a}$$

By using (C.3a), (C.3b), the right hand side of (C.4a) becomes

$$y = 0 : \lambda_{\mathrm{w}} \partial_y T_{\mathrm{w}} = \lambda_{\mathrm{w}} \mathsf{A}. \tag{C.4b}$$

We then shrink the wall thickness to zero: As already noted, the wall is just a boundary that serves as a heat source and its thickness is of no consequence. The resulting solution will be then used in the development of a boundary condition for the liquid. Taking the limit of (C.3b) as $h_{\mathrm{w}} \to 0$ gives

$$\mathsf{A} = \frac{-q_{\mathrm{w}} + \alpha_{\mathrm{w}}(T - T_{\infty})}{\lambda_{\mathrm{w}}},$$

so that (C.4a) becomes

$$y = 0 : \lambda \partial_y T = -q_{\mathrm{w}} + \alpha_{\mathrm{w}}(T - T_{\infty}). \tag{C.5}$$

Of course at the liquid–solid interface we also have Newton's law of cooling in (2.2) with $\mathbf{n} = \mathbf{j}$,

$$y = 0 : -\lambda_{\mathrm{w}} \partial_y T_{\mathrm{w}} = \alpha^{\mathrm{w}}(T_{\mathrm{w}} - T_{\mathrm{liq}}), \tag{C.6}$$

where α^{w} is the heat transfer coefficient between the wall and the liquid and T_{liq} is the liquid temperature right outside the thermal resistance layer in the immediate vicinity of the wall (see also our discussion on Newton's law of cooling (2.2) in Sect. 2.1); so it happens that the temperature gradient in the liquid is linear throughout for the Nusselt flat film solution in (2.15a)–(2.15f) and strictly speaking we do not have a thermal resistance layer in the immediate vicinity of the wall. At this stage, however, we do not know a priori what the temperature distribution in the liquid will be; as a matter of fact we are utilizing the concept of a thermal resistance layer precisely so we may obtain the thermal boundary condition for the HF case. Besides, we shall eventually demonstrate that for the boundary condition we are after, the heat transfer characteristics at the liquid–solid interface are good to the point that there is no resistance to heat transfer in the immediate vicinity of the wall and the layer there does not exist.

The constants A and B in (C.3a) are now replaced by

$$\mathsf{A} = \frac{-q_{\mathrm{w}}(1 + \frac{h_{\mathrm{w}} \alpha_{\mathrm{w}}}{2\lambda_{\mathrm{w}}}) + \alpha_{\mathrm{w}}(T_{\mathrm{liq}} - T_{\infty})}{\lambda_{\mathrm{w}}(1 + \alpha_{\mathrm{w}} h_{\mathrm{w}} + \frac{\alpha_{\mathrm{w}}}{\alpha^{\mathrm{w}}})}, \tag{C.7a}$$

$$\mathsf{B} = -\frac{\lambda_{\mathrm{w}}}{\alpha^{\mathrm{w}}}\mathsf{A} + T_{\mathrm{liq}}. \tag{C.7b}$$

The true boundary condition felt by the liquid is (C.4a), which with (C.6) becomes

$$y = 0 : \lambda \partial_y T = \alpha^{\mathrm{w}}(T_{\mathrm{liq}} - T_{\mathrm{w}}). \tag{C.8}$$

Via (C.3a) and (C.7b) the right hand side of this equation can be written as $\alpha^{\mathrm{w}}(T_{\mathrm{liq}} - T_{\mathrm{w}}) = \lambda_{\mathrm{w}}\mathsf{A}$ at $y = 0$. As before we take the limit of (C.7a) as $h_{\mathrm{w}} \to 0$ which yields

$$\lambda_{\mathrm{w}}\mathsf{A} = \frac{-q_{\mathrm{w}} + \alpha_{\mathrm{w}}(T_{\mathrm{liq}} - T_{\infty})}{1 + \frac{\alpha_{\mathrm{w}}}{\alpha^{\mathrm{w}}}}.$$

Further, it is quite natural to assume that α^{w} is large so that the above expression is further simplified to

$$\lambda_{\mathrm{w}}\mathsf{A} = -q_{\mathrm{w}} + \alpha_{\mathrm{w}}(T_{\mathrm{liq}} - T_{\infty}).$$

The boundary condition in (C.8) then becomes

$$y = 0 : \lambda \partial_y T = -q_{\mathrm{w}} + \alpha_{\mathrm{w}}(T_{\mathrm{liq}} - T_{\infty}), \tag{C.9}$$

which is the same with (C.5) but with T_{liq} instead of T on the right hand side. However, from (C.8), $T_{\mathrm{liq}} - T_{\mathrm{w}}|_{y=0} = (1/\alpha^{\mathrm{w}})\lambda \partial_y T|_{y=0}$, which for large α^{w} gives $T_{\mathrm{liq}} \to T_{\mathrm{w}}|_{y=0}$ (α^{w} is large and $T_{\mathrm{liq}} - T_{\mathrm{w}}|_{y=0}$ small, but the product $\partial_y T|_{y=0}$ is finite). But $T_{\mathrm{w}}|_{y=0} = T|_{y=0}$—continuity of temperatures at the substrate always holds. Hence, the temperature variation in the thermal resistance layer in the immediate vicinity of the wall is negligible and $T_{\mathrm{liq}} \to T|_{y=0}$ so that (C.9) and (C.5) are identical.

The condition of large α^{w} implies that the liquid thermal resistance layer is very thin. Indeed, using a linear profile to approximate the liquid temperature in the layer, we can estimate the layer's thickness, say δ_{TRL}: from $\delta_{\mathrm{TRL}} \sim (T_{\mathrm{liq}} - T|_{y=0})/(\partial_y T|_{y=0}) \to 0$ as $T_{\mathrm{liq}} \to T|_{y=0}$. Physically, the heat transfer process in the immediate vicinity of the wall is good to the point that the thermal resistance layer does not exist.

To summarize, it is by approximating T_{liq} with $T|_{y=0}$ in the second derivation, that we obtain (C.5). But this requires one additional condition, that of large α^{w}, compared to the first derivation, where only $h_{\mathrm{w}} \to 0$ is assumed. This additional condition then effectively gets rid of α^{w} and the boundary condition at $y = 0$ in (C.6) that involves α^{w}. And that is precisely why the final forms of the wall boundary condition obtained from the two derivations are the same.

C.2 Surface Gradient Operator

The *surface gradient operator* is defined as

$$\nabla_s = (\mathbf{I} - \mathbf{n} \otimes \mathbf{n}) \cdot \nabla, \tag{C.10}$$

where $\mathbf{I}$ is the identity matrix and $\mathbf{n}\otimes\mathbf{n}$ is the dyadic product of the normal vector $\mathbf{n}$ with itself, i.e.,

$$\mathbf{n}\otimes\mathbf{n}=\frac{1}{n^2}\begin{pmatrix}(\partial_x h)^2 & -\partial_x h & \partial_x h\partial_z h\\ -\partial_x h & 1 & -\partial_z h\\ \partial_x h\partial_z h & -\partial_z h & (\partial_z h)^2\end{pmatrix}.$$

The tensor $\mathbf{I}-\mathbf{n}\otimes\mathbf{n}$ singles out the tangential projection of a vector, e.g., $(\mathbf{I}-\mathbf{n}\otimes\mathbf{n})\cdot\mathbf{v}=\mathbf{v}_s$: $(\mathbf{I}-\mathbf{n}\otimes\mathbf{n})\cdot\mathbf{v}=\mathbf{I}\cdot\mathbf{v}-(\mathbf{n}\otimes\mathbf{n})\cdot\mathbf{v}=\mathbf{v}-(\mathbf{v}\cdot\mathbf{n})\mathbf{n}=\mathbf{v}-\mathbf{v}_n\mathbf{n}=\mathbf{v}-\mathbf{v}_n=\mathbf{v}_s+\mathbf{v}_n-\mathbf{v}_n=\mathbf{v}_s$, where $\mathbf{v}_n$ is the velocity component normal to the surface and we have used the identity $(\mathbf{n}\otimes\mathbf{n})\cdot\mathbf{v}\equiv(\mathbf{v}\cdot\mathbf{n})\mathbf{n}$.

C.3 On the Choice of the Unit Vectors Tangential to the Surface

When we gave the governing equations and boundary conditions in Chap. 2, we deliberately did not choose the set of orthogonal tangential vectors $(1/\tau_1)(1,0,\partial_x h)$ and $(1/\tau_2)(0,1,\partial_z h)$, since the only requirement for $\boldsymbol{\tau}_1$ and $\boldsymbol{\tau}_2$ is that they be linearly independent but not necessarily normal to each other. For example, $(1,0,\partial_x h)$ and $(0,1,\partial_z h)$ (with appropriate normalization coefficients) are two such vectors which also could have been chosen. To see this, let us write the tangential stress balance in the form $\mathbf{f}\cdot\boldsymbol{\tau}_i=0$, where $\mathbf{f}=\mathbf{P}\cdot\mathbf{n}-\nabla_s$. Consider now the two linearly independent tangential vectors $\boldsymbol{s}_i$; $i=1,2$. We then write $\boldsymbol{\tau}_1=a_1\boldsymbol{s}_1+a_2\boldsymbol{s}_2$ and $\boldsymbol{\tau}_2=b_1\boldsymbol{s}_1+b_2\boldsymbol{s}_2$, so that $\mathbf{f}\cdot\boldsymbol{\tau}_1=a_1(\mathbf{f}\cdot\boldsymbol{s}_1)+a_2(\mathbf{f}\cdot\boldsymbol{s}_2)=0$ and $\mathbf{f}\cdot\boldsymbol{\tau}_2=b_1(\mathbf{f}\cdot\boldsymbol{s}_1)+b_2(\mathbf{f}\cdot\boldsymbol{s}_2)=0$. But $\left|\begin{smallmatrix}a_1 & a_2\\ b_1 & b_2\end{smallmatrix}\right|\neq 0$ due to the linear independence of the vectors $\boldsymbol{s}_i$. Hence, the only solution to this system is the trivial solution, $\mathbf{f}\cdot\boldsymbol{s}_1=\mathbf{f}\cdot\boldsymbol{s}_2=0$. The general form of the tangential stress balance is then preserved. But the two new tangential boundary conditions will have in general a different functional form than the previous ones. Nevertheless, each new condition is simply a linear combination of the old equations, and so we can recover the old from the new. Indeed, with the decompositions $\boldsymbol{s}_1=c_1\boldsymbol{\tau}_1+c_2\boldsymbol{\tau}_2$ and $\boldsymbol{s}_2=d_1\boldsymbol{\tau}_1+d_2\boldsymbol{\tau}_2$, we have $\mathbf{f}\cdot\boldsymbol{s}_1=c_1(\mathbf{f}\cdot\boldsymbol{\tau}_1)+c_2(\mathbf{f}\cdot\boldsymbol{\tau}_2)=0$ and $\mathbf{f}\cdot\boldsymbol{s}_2=d_1(\mathbf{f}\cdot\boldsymbol{\tau}_1)+d_2(\mathbf{f}\cdot\boldsymbol{\tau}_2)=0$, which, since $\left|\begin{smallmatrix}c_1 & c_2\\ d_1 & d_2\end{smallmatrix}\right|\neq 0$ due to the linear independence now of $\boldsymbol{\tau}_1$ and $\boldsymbol{\tau}_2$, respectively give $\mathbf{f}\cdot\boldsymbol{\tau}_1=0$ and $\mathbf{f}\cdot\boldsymbol{\tau}_2=0$. In other words, $\mathbf{f}\cdot\boldsymbol{s}_i=0$ if and only if $\mathbf{f}\cdot\boldsymbol{\tau}_i=0$, so that in all cases we end up with the same set of equations for the tangential stress balance.

C.4 On the Evaluation of the Right Hand Side of the Tangential Stress Balance (2.13)

Here we comment on the evaluation of $\boldsymbol{\tau}_i\cdot\nabla_s\sigma$ in (2.13). Using the definition of the surface gradient operator (C.10) we obtain

$$\boldsymbol{\tau}_1\cdot\nabla_s=\frac{1}{\tau_1}(\partial_x+\partial_x h\partial_y)$$

and

$$\boldsymbol{\tau}_2 \cdot \nabla_s = \frac{1}{\tau_2}(\partial_z + \partial_z h \partial_y).$$

If we now operate on σ we have $\boldsymbol{\tau}_1 \cdot \nabla_s \sigma = (1/\tau_1)(\partial_x \sigma + \partial_x h \partial_y \sigma)$ and $\boldsymbol{\tau}_2 \cdot \nabla_s \sigma = (1/\tau_2)(\partial_z \sigma + \partial_z h \partial_y \sigma)$ at $y = h(x, z, t)$. From H6 in Chap. 2, $\sigma = \sigma(T_s)$, with $T_s = T(x, h(x, z, t), z, t) \equiv T_s(x, z, t)$. Hence, σ is only a function of x, z and t. As a result

$$\boldsymbol{\tau}_1 \cdot \nabla_s \sigma = \frac{1}{\tau_1} \partial_x \sigma$$

and

$$\boldsymbol{\tau}_2 \cdot \nabla_s \sigma = \frac{1}{\tau_2} \partial_z \sigma.$$

By using the equation of state in (2.1) we obtain,

$$\partial_x \sigma = \frac{d\sigma}{dT_s} \partial_x T_s = -\gamma \partial_x T_s,$$

and

$$\partial_z \sigma = \frac{d\sigma}{dT_s} \partial_z T_s = -\gamma \partial_z T_s.$$

The gradients of the interfacial temperature $\partial_x T_s$ and $\partial_z T_s$ can be further related to the temperature field T at $y = h(x, z, t)$. Using the chain rule,

$$\partial_x T_s = (\partial_x T + \partial_x h \partial_y T)|_{y=h}$$

and

$$\partial_z T_s = (\partial_z T + \partial_z h \partial_y T)|_{y=h},$$

where it is understood that we first take the derivatives on the right hand side with respect to x, y and z and then we substitute $y = h$. The final form of $\boldsymbol{\tau}_i \cdot \nabla_s \sigma$ in (2.13) is then

$$\boldsymbol{\tau}_1 \cdot \nabla_s \sigma = -\frac{\gamma}{\tau_1}(\partial_x T + \partial_x h \partial_y T)|_{y=h}$$

and

$$\boldsymbol{\tau}_2 \cdot \nabla_s \sigma = -\frac{\gamma}{\tau_2}(\partial_z T + \partial_z h \partial_y T)|_{y=h}.$$

The same expressions can also be obtained by noting that $\boldsymbol{\tau}_i \cdot \nabla \sigma$ is the "directional derivative" $\partial_{t_i} \sigma$ on the direction t_i defined by $\boldsymbol{\tau}_i$. We then have

$$\boldsymbol{\tau}_1 \cdot \nabla_s \sigma = \partial_{t_1} \sigma = -\gamma \partial_{t_1} T_s = -\gamma \boldsymbol{\tau}_1 \cdot \nabla T_s = -\frac{\gamma}{\tau_1} \partial_x T_s = -\frac{\gamma}{\tau_1}(\partial_x T + \partial_x h \partial_y T)|_{y=h},$$

and

$$\boldsymbol{\tau}_2 \cdot \nabla_s \sigma = \partial_{t_2} \sigma = -\gamma \partial_{t_2} T_s = -\gamma \boldsymbol{\tau_2} \cdot \nabla T_s = -\frac{\gamma}{\tau_2} \partial_z T_s = -\frac{\gamma}{\tau_2} (\partial_z T + \partial_z h \partial_y T)|_{y=h}.$$

C.5 Short Library of Weakly Nonlinear Model Equations: Bottom-up Dispersion Relation Approach

Several studies have examined the film flow dynamics within the framework of weakly nonlinear analyses [19, 20, 41, 42, 44, 53, 164, 185, 199]. The basic idea underlying these studies is that, sufficiently close to onset, the flow dynamics are determined by the properties of the linear stability of the base flow and that deviations from it remain small. Fluctuations are then decomposed into elementary instability waves of the "normal mode" form, $a(x,t)\exp(\lambda t + ikx)$, with k their (real) wavenumber and $\lambda = \lambda_\mathrm{r} + i\lambda_\mathrm{i}$ a complex eigenvalue whose real part λ_r is the (temporal) growth rate (subscripts "r" and "i" are used to denote real and imaginary parts, respectively) and imaginary part λ_i is the negative value of the (real angular) frequency (precise definitions of these terms are given in Chap. 3). The structure of the weakly nonlinear equations, or *amplitude equations*, giving the evolution of the envelope $a(x,t)$ is then determined by the dispersion relation, which expresses λ as a function of the wavenumber k.

It is then possible to invert the procedure by starting from the possible structure of the dispersion relation at the onset of the instability. Hence, writing from the outset generic amplitude equations without deriving them from the fully nonlinear system is a "bottom-up dispersion relation approach," a heuristic approach that guides qualitatively the understanding of the competing generic linear and nonlinear effects for small amplitude disturbances. In Chap. 5 the pertinent amplitude equations for the falling film problem are derived systematically with weakly nonlinear expansions from the BE.

Considering the hydrodynamic surface wave instability and the Marangoni instability described earlier, the transition from the uniform laminar flow to a wavy one can be understood as a transition from a steady to an oscillatory flow. Typically, "oscillatory instabilities" occur when "negative feedback" exists and hence a perturbation switches on some compensating mechanisms that try to diminish it. However, these mechanisms do not always suppress the perturbation, but sometimes they lead to "overshooting oscillations" ("overstability"). It seems essential that the destabilizing and stabilizing factors have different time scales, so that their counteraction is characterized by a certain effective "time delay." The asynchronous changes of fields of different physical variables leads to the appearance of oscillations instead of a monotonic growth or decay of the perturbation, in which case the instability is referred to as "monotonic" or "stationary." We give the precise definitions of the two basic types of instabilities, oscillatory and stationary, in Chap. 3.

A way to classify instabilities, oscillatory and otherwise, is obtained via the minimum of the neutral stability curve, that defines the critical value of the control parameter (see Chap. 3 for the definitions of these terms). If the "critical wavenumber,"

i.e., the wavenumber of the fastest growing perturbation at the instability onset, k_0, is nonzero, the oscillatory instability is, generally, short wavelength; otherwise (if $k_0 = 0$), it is a long wavelength instability. For the long wavelength instability, it is necessary to further distinguish between two cases.

In the first case, the eigenvalue $\lambda(k, \Sigma)$ that determines the (temporal) growth rate λ_r and the (real angular) frequency of the oscillations $-\lambda_i$ as a function of a given control parameter Σ (used as a generic quantity whose definition now is not needed), can be expanded into a Taylor series near the critical point ($k_0 = 0$, Σ_c) as

$$\lambda_r = (\partial_\Sigma \lambda_r)_0(\Sigma - \Sigma_c) + \frac{1}{2}(\partial_{kk}\lambda_r)_0 k^2 + \cdots, \tag{C.11a}$$

$$\lambda_i = (\lambda_i)_0 + (\partial_k \lambda_i)_0 k + (\partial_\Sigma \lambda_i)_0(\Sigma - \Sigma_c) + \frac{1}{2}(\partial_{kk}\lambda_i)_0 k^2 + \cdots, \tag{C.11b}$$

where the subscript 0 denotes that the corresponding quantity is evaluated at the critical point. In this case, the spatially homogeneous perturbation with $k = 0$ oscillates and grows with the largest growth rate, $(\partial_\Sigma \lambda_r)_0(\Sigma - \Sigma_c)$. This type of oscillatory instability occurs frequently in reaction–diffusion systems.

However, there is a wide class of problems where growth of a spatially homogeneous disturbance is forbidden by a "conservation law." An example is the falling film problem. It is a system that involves liquid flow from an inlet and the conservation law is imposed by the inlet flow rate. A homogeneous change of the base state film thickness is only possible through a change in the flow rate, but it is not allowed if the flow rate remains fixed. The mode associated with a homogeneous change of the base state is called *Goldstone mode* in condensed matter physics (e.g., [58]; we return to this mode on several occasions in this monograph) and is characterized by

$$\lambda(0, \Sigma) = 0 \tag{C.12}$$

for any Σ, which can produce a long wavelength instability for small but nonzero k. In the latter case, it is not $\lambda_r(0, \Sigma)$ but $\partial_{kk}\lambda_r(0, \Sigma)$ that changes sign at the threshold of the instability, $\Sigma = \Sigma_c$:

$$\lambda_r = \frac{1}{2}(\partial_{kk\Sigma}\lambda_r)_0 k^2(\Sigma - \Sigma_c) + \frac{1}{24}(\partial_{kkkk}\lambda_r)_0 k^4 + \cdots, \tag{C.13a}$$

$$\lambda_i = (\partial_k \lambda_i)_0 k + (\partial_{k\Sigma}\lambda_i)_0 k(\Sigma - \Sigma_c) + \frac{1}{6}(\partial_{kkk}\lambda_i)_0 k^3 + \cdots. \tag{C.13b}$$

Past the instability threshold, the growth rate is proportional to k^2 at small k (this effect appears akin to the role of an effective "negative viscosity").

Equations (C.13a), (C.13b) correspond precisely to the H-mode of instability for a falling liquid film. The dispersion relation for the growth rate λ_r features a band of unstable modes extending from zero up to a "cut-off wavenumber" k_c, above which the system is stable, $k_c = [-12(\partial_{kk\Sigma}\lambda_r)_0(\Sigma - \Sigma_c)/(\partial_{kkkk}\lambda_r)_0]^{1/2}$. The unstable band $0 \le k \le k_c$ contains the "maximum growing wavenumber" k_{max} with the largest positive growth rate, $\lambda_r(k_{max})$. We notice that even though at the critical

wavenumber $k = 0$, λ_i vanishes, the instability is oscillatory. As a matter of fact, $k \to 0$ is a "degenerate" limit where from (C.12) the exponential part of the disturbances reduces to $\exp 0 = 1$ corresponding to a uniform shift of the base state (by changing the flow rate), the Goldstone mode defined earlier (it is neither damped nor amplified). Infinitely long waves are a mathematical artifact and finite-size effects (finite length of the channel) will remove the degeneracy (because of the discrete spectrum of modes imposed by the finite size, while the smallest wavenumber scales as $k \sim 1/L$ with L the channel's length)[1] so that a true "Hopf bifurcation" with $\lambda_i \neq 0$ occurs. In the linear regime the disturbance will grow at rate $\lambda_r(k_{max})$ and at the same time it is periodic in space with wavenumber k_{max} and oscillates in time with frequency $-\lambda_i(k_{max})$. The combination of periodicity in space and oscillatory behavior in time leads to a traveling wave.

The behavior of the eigenvalue in the vicinity of the point (k_0, Σ_c) is crucial for the evolution of the weakly nonlinear waves generated by the oscillatory instability. In the case of a short wavelength instability where the fastest growing disturbance has a finite wavenumber, $k_0 \neq 0$, the *complex Ginzburg–Landau equation*

$$\partial_t a = \gamma_0 a + \gamma_2 \partial_{xx} a - \delta_0 |a|^2 a \tag{C.14}$$

is a universal equation for a complex envelope function $a(x, t)$ describing the modulation of the waves; here γ_0, γ_2 and δ_0 are complex constant coefficients. The space-independent case (formally $\gamma_2 = 0$) is called the "Landau equation" in several areas of physics such as phase transitions. It was introduced by Stuart (e.g., [263]) to study flow instabilities with transition between steady fluid motions and is also frequently referred to as the "Landau–Stuart equation."

The Ginzburg–Landau equation (C.14) can also be used to describe the transition when an unstable wave motion of given ("fundamental") wavenumber interacts with its first stable harmonics (in fact, the Ginzburg–Landau equation is only valid when the fundamental wavenumber is weakly unstable—i.e., just below k_c—while the overtone with a wavenumber twice that of the fundamental is stable [53, 274]). This situation occurs for monochromatic waves excited on a falling film by forcing at the inlet with a frequency close to the cut-off frequency, which then yields a wavenumber k close to the cut-off wavenumber k_c (details are given in Chap. 7) determined by the balance of the H-instability mechanism and the damping effect of surface tension. Using (C.14), Lin [164] showed that such monochromatic waves are sideband stable.[2] This, however, was in contradiction with the experimental results by Liu and Gollub [168]. Later on, Oron and Gottlieb [199] corrected Lin's

[1] In a finite-size container, e.g., the annular container used to investigate the propagation of waves due to solutocapillary Marangoni effect in [189, 300], the $\lambda = k = 0$ mode is removed. Clearly, due to the conservation law, i.e., conservation of fluid volume, a homogeneous change of the layer's thickness is not allowed.

[2] In general, the term "sideband instability" of a wave refers to a resonance between three frequencies, the frequency of the wave, say f, and two frequencies, $f + \delta f$ and $f - \delta f$ with δf small. Sideband instabilities in three dimensions are examined in Chap. 8.

analysis and demonstrated that excited monochromatic waves at $k \lesssim k_c$ can be sideband unstable.

It is then evident that for the falling liquid film, and more general long wave instabilities with $k_0 = 0$ and with the dependence $\lambda(k, \Sigma)$ determined by (C.13a), (C.13b), the Ginzburg–Landau equation (or its simplified version, the Landau–Stuart equation) has a limited applicability, since as already emphasized above it is only valid when the fundamental wavenumber is weakly unstable. For example, the maximum growing wavenumber $k_{max} \in [0, k_c]$, which, in general, is not weakly unstable (unless we are very close to criticality), cannot be captured by (C.14). As a matter of fact, due to the multiplicity of the dominant Fourier modes more than one amplitude equation must be considered [42]. Alternatively, the Kuramoto–Sivashinsky equation introduced later (which is not necessarily valid only for conditions very close to criticality—Chap. 4) can accommodate a large band of Fourier modes.

Let us consider now the case of a negative viscosity (dispersion relations (C.13a), (C.13b)) caused by a conservation law. The structure of an amplitude equation compatible with a conservation law is

$$\partial_t a = \mathcal{L}_x a + \partial_x \mathcal{F}(a), \tag{C.15a}$$

where the linear operator $\mathcal{L}_x$ involves derivatives with respect to x only and has the structure

$$\mathcal{L}_x = \gamma_1 \partial_x + \gamma_2 (\Sigma - \Sigma_c)\partial_{xx} + \gamma_3 \partial_{xxx} + \gamma_4 \partial_{xxxx} + \cdots, \tag{C.15b}$$

where

$$\gamma_1 = (\partial_k \lambda_i)_0 + (\partial_{k\Sigma} \lambda_i)_0 (\Sigma - \Sigma_c), \qquad \gamma_2 = -\frac{1}{2}(\partial_{kk\Sigma} \lambda_r)_0, \tag{C.15c}$$

$$\gamma_3 = -\frac{1}{6}(\partial_{kkk} \lambda_i)_0, \qquad \gamma_4 = \frac{1}{24}(\partial_{kkkk} \lambda_r)_0, \ldots, \tag{C.15d}$$

and

$$\mathcal{F}(a) = \delta_1 a^2 + \delta_2 \partial_x \left(a^2\right) + \cdots. \tag{C.15e}$$

It should be noted that if the conservation law is an approximate one, the amplitude equation can contain additional small terms not differentiated with respect to x. The term containing γ_1 can be removed by a *Galilean transformation* to a suitable moving reference frame. It should also be noted that the nonlinearity in the amplitude equation (C.15a) is actually a guess, while the linear operator in (C.15a) gives precisely the dispersion relation (C.13a), (C.13b) (which can be either exact, i.e., obtained from the fully nonlinear system, or a guess).

First, let us consider the generic case where all the coefficients γ_n, $n = 1, 2, \ldots$ in (C.15a)–(C.15e) are of $\mathcal{O}(1)$. A weakly nonlinear prototype can be obtained from (C.15a)–(C.15e) by utilizing multiple scale-type arguments. Taking $\Sigma - \Sigma_c = \mathcal{O}(\epsilon^2)$ where $\epsilon \ll 1$, the expression for the cut-off wavenumber, $k_c =$

$[-12(\partial_{kk\Sigma}\lambda_r)_0(\Sigma-\Sigma_c)/(\partial_{kkk}\lambda_r)_0]^{1/2}$, shows that $k_c \sim \epsilon$ so that $x \sim \epsilon^{-1}$, a long scale, or equivalently $\partial_x = \mathcal{O}(\epsilon)$ (the order of magnitude of the spatial gradient is dictated by the order of the cut-off wavelength, which is the wavelength of the instability pattern emerging at the onset). Assuming that the largest nonlinear term $\delta_1\partial_x(a^2)$ is balanced by the dispersion term $\gamma_3\partial_{xxx}a$ (the term "dispersion" is used to denote that the wave velocity depends on wavelength or "color" as in optics—this is clarified in Sects. 5.1.4, 5.2.1), we find that $a = \mathcal{O}(\epsilon^2)$, and the amplitude equation is

$$\partial_t a = \gamma_3\partial_{xxx}a + \delta_1\partial_x\left(a^2\right) + \gamma_2(\Sigma-\Sigma_c)\partial_{xx}a + \gamma_4\partial_{xxxx}a + \delta_2\partial_{xx}\left(a^2\right). \quad \text{(C.16)}$$

The first two terms on the right hand side of this equation are of $\mathcal{O}(\epsilon^5)$; the last three terms, describing the instability at long wavelengths, the stabilization at short wavelengths, and a nonlinear correction to the negative viscosity coefficient, are of $\mathcal{O}(\epsilon^6)$ (such that very close to criticality, instability at long wavelengths balances stability at short ones). Further, the time derivative balances the dispersive and nonlinear terms on the long time scale $t \sim \epsilon^{-3}$. Thus, we find that the generic amplitude equation in (C.16) is a *driven-dissipative Boussinesq–Korteweg–de Vries equation* (BKdV) which is effectively a perturbed "BKdV equation". The equation with $\gamma_4 = \delta_2 = 0$ is the "BKdV–Burgers equation." The terminology used here deserves a remark. We use *BKdV equation*, instead of the standard terminology "Korteweg–de Vries equation," because the former equation was first obtained by Boussinesq—actually written in a footnote: p. 360, Eq. (283 bis) in [30]!

In fact, it is not necessary to introduce the small parameter ϵ. We need only $\Sigma - \Sigma_c \ll 1$, a condition required to obtain the dispersion relation (C.13a), (C.13b). Now $k_c \sim (\Sigma-\Sigma_c)^{1/2} \ll 1$ and the appropriate long scale should be $x \sim k_c^{-1}\ (\Sigma-\Sigma_c)^{-1/2} \gg 1$. Balancing the instability with the stability terms, $a(\Sigma-\Sigma_c)/x^2 \sim a/x^4$, gives $x \sim (\Sigma-\Sigma_c)^{-1/2}$, consistent with the above assignment (to be expected, as the balance between the instability and stability terms is precisely what determines k_c). Balancing the nonlinearity with the dispersion term, $a\partial_x a \sim \partial_{xxx}a$ or $a \sim \Sigma - \Sigma_c$. The order of magnitude of the nonlinearity and dispersion terms then is $a\partial_x a \sim (\Sigma-\Sigma_c)^{5/2}$, while that of instability and stability, $a(\Sigma-\Sigma_c)/x^2 \sim (\Sigma-\Sigma_c)^3 \ll (\Sigma-\Sigma_c)^{5/2}$, and the relevant weakly nonlinear prototype is the BKdV equation. In other words, the BKdV equation is always the relevant weakly nonlinear prototype when $\Sigma - \Sigma_c \ll 1$ and all coefficients γ_i of the dispersion relation are of $\mathcal{O}(1)$.

If the dispersion coefficient is small, $\gamma_3 = \mathcal{O}(\epsilon)$ (for instance, this feature is characteristic of the modulational instability of periodic waves with small wavenumbers), it is balanced by the nonlinearity if $a = \mathcal{O}(\epsilon^3)$, and one obtains the *Kawahara equation* (e.g., [144]):

$$\partial_t a = \gamma_2(\Sigma-\Sigma_c)\partial_{xx}a + \gamma_3\partial_{xxx}a + \gamma_4\partial_{xxxx}a + \delta_1\partial_x\left(a^2\right), \quad \text{(C.17)}$$

with all terms on the right hand side of $\mathcal{O}(\epsilon^7)$. The time derivative now balances all terms on the right hand side on the long time scale $t \sim \epsilon^{-4}$.

If the dispersion coefficient vanishes ($\gamma_3 = 0$), the Kawahara equation is reduced to the *Kuramoto–Sivashinsky equation* (KS)

$$\partial_t a = \gamma_2(\Sigma - \Sigma_c)\partial_{xx} a + \gamma_4 \partial_{xxxx} a + \delta_1 \partial_x\left(a^2\right), \tag{C.18}$$

first derived by Homsy [118, 119] and typical for instabilities in a wide variety of nonlinear processes. Note that the Kawahara equation in (C.17) is also frequently referred to as the *generalized KS equation*.

The KS equation can also be obtained in the case where the instability region is no longer narrow as above because of large γ_4: This allows increase in the order of magnitude of the stability and hence instability (the two should always balance) as well as nonlinearity terms compared to dispersion. Consider, e.g., the case $\Sigma - \Sigma_c = \mathcal{O}(1)$, $\gamma_4 = \mathcal{O}(\epsilon^{-2})$ (of course the dispersion relation in (C.15a)–(C.15e) was obtained with an expansion for $\Sigma - \Sigma_c \ll 1$, but here we consider (C.15a)–(C.15e) as a model exact dispersion relation). The cut-off wavenumber then is $k_c \sim \sqrt{(\Sigma - \Sigma_c)/\gamma_4} \sim \epsilon$ so that the corresponding long scale is $x \sim 1/k_c \sim 1/\epsilon$. At this long scale the two terms representing instability at long wavelengths and stability at short ones balance as expected: $a(\Sigma - \Sigma_c)/x^2 \sim a\gamma_4/x^4$ or $x \sim 1/\epsilon$. To balance the nonlinearity with these two terms, $a\partial_x a \sim a/x^2$ or $a \sim \epsilon$. The order of instability, stability and nonlinearity then is $aa_x \sim \epsilon^3$ while that of dispersion is $\partial_{xxx} a \sim \epsilon^4$.

On the other hand, having large γ_4, small $\Sigma - \Sigma_c$ and $\gamma_3 = \mathcal{O}(1)$ gives the Kawahara equation. Consider, e.g., the case, $\Sigma - \Sigma_c = \mathcal{O}(\epsilon^2)$ and $\gamma_4 = \mathcal{O}(\epsilon^2)$. Then $k_c \sim \epsilon^2$ and $x \sim 1/k_c \sim \epsilon^{-2}$. Balance instability with stability, $(\Sigma - \Sigma_c)/x^2 \sim 1/x^4$ or $x \sim \epsilon^{-2}$, consistent with the above order (as expected). Balance the nonlinearity with the instability and stability terms, $a\partial_x a \sim a(\Sigma - \Sigma_c)/x^2$ or $a \sim \epsilon^4$. The order of instability, stability and nonlinearity terms then is $a\partial_x a \sim \epsilon^{10}$ while that of dispersion is $\partial_{xxx} a \sim \epsilon^{10}$, so that all terms are of the same order.

In Chap. 5 we demonstrate that both KS and Kawahara equations can be obtained from the governing equations of a falling liquid film via a weakly nonlinear expansion and multiple scale-type arguments similar to the ones adopted here. We also demonstrate in Chap. 5 that the second-order viscous effects are responsible for the dispersion term in the Kawahara equation.

The KS equation, which has both locally stable regular wavy solutions and spatio-temporal chaotic regimes, provides a paradigmatic example of the transition between regular and chaotic patterns, as well as a reference model for the application of the "dynamical systems" approach to spatio-temporal chaos. It suffices at this point to say that the path allowing the use of the theory of dynamical systems is the following. By a suitable Galilean boost we can look at the expected waves in their moving frame of reference. This change of reference frame converts a partial differential equation into an ordinary differential one, which underlines the corresponding dynamical system. A solitary wave then corresponds to a *homoclinic orbit* or trajectory of the dynamical system, while the presence of dissipation exhibits repelling and attractive directions on the orbit (these points are clarified in Chap. 7). When periodicity in time is present, as when a given steady wave solution becomes unstable through a (new) *Hopf bifurcation*, the new wave solution corresponds to

a *limit cycle* of the transformed problem. Other possibilities exist including chaotic solutions, and they are studied in this monograph.

It should be noted that the KS equation is formally equally valid for both oscillatory and stationary instabilities. The only "sign" of the "wavy" origin of this equation is the lack of the invariance of the nonlinear term to the parity (reflection) transformation $x \to -x$: The presence of $\partial_x(a^2)$ breaks this symmetry and is connected with the fact that the system has a preferred direction (this is a "mean flow" term in the context of fluid mechanics). However, the transformation $a = \partial_x h$ provides another form of the KS equation,

$$\partial_t h = \gamma_2(\Sigma - \Sigma_c)\partial_{xx} h + \gamma_4 \partial_{xxxx} h + \delta_1(\partial_x h)^2, \tag{C.19}$$

which is invariant to the parity transformation.

Finally, it is noteworthy that the analysis of the long wavelength instability just given was based on the assumption of the analyticity of the function $\lambda(k, \Sigma)$ at the point $k = 0$. If the analyticity condition does not hold, the amplitude equation can contain some nonlocal integral terms.

C.6 Negative Polarity in the BKdV Equation

Let us consider the BKdV equation with a dispersion coefficient δ_K:

$$\partial_u + u\partial_x u + \delta_K \partial_{xxx} u = 0. \tag{C.20a}$$

This equation is invariant under the transformation $u \to -u$, $x \to -x$ and $\delta_K \to -\delta_K$ (t is always > 0 and we do not change it). Alternatively, consider (C.20a) in the moving frame $x \to x - ct$,

$$-c\partial_x u + u\partial_x u + \delta_K \partial_{xxx} u = 0, \tag{C.20b}$$

which is invariant under the transformation $u \to -u$, $x \to -x$, $c \to -c$ and $\delta_K \to -\delta_K$. This symmetry shows that (C.20a) admits negative-hump waves traveling backward, but can we have such waves for $\delta_K > 0$ much like with the Kawahara equation as we point out in Sect. 5.3.2.

It is the sign of δ_K that determines the direction of propagation: $\delta_K > 0$ means that positive-hump solitary pulses travel forward while negative-hump ones travel backward. To see this consider the solution of (C.20a), $H = 3c\ \mathrm{sech}^2[(1/2)\sqrt{c/\delta_K}(x - ct)]$, corresponding to a solitary wave traveling with speed c. It is then clear that both c and δ_K must have the same sign for solitary waves to exist. Hence, as we note in Sect. 5.3.2, negative waves of the Kawahara equation with $\delta_K > 0$ no longer exist as the Kawahara equation approaches the perturbed BKdV one.

As far as the above mentioned symmetry is concerned, it is lost with the transformation,

$$u = \delta_K^{1/3}\overline{u}, \qquad x = \delta_K^{1/3}\overline{x}, \tag{C.21a}$$

which converts (C.20a) into the BKdV equation

$$\partial_t \overline{u} + \overline{u}\partial_x \overline{u} + \partial_{xxx}\overline{u} = 0 \tag{C.21b}$$

with a dispersion coefficient of unity. This equation is not invariant under the transformation $\overline{u} \to -\overline{u}$ and $\overline{x} \to -\overline{x}$ and hence it does not admit negative-hump pulses traveling backward. In fact, integrating numerically (C.21b) with an initial condition a negative-hump wave obtained by simply inverting the positive-hump wave of the equation, shows that the negative-hump wave collapses and degenerates into a wave train that disperses and at the same time travels backward [82]. Accordingly, the equation $\partial_t \overline{u} + \overline{u}\partial_x \overline{u} - \partial_{xxx}\overline{u} = 0$ admits only negative-hump waves propagating backward. In essence, the transformation in (C.21a) collapses the two families of solitary wave solutions, positive-hump ones with $\delta_K > 0$ and negative-hump ones with $\delta_K < 0$ of (C.20a), into the single family of positive-hump solutions with $\delta_K = 1$ of (C.21b).

C.7 Padé Approximants

To remedy the singularity of the BE, Ooshida [196] developed a resummation technique inspired from the *Padé approximants technique* (see, e.g., [18, 115]). The technique relies on the basic idea that the divergence of a power series representation of a function $Q(x)$, namely, $Q(x) = \sum_{k=0,1,2,\ldots} Q_k x^k$ on $[0, a]$, is due to the hidden presence of poles. The divergence reflects the inability of the polynomial representation to approximate the function adequately near a singularity. This leads us to express $Q(x)$ as the ratio of two polynomials $F_N(x)$ and $G_M(x)$ of degrees N and M, respectively, where the zeros of G_M are supposed to capture the causes of the divergence. Let us define the rational function

$$R_{N,M} = \frac{F_N(x)}{G_M(x)} \quad \text{for } 0 \le x \le a.$$

We wish to make the maximum error between this function and $Q(x)$ as small as possible. The Padé approximants technique then requires that $Q(x)$ and its derivatives be continuous at a point, say, $x = 0$. The polynomials employed are of the form

$$F_N(x) = f_0 + f_1 x + \cdots + f_N x^N \quad \text{and} \quad G_M(x) = 1 + g_1 x + \cdots + g_M x^M.$$

They are constructed so that $Q(x)$ and $R_{N,M}$ and their derivatives up to degree $N + M$ agree at $x = 0$. For a fixed value of $N + M$ (the degrees of the polynomials F and G are open to choice) the error is smallest when $N = M$ or $N = M + 1$. The easiest way to obtain these coefficients is by writing, $Z(x) = Q(x)G_M(x) - F_N(x)$ and ensuring that the coefficients of x^k in $Z(x)$ vanish for $k = 0, \ldots, N + M$.

C.8 Center Manifold Projection for a Scalar Equation

Here we illustrate how to implement the center manifold approach for a scalar nonlinear partial differential equation. Assume that the evolution of a physical variable $u(x,t)$ is described by

$$\partial_t u = \mathcal{L}u + N(u,\varepsilon), \tag{C.22}$$

where ε is a control parameter, $\mathcal{L} \equiv \mathcal{L}_x$ is a linear differential operator that describes the "flow" close to the origin $(u,\varepsilon) = (0,0)$ and N is a nonlinear functional. We define the eigenvalue problem, $\mathcal{L}\Phi_k = \lambda_k \Phi_k; k = 0,1,2,\ldots$ associated with $\mathcal{L}$, where Φ_k and λ_k are the eigenfunctions and eigenvalues of $\mathcal{L}$, respectively, and where appropriate boundary conditions depending on the physical problem have been imposed. We also define the adjoint eigenvalue problem, $\mathcal{L}^*\hat{\Phi}_k = \bar{\lambda}_k \hat{\Phi}_k; k = 0,1,2,\ldots$, where the overbar is used to denote complex conjugation. The adjoint operator $\mathcal{L}^*$ can be defined with respect to an appropriately chosen inner product, e.g., in an infinite domain the $L^2(-\infty,+\infty)$ inner product, $\langle f|g\rangle = \int_{-\infty}^{+\infty} f\bar{g}\,dx$, for any two functions f and g decaying sufficiently fast at infinity and such that $\langle \mathcal{L}f|g\rangle = \langle f|\mathcal{L}^*g\rangle$.

Assume now for simplicity that the linear operator $\mathcal{L}$ has a single zero eigenvalue, $\lambda_0 = 0$, while all other eigenvalues have negative real parts (all eigenvalues assumed simple). We then decompose u into eigenmodes as $u = a\Phi_0 + \hat{u}$ where $\hat{u}$ is the "complement" with respect to the null eigenfunction Φ_0 and is given by

$$\hat{u} = \sum_{i\geq 1} u_i \Phi_i. \tag{C.23a}$$

By introducing the "projection operator", $\mathcal{P}$ to denote projection onto the null space,

$$\mathcal{P}f = \langle f|\hat{\Phi}_0\rangle \Phi_0,$$

and the "complementary projection operator", $\mathcal{F} - \mathcal{P}$ to denote projection onto the complement of Φ_0,

$$(\mathcal{F}-\mathcal{P})f = \sum_{i=1}^{\infty} \langle f|\hat{\Phi}_i\rangle \Phi_i$$

for any function f in the domain of $\mathcal{L}$, u can be written as

$$u = \mathcal{P}u + (\mathcal{F}-\mathcal{P})u. \tag{C.23b}$$

The above expansion is a real-valued function even when complex eigenvalues and eigenfunctions are present: For real operators complex eigenvalues and eigenfunctions appear in conjugate pairs and hence if $\langle u|\hat{\Phi}_k\rangle$ and $\langle u|\hat{\Phi}_{k+1}\rangle$ are the coefficients of Φ_k and Φ_{k+1} in the projection for u, respectively, with $\lambda_{k+1} = \bar{\lambda}_k$ and $\Phi_{k+1} = \bar{\Phi}_k$, we must have $\langle u|\hat{\Phi}_{k+1}\rangle = \int_{-\infty}^{\infty} u\bar{\hat{\Phi}}_{k+1}\,dx = \langle \hat{\Phi}_k|u\rangle = \overline{\langle u|\hat{\Phi}_k\rangle}$.

Substituting the projection for u into (C.22) and taking inner products of both sides with the adjoint eigenfunctions $\hat{\Phi}_0$, $\hat{\Phi}_i$ with $i \neq 0$ and using the orthogonality condition $\langle \Phi_i | \hat{\Phi}_j \rangle = \delta_{ij}$ leads to

$$\partial_t a = F(\hat{u}, a, \varepsilon) \tag{C.24a}$$

$$\hat{u} = \mathcal{L}\hat{u} + H(a, \hat{u}, \varepsilon), \tag{C.24b}$$

where the functions F and H are given from

$$F(\hat{u}, a, \varepsilon) = \langle N(a\Phi_0 + \hat{u}, \varepsilon) | \hat{\Phi}_0 \rangle \tag{C.24c}$$

and

$$H(a, \hat{u}, \varepsilon) = (\mathcal{F} - \mathcal{P}) N(a\Phi_0 + \hat{u}, \varepsilon). \tag{C.24d}$$

Assume now that we wish to study small solutions of (C.22) for $\varepsilon \ll 1$. The center manifold approach requires that the eigenvalues of $\mathcal{L}$ have zero or negative real parts and in addition the eigenvalues with zero real parts must be well isolated from those with negative ones. However, for the system in (C.24a)–(C.24d) it can very well happen that the associated linearized problem has eigenvalues that are positive (and small) for $\varepsilon \neq 0$ (see [38] for examples of application of the center manifold theorem to systems of nonlinear ordinary differential equations and to singular perturbation problems). Nevertheless, we can write the above system in the following "extended manner":

$$\partial_t a = F(\hat{u}, a, \varepsilon) \tag{C.25a}$$

$$\hat{u} = \mathcal{L}\hat{u} + H(a, \hat{u}, \varepsilon) \tag{C.25b}$$

$$\partial_t \varepsilon = 0, \tag{C.25c}$$

thus ensuring that all eigenvalues are either zero or negative. The addition of (C.25c) introduces a second zero eigenvalue.

According to the center manifold approach then, the system (C.25a)–(C.25c) has a two-dimensional center manifold given by the "adiabatic coupling" $\hat{u} = \hat{u}(a, \varepsilon) = \mathcal{O}(2)$ to leading order with respect to a, ε. To obtain the flow onto the center manifold we note that $\partial_t a = \mathcal{O}(2)$ so that $\partial_t \hat{u} = \mathcal{O}(3)$ and the leading-order center manifold projection, the so-called "tangent space approximation," is simply $\partial_t \hat{u} = 0$ or $\mathcal{L}\hat{u} = -H_2$ where H_2 contains the $\mathcal{O}(2)$ terms of H (terms of $\mathcal{O}(3)$ and higher are neglected). Note that $\mathcal{L}$ is a singular operator and hence the right hand side of (C.25b) must satisfy the Fredhölm alternative solvability condition (see Sect. 5.1), but it does so automatically since the null eigenfunction has already been removed in the projection that leads to (C.24a)–(C.24d) (see, e.g., [135] for an example on how this is done in practice). By inverting $\mathcal{L}$, i.e., taking inner products with the adjoint eigenfunctions, one then obtains explicitly $\hat{u}$:

$$\hat{u} = -\mathcal{L}^{-1} H_2 = -\sum_{i=1}^{\infty} \frac{1}{\lambda_i} \langle H_2 | \hat{\Phi}_i \rangle \Phi_i .$$

Substituting this result into (C.25a) eliminates $\hat{u}$ from the problem and leads to a partial differential equation for a:

$$\partial_t a = F\left(-\mathcal{L}^{-1} H_2, a, \varepsilon\right) \equiv G(a, \varepsilon).$$

Appendix D
Scalings, Dimensionless Groups and Physical Parameters

D.1 The Viscous-Gravity Scaling

In the falling liquid film the gravitational acceleration g causes flow, and the kinematic viscosity ν (friction) resists the flow. The balance between the two, which gives rise to the Nusselt flat film solution in (2.15a)–(2.15f), can be rendered explicit with the viscous-gravity length and time scales introduced in Sect. 2.2. These scales can be obtained from simple physical considerations without prior knowledge of the specific details of the system. In fact, straightforward dimensional analysis dictates that

$$g \sin\beta \sim \frac{l_\nu}{t_\nu^2} \quad \text{and} \quad \nu \sim \frac{l_\nu^2}{t_\nu},$$

from which l_ν and t_ν, can be readily obtained:

$$l_\nu = \left(\frac{\nu^2}{g \sin\beta}\right)^{1/3} \quad \text{and} \quad t_\nu = \left(\frac{\nu}{(g \sin\beta)^2}\right)^{1/3}.$$

Their ratio gives the characteristic velocity for viscous-gravitational drainage:

$$u_\nu \sim \frac{l_\nu}{t_\nu} \sim \frac{g \sin\beta l_\nu^2}{\nu} \sim (\nu g \sin\beta)^{1/3}.$$

With this definition of u_ν, viscous diffusion in the y direction and gravity in (2.4) balance automatically, i.e., $\mu \partial_{yy} u \sim \rho g \sin\beta$. The pressure scale is selected from balancing the pressure gradient with viscous forces in (2.4), i.e., $\partial_x p \sim \mu \partial_{yy} u$ or

$$p_\nu \sim \frac{\mu u_\nu}{l_\nu} \sim \rho u_\nu^2 \sim \rho (\nu g \sin\beta)^{2/3}.$$

With $\sin\beta \sim 1$ and for water at 25°C, $\nu \approx 10^{-2}$ cm^2 s^{-1}, which yields $l_\nu \approx 4.7 \times 10^{-3}$ cm. The corresponding Nusselt flat film thickness is then always small, e.g., with $Re = 50$, from (2.37) $\bar{h}_N \approx 0.25$ mm.

S. Kalliadasis et al., *Falling Liquid Films*, Applied Mathematical Sciences 176,
DOI 10.1007/978-1-84882-367-9, © Springer-Verlag London Limited 2012

The above scaling will be referred to as the *viscous-gravity scaling* as it expresses the importance of viscous and gravitational forces in our system. This scaling is relevant for inclined plates for which $\sin\beta$ is of order unity and film thickness $\bar{h}_\mathrm{N}$ of the order of the length scale l_ν. It allows us to assess the incompressibility assumption in H1, Sect. 2.1. For a film with thickness $\bar{h}_\mathrm{N} \sim l_\nu$, the Reynolds number $Re = g\sin\beta\bar{h}_\mathrm{N}^3/(3\nu^2)$ is of $\mathcal{O}(1)$ ($l_\nu^3 \sim \nu^2/(g\sin\beta)$) so that the "Grashof number" $Gr = \gamma_T \Delta T/Re$ is small since the thermal expansion coefficient γ_T is usually small for typical fluids (the "Boussinesq approximation"). The Grashof number decreases further as Re increases, i.e., the film thickness $\bar{h}_\mathrm{N}$ becomes large compared to l_ν. Hence, buoyancy can be neglected.

We can also assess the neglect of heat production by viscous dissipation in H8, Sect. 2.1. In fact, this is not just a complementary assumption but a direct consequence of a small $\bar{h}_\mathrm{N}$ and large constant pressure heat capacity. By comparing the strength of the dissipation function Φ_v[1] to the heat transport by the flow leads to the ratio $\nu^2/(c_p\Delta T\bar{h}_\mathrm{N}^2) = BqRe^2$ where $Bq = g\bar{h}_\mathrm{N}/(c_p\Delta T)$ is the "Boussinesq number." With $\bar{h}_\mathrm{N}$ very small and the constant pressure heat capacity of the liquid being generally high, the Boussinesq number is in general very small so that the group $BqRe^2$ has in general a negligible value, even with $Re > 1$.

By introducing the nondimensionalization,

$$\begin{aligned} &(x, y, z) \to l_\nu(x, y, z), \qquad h \to l_\nu h, \\ &t \to t_\nu t, \qquad (u, v, w) \to u_\nu(u, v, w), \end{aligned} \tag{D.1a}$$

$$p \to p_\infty + p_\nu p, \qquad T \to T_\infty + T\Delta T, \tag{D.1b}$$

where $\Delta T = T_\mathrm{w} - T_\infty$ for ST and $\Delta T = q_\mathrm{w} l_\nu/\lambda$ for HF (see Sect. 2.2), the dimensionless versions of the equations of motion and energy (2.3)–(2.5) and wall and free surface boundary conditions (2.6)–(2.9) and (2.12)–(2.14) contain the parameters in (2.29)–(2.34). The Reynolds number based on u_ν and l_ν, $u_\nu l_\nu/\nu$ does not appear in the equations as it is equal to unity. That is because with the viscous-gravity scaling inertia balances automatically all other terms in (2.4): $\rho\partial_t u \sim \mu\partial_{yy}u$ and $\rho\partial_t u \sim \rho u\partial_x u$.

However, the Reynolds number in (2.35) based on film thickness $\bar{h}_\mathrm{N}$ and average velocity $\bar{u}_\mathrm{N}$ is effectively hidden in the inlet boundary condition that defines the Nusselt flat film solution (2.15a)–(2.15f). Therefore, the dimensionless equations of motion and energy and wall and free surface boundary conditions obtained with the viscous-gravity scaling are governed by the dimensionless Nusselt flat film

[1] The "viscous dissipation function" is defined as [26]

$$\begin{aligned} \Phi_\mathrm{v} = \mu\big\{&2\big[(\partial_x u)^2 + (\partial_y v)^2 + (\partial_z w)^2\big] \\ &+ (\partial_x v + \partial_y u)^2 + (\partial_y w + \partial_z v)^2 + (\partial_z u + \partial_x w)^2\big\} \end{aligned}$$

such that the product $(\nu/c_p)\Phi_\mathrm{v}$ represents the viscous heating that would have been added to the energy equation (2.5) if significant. Curiously enough, the minimization of ϕ_v leads to the semiparabolic Nusselt flat film solution, as pointed out in the Introduction.

thickness $h_N = \bar{h}_N / l_\nu$ or, equivalently, the Reynolds number, which appears implicitly through h_N, $Re = h_N^3/3$ (see (2.37)), Ct and the four dimensionless groups, Γ, Ma, Pr and Bi for ST and the five dimensionless groups, Γ, Ma, Pr, Bi and Bi_w for HF. Hence, a complete investigation over the entire parameter space would be very cumbersome. However, for a fixed liquid and inclination angle β, the Prandtl and Kapitza numbers are fixed, thus reducing the number of relevant parameters by three. On the other hand, for given properties of the gas–liquid–solid system (physical properties of the gas–liquid system and wall heating conditions (wall temperature/heat flux)) and β, the only free parameter is the Reynolds number (through the inlet condition), which from Sect. 2.2 is the flow control parameter.

In other words, by using the above nondimensionalization, which is based on viscosity and gravity, we have ended up with only one parameter, Re, that depends on h_N, with the remaining parameters, Ct, Γ, Ma, Pr, Bi and Bi_w are all independent of h_N and fixed for a given gas–liquid–solid system and given β. Hence, the viscous-gravity scaling is experimentally quite relevant: In experiments the film thickness is modified by changing the flow rate and therefore for comparisons with experiments it is useful to have only one parameter that depends on h_N.

However, the Nusselt flat film solution can also be taken as the boundary condition $h \to h_N$ far from a local surface deformation like a solitary hump, which also corresponds to the inlet boundary condition as discussed above. Hence, for numerical purposes the formulation of a model in which the film thickness has been scaled out of the boundary conditions and the Nusselt flat film solution is fixed, thus allowing useful numerical comparisons to be made, seems desirable. Therefore, for convenience another scaling is employed based on h_N through the following transformation of the dimensionless variables in (D.1a)–(D.1b):

$$(x, y, z) \to h_N(x, y, z), \qquad h \to h_N h, \qquad t \to \tfrac{t}{h_N}, \tag{D.2a}$$

$$(u, v, w) \to h_N^2(u, v, w), \qquad p \to h_N p, \tag{D.2b}$$

$$\text{ST:} \quad T \to T, \tag{D.2c}$$

or

$$\text{HF:} \quad T \to h_N T, \tag{D.2d}$$

which converts the boundary condition $h \to h_N$ far from a solitary hump to $h \to 1$. The combination of (D.1a)–(D.1b) and (D.2a)–(D.2d) is precisely the scaling given in (2.16a)–(2.16f). This scaling is based on the Nusselt flat film solution (2.15a)–(2.15f) and is defined as the *Nusselt scaling*. Notice that the numerical factor of 3 appearing along with the Reynolds and Péclet numbers in the dimensionless momentum and energy equations (2.18)–(2.21) is due to the definition of the Reynolds number (2.35) based on the flow rate.

The Nusselt scaling explicitly scales out $\bar{h}_{\mathrm{N}}$ from the full equations of motion and energy and wall and free surface boundary conditions, but as a consequence all governing dimensionless groups, Pe, We, M, B, B_{w}, and of course Re, depend on the flow rate (through the dimensionless Nusselt flat film thickness h_{N}).

As an example, assume that we wish to construct numerically a local surface deformation like a solitary hump and examine the influence of the flow rate and the temperature difference between wall and ambient gas phase or wall heat flux (corresponding to the ST or HF cases, respectively) only on this deformation. We then need to fix β and the physical properties of the liquid–gas system, i.e., fix the viscous-gravity parameters Pr, Γ and Bi or Bi_{w} for ST or HF, respectively. The only free parameters then are Re or, equivalently, h_{N} and Ma. In the numerical scheme for the construction of the deformation, the Nusselt parameters Pe, We and B are then varied with h_{N} according to their definitions in (2.38), (2.39) and (2.41) while M is varied with both h_{N} and Ma according to (2.40a) for ST and (2.40b) for HF. The results of different characteristics of the deformation, e.g., amplitude, speed are then reported as a function of Re or h_{N}, different Ma and fixed β, Pr, Γ and Bi or Bi_{w} for ST or HF, respectively, reflecting precisely how the different parameters are input in the numerical scheme.

Hence, although the Nusselt scaling is the most widely used scaling in the literature, in this monograph it is used as in experiments (where it is much easier to fix the gas–liquid–solid system and β), instead of, e.g., varying independently Re and We, as is often the case in the literature.

D.2 On the Orders of Magnitude for the Different Groups in the Boundary Layer Equations

The orders of magnitude assignments for the different dimensionless groups in the derivation of the boundary layer equations in Sect. 4.1 are made for simplicity and in order to fix ideas. These assignments can be relaxed.

For example, let us relax the order of magnitude assignment on Re while the remaining groups have the assignments used in the derivation of the boundary layer equations in Sect. 4.1. For the second-order boundary layer equations then, the y component of the momentum equation (4.2c) shows that in order to neglect the $\mathcal{O}(\varepsilon^2 Re)$ cross-stream inertia terms on the left hand side of this equation compared to the smallest term on the right hand side, i.e., $\varepsilon\partial_{yy}v$, we must have $\varepsilon Re \ll 1$. Hence Re can only increase at a rate slower than $1/\varepsilon$. This also ensures automatically that $Re \ll We$, the condition for cross-stream inertia to be negligible compared to surface tension in the free surface pressure distribution across the film (4.4). At the same time, in order for the streamwise inertia terms in (4.2b) to be kept compared to the neglected $\mathcal{O}(\varepsilon^3)$ terms on the right hand side of this equation we must have $Re \gg \varepsilon^2$.

For the first-order boundary layer equations, εRe can be at most of $\mathcal{O}(1)$, the maximum order on the right hand side of the streamwise momentum balance (4.2b), which automatically satisfies $\varepsilon^2 Re \ll 1$ for cross-stream inertia to be negligible in

the y component of the momentum equation (4.2c) and it satisfies $Re \ll We$ for cross-stream inertia to be negligible compared to surface tension in the pressure distribution across the film (4.4). At the same time, for the streamwise inertia terms in (4.2b) to dominate over the neglected $\mathcal{O}(\varepsilon^2)$ terms of the right hand side in the same equation, $Re \gg \varepsilon$.

As an example, let us take the upper bound on Re for the first-order boundary layer equations, $Re \sim 1/\varepsilon$. Assume also that we are not too close to criticality, more specifically, $Re - Re_c = \mathcal{O}(1)$. As pointed out in Sect. 4.1, in this case $k \sim \varepsilon$. For a wavelength of the waves $\sim$1 mm, i.e., of the order of the capillary length (see Introduction) and $\bar{h}_N \sim 0.1$ mm, $k \sim 0.1$ so that $\varepsilon \sim 0.1$, which gives $Re \sim 10$, a moderate value.

Let us now relax the order of magnitude assignments for both Re and We in the second-order boundary layer equations while the remaining parameters remain of $\mathcal{O}(1)$. The y component of the momentum equation (4.2c) then shows that in order to neglect cross-stream inertia, $\varepsilon^2 Re \ll \varepsilon \partial_{yy} v$, i.e., $\varepsilon Re \ll 1$. The neglected terms in the pressure distribution (4.4) then are of $\mathcal{O}(\varepsilon^2, \varepsilon^2 Re)$, while for surface tension we require $\varepsilon^2 We$ at most of $\mathcal{O}(1)$. At the same time, for surface tension to dominate over these neglected terms we need $\varepsilon^2 We \gg \varepsilon^2$, or $We \gg 1$, and $\varepsilon^2 We \gg \varepsilon^2 Re$, or simply $Re \ll We$. The pressure distribution (4.4) is then substituted into the x component of the momentum equation (4.2b). Following the differentiation of this distribution once, the contribution of its neglected terms in (4.2b) is of $\mathcal{O}(\varepsilon^3, \varepsilon^3 Re)$. To keep the inertia terms on the left hand side of (4.2b), we need $\varepsilon Re \gg \varepsilon^3$ or $Re \gg \varepsilon^2$ and $\varepsilon Re \gg \varepsilon^3 Re$, which is automatically satisfied. Also, the viscous terms on the right hand side of (4.2b) must be kept compared to the $\mathcal{O}(\varepsilon^3 Re)$ neglected terms in $\varepsilon \partial_x p$, i.e., $\varepsilon^3 Re \ll \varepsilon^2$ or $\varepsilon Re \ll 1$, a condition we already have.

To summarize:

(i) The conditions on Re are $Re \gg \varepsilon^2$, $Re \ll We$ and $Re \ll \varepsilon^{-1}$ or $Re \ll \min\{We, \varepsilon^{-1}\}$.
(ii) The conditions on We are $\varepsilon^2 We$ at most of $\mathcal{O}(1)$, $We \gg 1$.

Assume now that for the first-order boundary layer equations, B, B_w remain of $\mathcal{O}(1)$, but we relax the orders of magnitude assignments for Re, We and M. The more general orders of magnitude assignments for these groups then are εRe at most of $\mathcal{O}(1)$, $Re \gg \varepsilon$, εM at most of $\mathcal{O}(1)$ and $M \gg \varepsilon$, and $\varepsilon^2 We$ at most of $\mathcal{O}(1)$ and $\varepsilon We \gg 1$ (i.e., $We \gg Re$, a condition that has already been utilized in the derivation of the above orders of magnitude assignments). However, the final (first- or second-order) boundary layer equations remain the same, and in fact the neglected terms are of $\mathcal{O}(\epsilon^2)$ for the first-order boundary layer equations and of $\mathcal{O}(\epsilon^3)$ for the second-order ones, as they should be: e.g., for the first-order equations the neglected terms are of $\mathcal{O}(\varepsilon^2, \varepsilon^3 Re, \varepsilon^3 M) \equiv \mathcal{O}(\varepsilon^2)$ since εRe, εM are at most of $\mathcal{O}(1)$ [207].

In all cases, We must be large, i.e., $We = \mathcal{O}(\varepsilon^{-2})$, $\mathcal{O}(\varepsilon^{-1})$ and $We = \mathcal{O}(\varepsilon^{-2})$, $\mathcal{O}(\varepsilon^{-3/2})$ are possible orders of magnitude assignments for the second- and first-order boundary layer equations, respectively. Large We is an essential requirement for the validity of the boundary layer approximation. This point is discussed in detail in Sect. 4.4.

D.3 Dimensionless Groups and Their Relationships for the ST Case

Reynolds number: $Re = \dfrac{\delta}{3\eta^{1/2}}$

Inclination number: $Ct = \dfrac{\zeta}{\eta^{1/2}}$

Kapitza number: $\Gamma = \dfrac{\delta^{2/3}}{\eta^{11/6}} = We(3Re)^{2/3}$

Marangoni number: $Ma = \dfrac{\mathcal{M}\delta^{2/3}}{\eta^{5/6}} = M(3Re)^{2/3}$

Biot number: $Bi = \dfrac{B}{(3Re)^{1/3}}$

Weber number: $We = \dfrac{1}{\eta^{3/2}} = \dfrac{\Gamma}{(3Re)^{2/3}}$

Film Marangoni number: $M = \dfrac{\mathcal{M}}{\eta^{1/2}} = \dfrac{Ma}{(3Re)^{2/3}}$

Film Biot number: $B = Bi\,(3Re)^{1/3}$

Reduced Reynolds number: $\delta = \dfrac{3Re}{We^{1/3}} = \dfrac{(3Re)^{11/9}}{\Gamma^{1/3}}$

Reduced inclination number: $\zeta = \dfrac{Ct}{We^{1/3}} = \dfrac{Ct(3Re)^{2/9}}{\Gamma^{1/3}}$

Viscous dispersion number: $\eta = \dfrac{1}{We^{2/3}} = \dfrac{(3Re)^{4/9}}{\Gamma^{2/3}}$

Reduced film Marangoni number: $\mathcal{M} = \dfrac{M}{We^{1/3}} = \dfrac{Ma}{\Gamma^{1/3}(3Re)^{4/9}}$

D.4 Physical Parameters

Table D.1 shows typical properties and parameter values for different liquids used in experiments [3, 131, 132, 239]. The Marangoni number is calculated with the

Table D.1 Physical properties of different liquids [296] and corresponding dimensionless parameters, with $\Delta T = 1$ K used for Ma and $\alpha = 100\ \mathrm{W\,m^{-2}\,K^{-1}}$ used for Bi

Liquid	l_ν (μm)	t_ν (ms)	Γ	Ma	Bi
Water at 20°C	47	2.2	3375	8.9	0.008
Water at 15°C	50	2.3	2950	7.7	0.009
FC–72 at 20°C	26	1.6	1100	9.7	0.045
MD–3F at 30°C	31	1.8	703	5.8	0.047
25% ethyl alcohol at 20°C	87	3.0	500	1.5	0.02

temperature difference $\Delta T = 1$ K and the Biot number with the heat transfer coefficient $\alpha = 100\ \mathrm{W\,m^{-2}\,K^{-1}}$. These are reference values and in practice, typical values would be 10 times larger for *Ma*, i.e., $\Delta T = 10$ K, and 5 times larger for *Bi*, i.e., $\alpha = 500\ \mathrm{W\,m^{-2}\,K^{-1}}$.

Appendix E
Model Details

E.1 Dynamical System Corresponding to the Full Second-Order Model

In the moving frame $\xi = x - ct$, the four-equation system (6.78) is transformed into a set of four ordinary differential equations. One corresponds to the mass balance $q' = ch'$, which after one integration gives $q = c\,h + q_0$. We can then eliminate q from the other three equations. Solving the system of equations for h''', ${s_1}'$ and ${s_2}'$ leads to an autonomous five-dimensional *dynamical system* in the phase space spanned by $\mathbf{U} = (U_1, U_2, U_3, U_4, U_5)$ where $U_1 = h$, $U_2 = h'$, $U_3 = h''$, $U_4 = s_1$ and $U_5 = s_2$:

$$U_1' = U_2, \qquad U_2' = U_3, \tag{E.1a}$$

$$\begin{aligned}
U_3' = {} & 3\frac{q_0}{U_1^3} + 3\frac{c}{U_1^2} - 1 + \frac{1}{U_1^3\left(c^2U_1^2 + \frac{152}{11}cq_0U_1 - \frac{444}{11}q_0^2\right)} \\
& \times \left\{\left[\delta\left(\frac{2160}{121}q_0^4 - \frac{720}{11}cq_0^3U_1 - \frac{3060}{121}c^2q_0^2U_1^2 + \frac{540}{121}c^3q_0U_1^3 + \frac{580}{363}c^4U_1^4\right)\right.\right. \\
& + BU_1^3\left(c^2U_1^2 + \frac{152}{11}cq_0U_1 - \frac{444}{11}q_0^2\right) \\
& + \delta\left(\frac{10080}{121}q_0^3 + \frac{7056}{121}cq_0^2U_1 - \frac{24584}{121}c^2q_0U_1^2 - \frac{504}{11}c^3U_1^3\right)U_4 \\
& \left.\left. + \delta\left(\frac{25920}{121}q_0^3 + \frac{74376}{121}cq_0^2U_1 + \frac{27336}{121}c^2q_0U_1^2 - \frac{324}{11}c^3U_1^3\right)U_5\right]U_2\right. \\
& + \eta\left(\frac{909}{4}q_0^3 - \frac{1971}{11}cq_0^2U_1 - \frac{42589}{352}c^2q_0U_1^2 - \frac{4525}{176}c^3U_1^3\right)U_2^2 \\
& \left. + \eta\left(-\frac{15957}{88}q_0^3 + \frac{7221}{88}cq_0^2U_1 + \frac{6727}{704}c^2q_0U_1^2 - \frac{9071}{2112}c^3U_1^3\right)U_1U_3\right\},
\end{aligned} \tag{E.1b}$$

S. Kalliadasis et al., *Falling Liquid Films*, Applied Mathematical Sciences 176,
DOI 10.1007/978-1-84882-367-9, © Springer-Verlag London Limited 2012

$$
\begin{aligned}
U_4' = & \frac{1}{\delta U_1 (c^2 U_1^2 + \frac{152}{11} c q_0 U_1 - \frac{444}{11} q_0^2)} \\
& \times \Bigg\{ \left(\frac{13689}{11} q_0 + \frac{949}{11} c U_1 \right) U_4 + \left(\frac{91143}{22} q_0 + \frac{37479}{11} c U_1 \right) U_5 \\
& + \Bigg[\delta \left(\frac{45942}{4235} q_0^3 + \frac{24986}{4235} c q_0^2 U_1 - \frac{533}{8470} c^2 q_0 U_1^2 - \frac{16003}{25410} c^3 U_1^3 \right) \\
& + \delta \left(-\frac{50772}{605} q_0^2 + \frac{5850}{121} c q_0 U_1 + \frac{1069}{55} c^2 U_1^2 \right) U_4 \\
& + \delta \left(-\frac{166644}{4235} q_0^2 - \frac{96825}{847} c q_0 U_1 + \frac{5058}{385} c^2 U_1^2 \right) U_5 \Bigg] U_2 \\
& + \eta \left(-\frac{905931}{24640} q_0^2 + \frac{436553}{12320} c q_0 U_1 + \frac{35659}{3080} c^2 U_1^2 \right) U_2^2 \\
& + \eta \left(-\frac{1647087}{49280} q_0^2 U_1 + \frac{61217}{9856} c q_0 U_1^2 + \frac{50167}{18480} c^2 U_1^3 \right) U_3 \Bigg\}, \qquad \text{(E.1c)}
\end{aligned}
$$

$$
\begin{aligned}
U_5' = & \frac{1}{\delta U_1 (c^2 U_1^2 + \frac{152}{11} c q_0 U_1 - \frac{444}{11} q_0^2)} \\
& \times \Bigg\{ \left(\frac{4186}{11} q_0 + \frac{728}{33} c U_1 \right) U_4 + \left(\frac{4559}{11} q_0 - \frac{1729}{11} c U_1 \right) U_5 \\
& + \Bigg[\delta \left(\frac{1404}{605} q_0^3 + \frac{312}{605} c q_0^2 U_1 - \frac{13}{605} c^2 q_0 U_1^2 + \frac{416}{5445} c^3 U_1^3 \right) \\
& + \delta \left(\frac{6552}{605} q_0^2 + \frac{6188}{363} c q_0 U_1 - \frac{182}{165} c^2 U_1^2 \right) U_4 \\
& + \delta \left(-\frac{51528}{605} q_0^2 + \frac{1146}{121} c q_0 U_1 - \frac{94}{55} c^2 U_1^2 \right) U_5 \Bigg] U_2 \\
& + \eta \left(\frac{75179}{1760} q_0^2 + \frac{3913}{5280} c q_0 U_1 - \frac{3497}{2640} c^2 U_1^2 \right) U_2^2 \\
& + \eta \left(\frac{16783}{3520} q_0^2 U_1 - \frac{611}{528} c q_0 U_1^2 - \frac{11947}{31680} c^2 U_1^3 \right) U_3 \Bigg\}. \qquad \text{(E.1d)}
\end{aligned}
$$

This dynamical system becomes singular with $\mathbf{U}'$ not defined at points where the denominator of (E.1b)–(E.1d) vanishes:

$$
\delta U_1 \left(c^2 U_1^2 + \frac{152}{11} c q_0 U_1 - \frac{444}{11} q_0^2 \right) = 0. \qquad \text{(E.2)}
$$

$U_1 = 0$ corresponds to the onset of dry patches on the inclined plate. However, physically the formation of dry patches requires forces of nonhydrodynamic origin, such as long-range attractive intermolecular interactions that are not con-

sidered in this monograph. The touch down with $U_1 = 0$ of a trajectory in the phase plane therefore is a nonphysical solution. The other two roots of (E.2) are $U_{\text{sing}\pm} = \frac{2}{11} q_0(-38 \pm \sqrt{2665})/c$. At least one of these roots is positive. The presence of the singular planes $U_1 = U_{\text{sing}\pm}$ in the phase space is a sign of the complexity of the full second-order model and does not result from any actual physical limitations. It is rather a direct consequence of the projection of the velocity field on a small set of polynomials.

On the other hand, the three-dimensional dynamical system (7.42) does not have any denominators and the above difficulty is avoided. This is due to the simplicity of the corresponding models. Notice, however, that the choice of only one test function does not necessarily sidestep the onset of singular planes in the phase space. The formulation adopted by Lee and Mei [161] by retaining cross-stream inertial terms while using the assumption of a self-similar parabolic velocity profile also led to the presence of singular planes in a three-dimensional phase plane.

By setting q_0 to $1/3 - c$ as in (7.39), the two fixed points of the flow (E.1a)–(E.1d) verify $U_2 = U_3 = U_4 = U_5 = 0$ and (7.44). To simplify notations, the two fixed points are denoted with the same symbols used for the fixed points $\mathbf{U}_{\text{I}}$ and $\mathbf{U}_{\text{II}}$ of the three-dimensional system (7.42). Heteroclinic orbits must connect the two fixed points without encountering one of the singular planes. For $c > 1/3$, $q_0 < 0$ and only $U_{\text{sing}-} = \frac{2}{11}(38 + \sqrt{2665})(1 - 1/(3c))$ is positive. $U_{\text{sing}-} = 1$ admits a root

$$c_- = \frac{2}{3} \frac{38 + \sqrt{2665}}{65 + 2\sqrt{2665}} \approx 0.355127.$$

Similarly, $U_{\text{sing}-} = h_{\text{II}}$ leads to $c = 1/3$ or to the second-order equation,

$$\frac{16436}{1089} + \frac{304\sqrt{2665}}{1089} - \left(\frac{17272}{363} + \frac{326\sqrt{2665}}{363} \right) c + c^2 = 0,$$

which admits two roots, $c_- \approx 0.315117$ and $c_+ \approx 93.6279$. The first value is lower than the limiting value $1/3$, below which the second fixed point $\mathbf{U}_{\text{II}}$ vanishes. The second one is much larger than the usual speed of observed waves. The limiting speeds c_- and c_+ correspond to extreme positions of the fixed point $\mathbf{U}_{\text{II}}$, either very close to the origin, $\mathbf{U}_{\text{II}} \approx 0.0615879$, or very far from it, $\mathbf{U}_{\text{II}} \approx 16.2372$. Therefore, the condition

$$c_- < c < c_+ \tag{E.3}$$

is not restrictive and does not limit the exploration of the pertinent solutions (limit cycles, homoclinic and heteroclinic orbits) to the dynamical system.

The position of the fixed points influences the orbits in the phase space. Homoclinic orbits connecting $\mathbf{U}_{\text{I}}$ to itself spiral around $\mathbf{U}_{\text{II}}$ such that the maximum amplitudes of $U_2, \ldots, U_5$ increase with the distance separating the two fixed points. The two values $1 - c_-$ and $c_+ - 1$ can be viewed as upper limits on the distance between the two fixed points, which in turn correspond to upper limits on the wave amplitude.

E.2 Three-Dimensional Full Second-Order Model

Following the weighted residuals methodology detailed in Chap. 6, the velocity field is projected onto the polynomials F_0, F_1 and F_2 defined in (6.74) and repeated below for convenience:

$$F_0 = \bar{y} - \frac{1}{2}\bar{y}^2 \tag{E.4a}$$

$$F_1 = \bar{y} - \frac{17}{6}\bar{y}^2 + \frac{7}{3}\bar{y}^3 - \frac{7}{12}\bar{y}^4 \tag{E.4b}$$

$$F_2 = \bar{y} - \frac{13}{2}\bar{y}^2 + \frac{57}{4}\bar{y}^3 - \frac{111}{8}\bar{y}^4 + \frac{99}{16}\bar{y}^5 - \frac{33}{32}\bar{y}^6. \tag{E.4c}$$

The streamwise and spanwise velocity distributions thus read

$$u = \frac{3}{h}(q_\parallel - s_1 - s_2)g_0(\bar{y}) + 45\frac{s_1}{h}g_1(\bar{y}) + 210\frac{s_2}{h}g_2(\bar{y}) \tag{E.5a}$$

$$w = \frac{3}{h}(p - r_1 - r_2)g_0(\bar{y}) + 45\frac{r_1}{h}g_1(\bar{y}) + 210\frac{r_2}{h}g_2(\bar{y}), \tag{E.5b}$$

where $\bar{y} = y/h$ and the streamwise and spanwise flow rates $q_\parallel = \int_0^h u\,dy$ and $q_\perp = \int_0^h w\,dy$, respectively, appear with two corrections each, namely s_1, s_2 and r_1, r_2.

Applying the Galerkin method, which consists of integrating the boundary layer equations (4.5a), (4.5b) across the film, substituting the projections (E.5a)–(E.5b) into the integrated equations, taking the test functions (E.4a)–(E.4c) as weight functions and using the boundary conditions (4.2f), (4.2k), (4.2l) yields the full second-order model for three-dimensional flows. Let us define two fictitious parameters, $\epsilon_x \equiv 1$ and $\epsilon_z \equiv 0$. They will be used as "tracers" to identify in-plane gravity terms that are equal to zero for the momentum equations in the transverse z direction. The evolution equations for $q_\parallel$, s_1 and s_2 read

$$\begin{aligned}
\delta\partial_t q_\parallel = {} & \epsilon_x\frac{27}{28}h - \frac{81}{28}\frac{q_\parallel}{h^2} - 33\frac{s_1}{h^2} - \frac{3069}{28}\frac{s_2}{h^2} + \delta\bigg(-\frac{12}{5}\frac{q_\parallel s_1\partial_x h}{h^2} - \frac{126}{65}\frac{q_\parallel s_2\partial_x h}{h^2} \\
& + \frac{12}{5}\frac{s_1\partial_x q_\parallel}{h} + \frac{171}{65}\frac{s_2\partial_x q_\parallel}{h} + \frac{12}{5}\frac{q_\parallel\partial_x s_1}{h} + \frac{1017}{455}\frac{q_\parallel\partial_x s_2}{h} + \frac{6}{5}\frac{q_\parallel^2\partial_x h}{h^2} \\
& - \frac{12}{5}\frac{q_\parallel\partial_x q_\parallel}{h} - \frac{6}{5}\frac{q_\parallel\partial_z q_\perp}{h} - \frac{6}{5}\frac{q_\perp\partial_z q_\parallel}{h} + \frac{6}{5}\frac{q_\parallel q_\perp\partial_z h}{h^2} - \frac{6}{5}\frac{q_\parallel r_1\partial_z h}{h^2} \\
& - \frac{63}{65}\frac{q_\parallel r_2\partial_z h}{h^2} - \frac{6}{5}\frac{q_\perp s_1\partial_z h}{h^2} - \frac{63}{65}\frac{q_\perp s_2\partial_z h}{h^2} + \frac{6}{5}\frac{s_1\partial_z q_\perp}{h} + \frac{108}{65}\frac{s_2\partial_z q_\perp}{h} \\
& + \frac{6}{5}\frac{r_1\partial_z q_\parallel}{h} + \frac{63}{65}\frac{r_2\partial_z q_\parallel}{h} + \frac{6}{5}\frac{q_\parallel\partial_z r_1}{h} + \frac{576}{455}\frac{q_\parallel\partial_z r_2}{h} + \frac{6}{5}\frac{q_\perp\partial_z s_1}{h} \\
& + \frac{63}{65}\frac{q_\perp\partial_z s_2}{h}\bigg) + \eta\bigg(\frac{5025}{896}\frac{q_\parallel(\partial_x h)^2}{h^2} - \frac{5055}{896}\frac{\partial_x q_\parallel\partial_x h}{h} - \frac{10851}{1792}\frac{q_\parallel\partial_{xx} h}{h}
\end{aligned}$$

$$+\frac{2027}{448}\partial_{xx}q_{\parallel}+\partial_{zz}q_{\parallel}-\frac{2463}{1792}\frac{\partial_z q_{\parallel}\partial_z h}{h}+\frac{2433}{1792}\frac{q_{\parallel}(\partial_z h)^2}{h^2}-\frac{5361}{3584}\frac{q_{\parallel}\partial_{zz}h}{h}$$
$$+\frac{7617}{1792}\frac{q_{\perp}\partial_x h\partial_z h}{h^2}-\frac{4749}{3584}\frac{\partial_z q_{\perp}\partial_x h}{h}-\frac{10545}{3584}\frac{\partial_x q_{\perp}\partial_z h}{h}-\frac{16341}{3584}\frac{q_{\perp}\partial_{xz}h}{h}$$
$$+\frac{1579}{448}\partial_{xz}q_{\perp}\Big)-\frac{27}{28}\zeta h\,\partial_x h+\frac{27}{28}h(\partial_{xxx}+\partial_{xzz})h \tag{E.6a}$$

$$\delta\partial_t s_1=\epsilon_x\frac{1}{10}h-\frac{3}{10}\frac{q_{\parallel}}{h^2}-\frac{126}{5}\frac{s_1}{h^2}-\frac{126}{5}\frac{s_2}{h^2}+\delta\Big(\frac{1}{35}\frac{q_{\parallel}\partial_x q_{\parallel}}{h}-\frac{3}{35}\frac{q_{\parallel}^2\partial_x h}{h^2}$$
$$+\frac{108}{55}\frac{q_{\parallel}s_1\partial_x h}{h^2}-\frac{5022}{5005}\frac{q_{\parallel}s_2\partial_x h}{h^2}-\frac{103}{55}\frac{s_1\partial_x q_{\parallel}}{h}+\frac{9657}{5005}\frac{s_2\partial_x q_{\parallel}}{h}$$
$$-\frac{39}{55}\frac{q_{\parallel}\partial_x s_1}{h}+\frac{10557}{10010}\frac{q_{\parallel}\partial_x s_2}{h}-\frac{2}{35}\frac{q_{\parallel}\partial_z q_{\perp}}{h}+\frac{3}{35}\frac{q_{\perp}\partial_z q_{\parallel}}{h}$$
$$-\frac{3}{35}\frac{q_{\parallel}q_{\perp}\partial_z h}{h^2}+\frac{54}{55}\frac{q_{\parallel}r_1\partial_z h}{h^2}+\frac{54}{55}\frac{q_{\perp}s_1\partial_z h}{h^2}-\frac{54}{55}\frac{r_1\partial_z q_{\parallel}}{h}$$
$$-\frac{54}{55}\frac{q_{\perp}\partial_z s_1}{h}-\frac{2511}{5005}\frac{q_{\perp}s_2\partial_z h}{h^2}-\frac{2511}{5005}\frac{q_{\parallel}r_2\partial_z h}{h^2}+\frac{2511}{5005}\frac{r_2\partial_z q_{\parallel}}{h}$$
$$+\frac{2511}{5005}\frac{q_{\perp}\partial_z s_2}{h}-\frac{49}{55}\frac{s_1\partial_z q_{\perp}}{h}+\frac{7146}{5005}\frac{s_2\partial_z q_{\perp}}{h}+\frac{3}{11}\frac{q_{\parallel}\partial_z r_1}{h}$$
$$+\frac{1107}{2002}\frac{q_{\parallel}\partial_z r_2}{h}\Big)+\eta\Big(\frac{93}{40}\frac{q_{\parallel}(\partial_x h)^2}{h^2}-\frac{69}{40}\frac{\partial_x h\partial_x q_{\parallel}}{h}+\frac{21}{80}\frac{q_{\parallel}\partial_{xx}h}{h}$$
$$-\frac{9}{40}\partial_{xx}q_{\parallel}-\frac{57}{80}\frac{\partial_z q_{\parallel}\partial_z h}{h}+\frac{81}{80}\frac{q_{\parallel}(\partial_z h)^2}{h^2}-\frac{3}{40}\frac{q_{\parallel}\partial_{zz}h}{h}+\frac{27}{80}\frac{q_{\perp}\partial_{xz}h}{h}$$
$$+\frac{21}{16}\frac{q_{\perp}\partial_x h\partial_z h}{h^2}-\frac{63}{80}\frac{\partial_z q_{\perp}\partial_x h}{h}-\frac{9}{40}\frac{\partial_z h\partial_x q_{\perp}}{h}-\frac{9}{40}\partial_{xz}q_{\perp}\Big)$$
$$-\frac{1}{10}\zeta h\partial_x h+\frac{1}{10}h(\partial_{xxx}+\partial_{xzz})h \tag{E.6b}$$

$$\delta\partial_t s_2=\epsilon_x\frac{13}{420}h-\frac{13}{140}\frac{q_{\parallel}}{h^2}-\frac{39}{5}\frac{s_1}{h^2}-\frac{11817}{140}\frac{s_2}{h^2}+\delta\Big(-\frac{4}{11}\frac{q_{\parallel}s_1\partial_x h}{h^2}+\frac{18}{11}\frac{q_{\parallel}s_2\partial_x h}{h^2}$$
$$-\frac{2}{33}\frac{s_1\partial_x q_{\parallel}}{h}-\frac{19}{11}\frac{s_2\partial_x q_{\parallel}}{h}+\frac{6}{55}\frac{q_{\parallel}\partial_x s_1}{h}-\frac{288}{385}\frac{q_{\parallel}\partial_x s_2}{h}-\frac{2}{11}\frac{q_{\parallel}r_1\partial_z h}{h^2}$$
$$-\frac{2}{11}\frac{q_{\perp}s_1\partial_z h}{h^2}+\frac{2}{11}\frac{r_1\partial_z q_{\parallel}}{h}+\frac{2}{11}\frac{q_{\perp}\partial_z s_1}{h}+\frac{9}{11}\frac{q_{\parallel}r_2\partial_z h}{h^2}+\frac{9}{11}\frac{q_{\perp}s_2\partial_z h}{h^2}$$
$$-\frac{9}{11}\frac{r_2\partial_z q_{\parallel}}{h}-\frac{9}{11}\frac{q_{\perp}\partial_z s_2}{h}-\frac{8}{33}\frac{s_1\partial_z q_{\perp}}{h}-\frac{10}{11}\frac{s_2\partial_z q_{\perp}}{h}-\frac{4}{55}\frac{q_{\parallel}\partial_z r_1}{h}$$

$$+\frac{27}{385}\frac{q_\parallel\partial_z r_2}{h}\Big)+\eta\Big(-\frac{3211}{4480}\frac{q_\parallel(\partial_x h)^2}{h^2}+\frac{2613}{4480}\frac{\partial_x h\partial_x q_\parallel}{h}-\frac{2847}{8960}\frac{q_\parallel\partial_{xx}h}{h}$$
$$+\frac{559}{2240}\partial_{xx}q_\parallel+\frac{3029}{8960}\frac{\partial_z q_\parallel\partial_z h}{h}-\frac{3627}{8960}\frac{q_\parallel(\partial_z h)^2}{h^2}+\frac{299}{17920}\frac{q_\parallel\partial_{zz}h}{h}$$
$$-\frac{559}{1792}\frac{q_\perp\partial_x h\partial_z h}{h^2}+\frac{4927}{17920}\frac{\partial_z q_\perp\partial_x h}{h}-\frac{533}{17920}\frac{\partial_x q_\perp\partial_z h}{h}-\frac{5993}{17920}\frac{q_\perp\partial_{xz}h}{h}$$
$$+\frac{559}{2240}\partial_{xz}q_\perp\Big)-\frac{13}{420}\zeta h\partial_x h+\frac{13}{420}h(\partial_{xxx}+\partial_{xzz})h. \tag{E.6c}$$

The equations for $q_\perp$, r_1 and r_2 are obtained from (E.6a)–(E.6c) through the exchanges $\{x\leftrightarrow z,\ q_\parallel\leftrightarrow q_\perp,\ s_{1,2}\leftrightarrow r_{1,2},\ \epsilon_x\leftrightarrow\epsilon_z\}$ (hence the introduction of the "tracers" $\epsilon_{x,z}$ reduces to a minimum the set of equations to be written). The set of equations is completed by the mass conservation $\partial_t h=-\partial_x q_\parallel-\partial_z q_\perp$.

E.3 Three-Dimensional Regularized Second-Order Model

$$\partial_t h=-\partial_x q_\parallel-\partial_z q_\perp \tag{E.7a}$$

$$\delta\partial_t q_\parallel=\delta\Big[\frac{9}{7}\frac{q_\parallel^2}{h^2}\partial_x h-\frac{17}{7}\frac{q_\parallel}{h}\partial_x q_\parallel\Big]+\Big[\frac{5}{6}h-\frac{5}{2}\frac{q_\parallel}{h^2}$$
$$+\delta\Big(-\frac{8}{7}\frac{q_\parallel\partial_z q_\perp}{h}-\frac{9}{7}\frac{q_\perp\partial_z q_\parallel}{h}+\frac{9}{7}\frac{q_\parallel q_\perp\partial_z h}{h^2}\Big)$$
$$+\eta\Big(4\frac{q_\parallel(\partial_x h)^2}{h^2}-\frac{9}{2}\frac{\partial_x q_\parallel\partial_x h}{h}-6\frac{q_\parallel\partial_{xx}h}{h}+\frac{9}{2}\partial_{xx}q_\parallel$$
$$+\frac{13}{4}\frac{q_\perp\partial_x h\partial_z h}{h^2}-\frac{\partial_z q_\parallel\partial_z h}{h}-\frac{43}{16}\frac{\partial_x q_\perp\partial_z h}{h}-\frac{13}{16}\frac{\partial_z q_\perp\partial_x h}{h}$$
$$+\frac{3}{4}\frac{q_\parallel(\partial_z h)^2}{h^2}-\frac{23}{16}\frac{q_\parallel\partial_{zz}h}{h}-\frac{73}{16}\frac{q_\perp\partial_{xz}h}{h}+\partial_{zz}q_\parallel+\frac{7}{2}\partial_{xz}q_\perp\Big)$$
$$-\frac{5}{6}\zeta h\,\partial_x h+\frac{5}{6}h(\partial_{xxx}+\partial_{xzz})h\Big]\Big(1-\frac{\delta}{70}q_\parallel\partial_x h\Big)^{-1} \tag{E.7b}$$

$$\delta\partial_t q_\perp=\delta\Big(\frac{9}{7}\frac{q_\perp^2}{h^2}\partial_z h-\frac{17}{7}\frac{q_\perp}{h}\partial_z q_\perp\Big)-\frac{5}{2}\frac{q_\perp}{h^2}$$
$$+\delta\Big(-\frac{8}{7}\frac{q_\perp\partial_x q_\parallel}{h}-\frac{9}{7}\frac{q_\parallel\partial_x q_\perp}{h}+\frac{9}{7}\frac{q_\parallel q_\perp\partial_x h}{h^2}\Big)$$
$$+\eta\Big(4\frac{q_\perp(\partial_z h)^2}{h^2}-\frac{9}{2}\frac{\partial_z q_\perp\partial_z h}{h}-6\frac{q_\perp\partial_{zz}h}{h}+\frac{9}{2}\partial_{zz}q_\perp$$

$$+\frac{13}{4}\frac{q_\parallel \partial_x h \partial_z h}{h^2}-\frac{\partial_x q_\perp \partial_x h}{h}-\frac{43}{16}\frac{\partial_z q_\parallel \partial_x h}{h}-\frac{13}{16}\frac{\partial_x q_\parallel \partial_z h}{h}$$
$$+\frac{3}{4}\frac{q_\perp(\partial_x h)^2}{h^2}-\frac{23}{16}\frac{q_\perp \partial_{xx} h}{h}-\frac{73}{16}\frac{q_\parallel \partial_{xz} h}{h}+\partial_{xx} q_\perp+\frac{7}{2}\partial_{xz} q_\parallel\Big)$$
$$-\frac{5}{6}\zeta h\partial_z h+\frac{5}{6}h(\partial_{xxz}+\partial_{zzz})h. \tag{E.7c}$$

E.4 Full Second-Order Model for the ST Case

$$\partial_t h=-\partial_x q \tag{E.8a}$$
$$\delta\partial_t q=\frac{30}{31}h-\frac{90}{31}\frac{q}{h^2}-\frac{1050}{31}\frac{s_1}{h^2}-\frac{3690}{31}\frac{s_2}{h^2}-\frac{9066}{31}\frac{s_3}{h^2}$$
$$+\delta\Big(\frac{6}{5}\frac{q^2\partial_x h}{h^2}-\frac{12}{5}\frac{q\partial_x q}{h}-\frac{12}{5}\frac{q s_1\partial_x h}{h^2}-\frac{4248}{2015}\frac{q s_2\partial_x h}{h^2}$$
$$-\frac{5296}{3875}\frac{q s_3\partial_x h}{h^2}+\frac{12}{5}\frac{s_1\partial_x q}{h}+\frac{1026}{403}\frac{s_2\partial_x q}{h}+\frac{11722}{3875}\frac{s_3\partial_x q}{h}$$
$$+\frac{12}{5}\frac{q\partial_x s_1}{h}+\frac{4626}{2015}\frac{q\partial_x s_2}{h}+\frac{1538}{775}\frac{q\partial_x s_3}{h}\Big)-\frac{213}{248}\mathcal{M}\partial_x\theta$$
$$+\eta\Big(\frac{1569}{248}\frac{q(\partial_x h)^2}{h^2}-\frac{1569}{248}\frac{\partial_x q\partial_x h}{h}-\frac{2847}{496}\frac{q\partial_{xx} h}{h}+\frac{1069}{248}\partial_{xx} q\Big)$$
$$-\frac{30}{31}\zeta h\,\partial_x h+\frac{30}{31}h\partial_{xxx}h \tag{E.8b}$$
$$\delta\partial_t s_1=\frac{1}{10}h-\frac{3}{10}\frac{q}{h^2}-\frac{126}{5}\frac{s_1}{h^2}-\frac{126}{5}\frac{s_2}{h^2}-\frac{126}{5}\frac{s_3}{h^2}$$
$$+\delta\Big(-\frac{3}{35}\frac{q^2\partial_x h}{h^2}+\frac{1}{35}\frac{q\partial_x q}{h}+\frac{108}{55}\frac{q s_1\partial_x h}{h^2}-\frac{5022}{5005}\frac{q s_2\partial_x h}{h^2}$$
$$+\frac{6}{35}\frac{q s_3\partial_x h}{h^2}-\frac{103}{55}\frac{s_1\partial_x q}{h}+\frac{9657}{5005}\frac{s_2\partial_x q}{h}-\frac{1}{35}\frac{s_3\partial_x q}{h}$$
$$-\frac{39}{55}\frac{q\partial_x s_1}{h}+\frac{10557}{10010}\frac{q\partial_x s_2}{h}+\frac{19}{70}\frac{q\partial_x s_3}{h}\Big)+\frac{3}{8}\mathcal{M}\partial_x\theta$$
$$+\eta\Big(\frac{93}{40}\frac{q(\partial_x h)^2}{h^2}-\frac{69}{40}\frac{\partial_x h\partial_x q}{h}+\frac{21}{80}\frac{q\partial_{xx} h}{h}-\frac{9}{40}\partial_{xx} q\Big)$$
$$-\frac{1}{10}\zeta h\partial_x h+\frac{1}{10}h\partial_{xxx}h \tag{E.8c}$$

$$\begin{aligned}\delta\partial_t s_2 = {} & \frac{13}{420}h - \frac{13}{140}\frac{q}{h^2} - \frac{39}{5}\frac{s_1}{h^2} - \frac{11817}{140}\frac{s_2}{h^2} - \frac{11817}{140}\frac{s_3}{h^2} \\ & + \delta\Bigg(-\frac{4}{11}\frac{q s_1 \partial_x h}{h^2} + \frac{18}{11}\frac{q s_2 \partial_x h}{h^2} - \frac{38}{25}\frac{q s_3 \partial_x h}{h^2} - \frac{2}{33}\frac{s_1 \partial_x q}{h} \\ & - \frac{19}{11}\frac{s_2 \partial_x q}{h} + \frac{76}{25}\frac{s_3 \partial_x q}{h} + \frac{6}{55}\frac{q \partial_x s_1}{h} - \frac{288}{385}\frac{q \partial_x s_2}{h} \\ & + \frac{73}{70}\frac{q \partial_x s_3}{h}\Bigg) - \frac{13}{64}\mathcal{M}\partial_x\theta \\ & + \eta\Bigg(-\frac{3211}{4480}\frac{q(\partial_x h)^2}{h^2} + \frac{2613}{4480}\frac{\partial_x h \partial_x q}{h} - \frac{2847}{8960}\frac{q\partial_{xx}h}{h} + \frac{559}{2240}\partial_{xx}q\Bigg) \\ & - \frac{13}{420}\zeta h \partial_x h + \frac{13}{420}h\partial_{xxx}h \end{aligned} \tag{E.8d}$$

$$\begin{aligned}\delta\partial_t s_3 = {} & \frac{8}{868}h - \frac{9}{868}\frac{q}{h^2} - \frac{27}{31}\frac{s_1}{h^2} - \frac{8181}{868}\frac{s_2}{h^2} - \frac{158709}{868}\frac{s_3}{h^2} \\ & + \delta\Bigg(-\frac{342}{2015}\frac{q s_2 \partial_x h}{h^2} + \frac{9894}{3875}\frac{q s_3 \partial_x h}{h^2} - \frac{171}{2015}\frac{s_2 \partial_x q}{h} - \frac{9358}{3875}\frac{s_3 \partial_x q}{h} \\ & + \frac{171}{2821}\frac{q \partial_x s_2}{h} - \frac{13653}{10850}\frac{q \partial_x s_3}{h}\Bigg) + \frac{435}{1984}\mathcal{M}\partial_x\theta \\ & + \eta\Bigg(+\frac{19953}{27776}\frac{q(\partial_x h)^2}{h^2} - \frac{19023}{27776}\frac{\partial_x h \partial_x q}{h} + \frac{17517}{55552}\frac{q\partial_{xx}h}{h} \\ & - \frac{2973}{13888}\partial_{xx}q\Bigg) - \frac{3}{868}\zeta h\partial_x h + \frac{33}{868}h\partial_{xxx}h \end{aligned} \tag{E.8e}$$

$$\begin{aligned}Pr\delta\partial_t\theta = {} & \frac{30009}{1273}\left(\frac{1-(1+Bh)\theta}{h^2}\right) - \frac{130950}{1273}\frac{t_1}{h^2} - \frac{1384362}{6365}\frac{t_2}{h^2} - \frac{1863792}{6365}\frac{t_3}{h^2} \\ & + Pr\delta\Bigg(-\frac{3117}{203680}\frac{(1-\theta)\partial_x q}{h} - \frac{155877}{101840}\frac{q\partial_x\theta}{h} - \frac{3117}{81472}\frac{t_1\partial_x q}{h} \\ & + \frac{801101}{4480960}\frac{t_2\partial_x q}{h} - \frac{1768473}{1323920}\frac{t_3\partial_x q}{h} + \frac{3117}{40736}\frac{q\partial_x t_1}{h} - \frac{364701}{2240480}\frac{q\partial_x t_2}{h} \\ & + \frac{7840671}{14563120}\frac{q\partial_x t_3}{h} - \frac{21819}{101840}\frac{(1-\theta)\partial_x s_1}{h} - \frac{10066647}{21182720}\frac{(1-\theta)\partial_x s_2}{h} \\ & - \frac{949089}{8147200}\frac{(1-\theta)\partial_x s_3}{h} + \frac{245511}{50920}\frac{s_1\partial_x\theta}{h} - \frac{44102157}{10591360}\frac{s_2\partial_x\theta}{h} \\ & + \frac{295506139}{4073600}\frac{s_3\partial_x\theta}{h}\Bigg) + \eta\Bigg(\frac{27463}{1273}\frac{(1-\theta)(\partial_x h)^2}{h^2} - \frac{30009}{2546}B\frac{\theta(\partial_x h)^2}{h} \\ & + \frac{27463}{1273}\frac{\partial_x h\partial_x\theta}{h} + \frac{(1-\theta)\partial_{xx}h}{h} + \partial_{xx}\theta\Bigg) \end{aligned} \tag{E.8f}$$

$$
\begin{aligned}
Pr\delta\partial_t t_1 = {} & \frac{8176}{1273}\left(\frac{1-(1+Bh)\theta}{h^2}\right) - \frac{40880}{1273}\frac{t_1}{h^2} - \frac{34874}{1273}\frac{t_2}{h^2} - \frac{28784}{1273}\frac{t_3}{h^2} \\
& + Pr\delta\left(-\frac{97063}{407360}\frac{(1-\theta)\partial_x q}{h} - \frac{56327}{203680}\frac{q\partial_x\theta}{h} - \frac{166435}{488832}\frac{t_1\partial_x q}{h}\right. \\
& - \frac{20340413}{26885760}\frac{t_2\partial_x q}{h} - \frac{28729997}{174757440}\frac{t_3\partial_x q}{h} - \frac{225649}{244416}\frac{q\partial_x t_1}{h} \\
& + \frac{222059}{4480960}\frac{q\partial_x t_2}{h} + \frac{16530119}{43689360}\frac{q\partial_x t_3}{h} + \frac{1849169}{1222080}\frac{(1-\theta)\partial_x s_1}{h} \\
& + \frac{70164667}{42365440}\frac{(1-\theta)\partial_x s_2}{h} - \frac{11651371}{9776640}\frac{(1-\theta)\partial_x s_3}{h} + \frac{294637}{76380}\frac{s_1\partial_x\theta}{h} \\
& \left. - \frac{122474147}{21182720}\frac{s_2\partial_x\theta}{h} + \frac{88699283}{4888320}\frac{s_3\partial_x\theta}{h}\right) + \eta\left(\frac{8176}{1273}\frac{\partial_x h\partial_x\theta}{h}\right. \\
& \left. + \frac{8176}{1273}\frac{(1-\theta)(\partial_x h)^2}{h^2} - \frac{4088}{1273}B\frac{\theta(\partial_x h)^2}{h}\right) \qquad \text{(E.8g)}
\end{aligned}
$$

$$
\begin{aligned}
Pr\delta\partial_t t_2 = {} & \frac{44838}{6365}\left(\frac{1-(1+Bh)\theta}{h^2}\right) - \frac{44838}{1273}\frac{t_1}{h^2} - \frac{3231144}{31825}\frac{t_2}{h^2} - \frac{2306304}{31825}\frac{t_3}{h^2} \\
& + Pr\delta\left(\frac{158337}{2036800}\frac{(1-\theta)\partial_x q}{h} + \frac{158337}{1018400}\frac{q\partial_x\theta}{h} + \frac{2674149}{5703040}\frac{t_1\partial_x q}{h}\right. \\
& + \frac{13678523}{313667200}\frac{t_2\partial_x q}{h} - \frac{446443197}{509709200}\frac{t_3\partial_x q}{h} - \frac{1222929}{2851520}\frac{q\partial_x t_1}{h} \\
& - \frac{204549663}{156833600}\frac{q\partial_x t_2}{h} - \frac{336704427}{1019418400}\frac{q\partial_x t_3}{h} + \frac{97173}{2036800}\frac{(1-\theta)\partial_x s_1}{h} \\
& - \frac{490225113}{211827200}\frac{(1-\theta)\partial_x s_2}{h} - \frac{64692369}{81472000}\frac{(1-\theta)\partial_x s_3}{h} - \frac{352833}{254600}\frac{s_1\partial_x\theta}{h} \\
& \left. - \frac{302607783}{105913600}\frac{s_2\partial_x\theta}{h} + \frac{1304283921}{40736000}\frac{s_3\partial_x\theta}{h}\right) + \eta\left(\frac{44838}{6365}\frac{\partial_x h\partial_x\theta}{h}\right. \\
& \left. + \frac{44838}{6365}\frac{(1-\theta)(\partial_x h)^2}{h^2} - \frac{22419}{6365}B\frac{\theta(\partial_x h)^2}{h}\right) \qquad \text{(E.8h)}
\end{aligned}
$$

$$
\begin{aligned}
Pr\delta\partial_t t_3 = {} & \frac{45232}{6365}\left(\frac{1-(1+Bh)\theta}{h^2}\right) - \frac{45232}{1273}\frac{t_1}{h^2} - \frac{2818816}{31825}\frac{t_2}{h^2} - \frac{6293056}{31825}\frac{t_3}{h^2} \\
& + Pr\delta\left(-\frac{7579}{254600}\frac{(1-\theta)\partial_x q}{h} - \frac{7579}{127300}\frac{q\partial_x\theta}{h} - \frac{260999}{2138640}\frac{t_1\partial_x q}{h}\right. \\
& + \frac{6804757}{10693200}\frac{t_2\partial_x q}{h} - \frac{62613409}{139011600}\frac{t_3\partial_x q}{h} + \frac{210079}{1069320}\frac{q\partial_x t_1}{h} \\
& \left. - \frac{555439}{1782200}\frac{q\partial_x t_2}{h} - \frac{58821361}{69505800}\frac{q\partial_x t_3}{h} - \frac{133699}{381900}\frac{(1-\theta)\partial_x s_1}{h}\right.
\end{aligned}
$$

$$+\frac{8441321}{26478400}\frac{(1-\theta)\partial_x s_2}{h}+\frac{121848419}{30552000}\frac{(1-\theta)\partial_x s_3}{h}-\frac{95509}{190950}\frac{s_1\partial_x\theta}{h}$$
$$+\frac{55645211}{13239200}\frac{s_2\partial_x\theta}{h}+\frac{284237129}{15276000}\frac{s_3\partial_x\theta}{h}\Big)+\eta\Big(\frac{45232}{6365}\frac{\partial_x h\partial_x\theta}{h}$$
$$+\frac{45232}{6365}\frac{(1-\theta)(\partial_x h)^2}{h^2}-\frac{22616}{6365}B\frac{\theta(\partial_x h)^2}{h}\Big). \tag{E.8i}$$

E.5 Second-Order Inertia Corrections to the Regularized Model (9.33a), (9.33b) for the ST Case

$$\mathcal{K}=\frac{1}{210}h^2\partial_{tt}q+\frac{17}{630}hq\partial_{xt}q-\frac{1}{105}q\partial_x h\partial_t q+\frac{1}{42}h\partial_x q\partial_t q-\frac{26}{231}\frac{q^2\partial_x h\partial_x q}{h}$$
$$+\frac{653}{8085}q(\partial_x q)^2+\frac{386}{8085}q^2\partial_{xx}q+\frac{104}{2695}\frac{q^3(\partial_x h)^2}{h^2}-\frac{78}{2695}\frac{q^3\partial_{xx}h}{h} \tag{E.9a}$$
$$\mathcal{K}^M=\frac{5}{112}q\partial_x h\partial_x\theta+\frac{19}{336}h\partial_x q\partial_x\theta+\frac{1}{48}h^2\partial_{xt}\theta+\frac{15}{224}hq\partial_{xx}\theta \tag{E.9b}$$
$$\mathcal{K}_{\theta q}=-\frac{19}{1400}\big[(1-\theta)\partial_x h-h\partial_x\theta\big]\partial_t q-\frac{19}{2800}(1-\theta)\partial_{xt}q$$
$$+\frac{47}{4800}(1-\theta)\frac{\partial_x h\partial_x q}{h}-\frac{613}{33600}(1-\theta)\big[(\partial_x q)^2+q\partial_{xx}q\big]$$
$$-\frac{157}{1600}\frac{q^2\partial_x h\partial_x\theta}{h}+\frac{613}{16800}q\partial_x q\partial_x\theta+\frac{157}{11200}\frac{(1-\theta)q^2\partial_{xx}h}{h} \tag{E.9c}$$
$$\mathcal{K}_\theta=\frac{1}{15}h^2\partial_{tt}\theta+\frac{23}{140}(qh\partial_{xt}\theta+q\partial_x h\partial_t\theta)+\frac{23}{280}h\partial_t q\partial_x\theta-\frac{33}{280}h\partial_x q\partial_t\theta$$
$$-\frac{31}{1680}(1-\theta)h\partial_{xt}q-\frac{491}{22400}(1-\theta)\Big(\frac{\partial_x h\partial_x q}{h}+q\partial_{xx}q\Big)$$
$$+\frac{1391}{67200}(1-\theta)(\partial_x q)^2+\frac{573}{5600}\Big(\frac{q^2\partial_x h\partial_x\theta}{h}+q^2\partial_{xx}\theta\Big)$$
$$+\frac{113}{2800}q\partial_x q\partial_x\theta \tag{E.9d}$$
$$\mathcal{K}_\theta^M=\frac{3}{40}h(\partial_x\theta)^2-\frac{3}{40}(1-\theta)\partial_x h\partial_x\theta-\frac{3}{80}(1-\theta)h\partial_{xx}\theta. \tag{E.9e}$$

E.6 Weighted Residuals Modeling for the HF Case

Up to now, the weighted residual approach has been applied for the problem of a uniformly heated film corresponding to the ST condition. Here we develop the

weighted residuals modeling for the HF condition which takes into account heat losses from the wall to the gas phase in contact with the wall. The condition is given in (2.23b) and is rewritten here for clarity:

$$\partial_y T|_0 = -1 + B_\mathrm{w} T|_0. \tag{E.10}$$

As emphasized in Sect. 9.4, at zeroth order the heat transfer and mechanical equilibrium of the film are decoupled from each other. The coupling between the two appears at first order through the presence of interfacial deformations. Moreover, the zeroth-order formulation of the surface temperature (5.4b)

$$\theta^{(0)} = \frac{1}{B + B_\mathrm{w}(1 + Bh)} \tag{E.11}$$

yields the same formulation of the second-order terms $\mathcal{K}^M$ (recall that these terms are induced in the momentum equation by the Marangoni flow produced by the gradient of temperature at the film surface) as obtained in (9.40) for ST. Therefore, the momentum equation (9.43b) of the reduced model will remain unaltered with HF and we hence focus only on the energy equation in what follows. In addition, the Galerkin averaging procedure for the energy equation is overall similar to the one presented in Sect. 9.2, but with some modifications.

Much like with the ST case, we wish to have the film surface temperature θ in the formulation of the averaged model. Let us then rewrite the linear zeroth-order temperature profile across the film (5.3f) in terms of the surface temperature θ:

$$T^{(0)} = \theta + \mathbb{F}(h - y) \quad \text{where } \mathbb{F} = \frac{1 - B_\mathrm{w}\theta}{1 + B_\mathrm{w} h}. \tag{E.12}$$

The *effective heat flux* $\mathbb{F}(x,t)$ at the wall decreases with the intensity B_w of the heat losses from the liquid to the wall and with the increase of the film surface temperature θ. To satisfy the boundary condition (E.10), we write the temperature field as

$$T(x,y,t) = -\mathbb{F}(x,t)\ y + \sum_{i=0}^{i_\mathrm{max}} b_i(x,t) g_i\left(\frac{y}{h(x,t)}\right), \tag{E.13}$$

where $g_0 = 1$ corresponds to the base state, and the set of test functions is completed with $g_i(\bar{y}) = \bar{y}^{i+1}$, $i \leq 1$, to obtain the polynomial basis for the projection.

E.6.1 Formulation at First-Order

Turning to the weighted residuals for the energy equation (9.7b) and with the same arguments as in Sect. 9.2, the unknowns b_i, $i \geq 1$, may only play a role through the integral, $\int_0^h w_j \partial_{yy} T$. With two integrations by parts and making use of the boundary

condition at the surface (9.6f) and the heat flux condition at the wall (E.10), we obtain

$$\int_0^h w_j\left(\frac{y}{h}\right)\partial_{yy}T\,dy = -Bw_j(1)T|_h + w_j(0)(1-B_{\rm w}T|_0) + \frac{1}{h}\left(w_j{}'(0)T|_0 - w_j{}'(1)T|_h\right) + \frac{1}{h^2}\int_0^h w_j{}''\left(\frac{y}{h}\right)T\,dy. \tag{E.14}$$

In order to put the emphasis on $\theta \equiv T|_h$, we choose for the first weight function $w'_{i_{\max}}(0) = 0$, $w''_{i_{\max}} = 0$, so that $w_{i_{\max}} \propto 1 = g_0$. It is next appropriate to replace the physically meaningless unknown b_0 by θ through the substitution

$$b_0 = \mathbb{F}h + \theta - \sum_{i=1}^{i_{\max}} b_i. \tag{E.15}$$

The evaluation of the first residual (9.7b) corresponding to $w_{i_{\max}} = g_0 = 1$ then yields

$$3\varepsilon Pe\left[\mathbb{F}\partial_t h + \frac{1}{2}h\partial_t\mathbb{F} + \partial_t\theta + \frac{3}{8}\left(\frac{\mathbb{F}q\partial_x h}{h} + \mathbb{F}\partial_x q + q\,\partial_x\mathbb{F}\right) + \frac{q\,\partial_x\theta}{h}\right] - \frac{(\mathbb{F}-B\theta)}{h} = 0. \tag{E.16}$$

Substituting now $\mathbb{F} = (1-B_{\rm w}\theta)/(1+B_{\rm w}h)$ and using the kinematic equivalence, $\partial_t h = -\partial_x q$, leads to the following equation for θ:

$$3\varepsilon Pe\partial_t\theta = \left\{\frac{(1-B_{\rm w}\theta)}{h(1+B_{\rm w}h)} - \frac{B\theta}{h} + 3\varepsilon Pe\left[\frac{(5+B_{\rm w}h)(1-B_{\rm w}\theta)}{8(1+B_{\rm w}h)^2}\partial_x q - \frac{3}{8}\frac{(1-B_{\rm w}\theta)}{(1+B_{\rm w}h)^2}\frac{q}{h}\partial_x h - \left(1-\frac{3}{8}\frac{B_{\rm w}h}{(1+B_{\rm w}h)}\right)\frac{q}{h}\partial_x\theta\right]\right\} \times \left(1-\frac{B_{\rm w}h}{2+2B_{\rm w}h}\right)^{-1}, \tag{E.17}$$

where the unknowns b_i do not appear. This equation is consistent at $\mathcal{O}(\varepsilon)$ and can be substituted for (9.17c) into (9.17a)–(9.17c) to get the first-order model for the heat flux condition; the model consists of three coupled evolution equations for h, q and θ.

E.6.2 Formulation at Second-Order

As in Sect. 9.3, we extend here the first-order formulation to take into account the second-order thermal effects. For this purpose, we need the explicit expressions for

the amplitudes b_j of the projection at first order. This is done by eliminating the coefficients of the polynomial obtained by substituting the temperature field (E.13) and the velocity field (9.2a) into the second-order energy equation (4.6b). Since the amplitudes a_i are known from (9.18a)–(9.18e) and b_0 from (E.15), and the b_i, $i \geq 1$, are at least of $\mathcal{O}(\varepsilon)$, the coefficients of the above polynomial provide the required expressions of the b_i as functions of h, θ, q and their derivatives:

$$b_1 = \frac{3}{2}\varepsilon Peh^2(h\partial_t\mathbb{F} + \partial_t\theta - \mathbb{F}\partial_x q) \tag{E.18a}$$

$$b_2 = -\frac{1}{2}\varepsilon Peh\big[h^2\partial_t\mathbb{F} - 3q(\mathbb{F}\partial_x h + h\partial_x\mathbb{F} + \partial_x\theta)\big] \tag{E.18b}$$

$$b_3 = -\frac{3}{8}\varepsilon Peh\big[-h\mathbb{F}\partial_x q + q(3\mathbb{F}\partial_x h + 3h\partial_x\mathbb{F} + \partial_x\theta)\big] \tag{E.18c}$$

$$b_4 = \frac{3}{40}\varepsilon Peh\big[-h\mathbb{F}\partial_x q + 3q(\mathbb{F}\partial_x h + h\partial_x\mathbb{F})\big] \tag{E.18d}$$

$$b_i = 0, \quad i \geq 5. \tag{E.18e}$$

In contrast to the ST case, here the amplitude b_1 is nonzero. Therefore, the temperature T at first order is a combination of five independent fields, namely, θ, b_1, b_2, b_3 and b_4. As a consequence, a consistent formulation of a model for the dynamics of the flow at second order would require 14 unknowns, instead of 13 for the ST case. However, rather than solving 14 equations, let us use the same approach as for the ST case and construct a set of orthogonal test functions for the temperature field from linear combinations of g_0, g_1, g_2, g_3 and g_4 such that $G_0 \equiv g_0$:

$$G_0 = 1 \tag{E.19a}$$

$$G_1 = 1 - 3\bar{y}^2 \tag{E.19b}$$

$$G_2 = 1 - 15\bar{y}^2 + 16\bar{y}^3 \tag{E.19c}$$

$$G_3 = 1 - 45\bar{y}^2 + 112\bar{y}^3 - 70\bar{y}^4 \tag{E.19d}$$

$$G_4 = 1 - 105\bar{y}^2 + 448\bar{y}^3 - 630\bar{y}^4 + 288\bar{y}^5. \tag{E.19e}$$

Therefore, the temperature field can be accurately described at $\mathcal{O}(\varepsilon)$ from

$$T = -\mathbb{F}y + (\mathbb{F}h + \theta - t_1 - t_2 - t_3 - t_4)G_0 + \frac{1}{2}\sum_{i=1}^{4}(-1)^i t_i G_i. \tag{E.20}$$

The set of test functions G_i must be completed at second order with 10 polynomials of degree up to 14. Nevertheless, since G_i'', $0 \leq i \leq 4$, are not linear combinations of G_i, $0 \leq i \leq 4$, the five first residuals do not form a closed set of equations for θ, t_1, t_2, t_3 and t_4. Yet, a basis for the set of polynomials of degree up to five satisfying the HF condition can be obtained by introducing only one polynomial orthogonal to

the first four G_i. This polynomial, G_5, is

$$G_5(\bar{y}) = 1 - \frac{70}{3}\bar{y} + 140\bar{y}^2 - 336\bar{y}^3 + 350\bar{y}^4 - 132\bar{y}^5. \tag{E.21}$$

The temperature field can now be written explicitly at second order as

$$\begin{aligned} T = &-\mathbb{F}y + (\mathbb{F}h + \theta - t_1 - t_2 - t_3 - t_4)G_0(\bar{y}) - \frac{1}{2}t_1 G_1(\bar{y}) \\ &+ \frac{1}{2}t_2 G_2(\bar{y}) - \frac{1}{2}t_3 G_3(\bar{y}) + \frac{1}{2}\left(t_4 - \sum_{i=6}^{9} t_i\right) G_4(\bar{y}) \\ &- 3t_5 G_5(\bar{y}) + \sum_{i=6}^{9} t_i \frac{G_i(\bar{y})}{G_i(1)}. \end{aligned} \tag{E.22}$$

The choice of this formulation ensures that the evaluation of $\int_0^h G_j''(\bar{y}) T\, dy$, $0 \leq j \leq 5$, does not require the definitions of G_j, $j \geq 6$. By applying next the Galerkin method to the energy equation we find that the first six residuals $\mathcal{R}_\theta(G_i)$, $0 \leq i \leq 5$, constitute a closed set. Since the amplitude t_5 is of $\mathcal{O}(\varepsilon^2)$, its space and time derivatives can be neglected at this order, so that an explicit formulation in terms of h, θ, t_1, t_2, t_3 and t_4 can be obtained, expressing the slaving of the former to the latter. We can then derive a set of five evolution equations for θ, t_1, t_2, t_3, t_4 that couple with the five other evolution equations (E.8a)–(E.8e) to provide the full second-order model, a system of 10 equations with 10 unknowns.

However, we will take a shortcut here based on considerations already developed in the ST case (see Sect. 9.4.3). In fact, the aim is once again to obtain a three-unknown regularized model for h, q and θ that remains asymptotically correct up to $\mathcal{O}(\varepsilon^2)$ with the long-wave theory. Yet, as temperature is coupled through its gradient in the momentum equation, the second-order terms in the energy equation do not enter the second-order gradient expansion. Further, recall that it is not possible to take into account the second-order corrections appearing in the averaged energy equation—which are induced by the deviations of the temperature and velocity profiles from the Nusselt flat film solution—if the temperature field is assumed to be slaved to the free surface temperature θ only. Hence, we restrict ourselves here to the second-order averaged energy equation obtained from the first residual, $\mathcal{R}_\theta(G_0)$ with $G_0 = 1$, as we did for the first order. The result written in terms of the Shkadov scaling is

$$\begin{aligned} &\frac{\mathbb{F} - B\theta}{h} - Pr\delta\left[\frac{1}{2}h\partial_t\mathbb{F} + \partial_t\theta + \frac{3}{8}q\left(\partial_x\mathbb{F} + \mathbb{F}\frac{\partial_x h}{h}\right)\right. \\ &\left. - \frac{5}{8}\mathbb{F}\partial_x q + \frac{q\partial_x\theta}{h}\right] + \eta\left[2\partial_x\mathbb{F}\partial_x h + \left(\mathbb{F} - \frac{1}{2}B\theta\right)\frac{(\partial_x h)^2}{h}\right. \\ &\left. + \frac{\partial_x h\partial_x\theta}{h} + \frac{1}{2}h\partial_{xx}\mathbb{F} + \mathbb{F}\partial_{xx}h + \partial_{xx}\theta\right] = 0, \end{aligned} \tag{E.23}$$

where the second bracketed expression contains the second-order thermal effects. Equation (E.23) should be coupled with the continuity and the momentum equations (9.43a), (9.43b). This three-equation system constitutes the *regularized model* for the HF case.

Appendix F
Numerical Schemes

F.1 Solving the Orr–Sommerfeld Equation by Continuation

Solving the Orr–Sommerfeld eigenvalue problem is not a straightforward task. Numerical schemes for its solution were proposed as early as 1964 [298] for the problem of a falling film with surfactants (the Orr–Sommerfeld problem for the purely hydrodynamic case was treated for the first time in [10]). The different schemes are based, for example, on the "shooting method" (see, e.g., [67] or [259]), "pseudo-spectral methods" (see, e.g., [44, 202]) or "finite differences." In the last two cases the aim is to discretize the (infinite-dimension) differential eigenvalue problem appropriately and thus convert it to a (finite-dimension) matrix eigenvalue problem, whereas, in the shooting method one looks for the parameter values for which the integration of the equation from one side of the domain (the wall) satisfies the boundary conditions at the other side (the free surface).

Here we present an alternative approach based on *continuation*, which demands a minimum of code writing due to a freely distributed software. The basic idea is the following: Suppose one trivial solution of the problem at hand is known and that this solution is not isolated in the parameter space but lies on a continuous branch of solutions, i.e., a continuous distribution of solutions as a function of a single parameter (a "codim 1 manifold"). One may then construct the whole branch of solutions in small steps, starting from the known trivial solution. An introduction to continuation methods can be found in the monograph by Allgower and Georg [8]. Based on the initial work by Keller [146], accurate continuation algorithms have been developed by Doedel et al. [80, 81] and implemented in the software package AUTO-07P, which can be downloaded from http://indy.cs.concordia.ca. The software is designed as a collection of subroutines that enables the solution of bifurcation problems for ordinary differential equations. It can be installed on most operating systems, including Windows and Linux. For details, we refer the reader to the documentation of the software. Here we provide the basic steps to using the software and how to implement it for the numerical solution of the Orr–Sommerfeld eigenvalue problem.

The user gives a name to the problem to be solved, say `xxx`, and defines it in the file `xxx.f`. The numerical constants of each run are specified in separate files

S. Kalliadasis et al., *Falling Liquid Films*, Applied Mathematical Sciences 176,
DOI 10.1007/978-1-84882-367-9, © Springer-Verlag London Limited 2012

`c.xxx.1`, `c.xxx.2` and so on. The computations are initiated by the command `@r`, by typing in a unix shell `@r xxx 1`, for example. The software then compiles the program using the routines defined in `xxx.f`, reads the numerical constants stored in `c.xxx` and the initial solution stored in the file `q.1` produced by a previous run.[1]

The results of the computation are stored using `@sv`. They can be plotted with the software PLAUT run by the command `@p`. Details can be found in the user manual, which contains numerous useful examples, i.e., a variety of dynamical systems, such as reaction-diffusion equations [79].

As an example, let us consider the search for the neutral stability curve of streamwise perturbations in terms of the wavenumber k versus angular frequency ω for an isothermal film falling down an inclined plate. We then need to solve numerically (3.22a) with boundary conditions (3.22c), (3.22g) and (3.22h), where η is given by (3.22f) and M is set to zero.

As the Orr–Sommerfeld system is linear, a constraint/normalization condition on the amplitude must be added. Here we choose the integral constraint

$$\int_0^1 \varphi \, dy = 1/3, \tag{F.1}$$

which is compatible with the normalization of φ_0 in (3.24). In practice, the search for the neutral stability conditions is facilitated by the long-wave nature of the instability. The onset of instability corresponds to a zero wavenumber k and the neutral stability curve emerges from the "trivial solution":

$$\varphi = y^2, \qquad k = 0, \qquad c = 1. \tag{F.2}$$

We therefore proceed in two steps.

Step 1: We start from the trivial solution (F.2) and follow the horizontal axis $\omega = k = 0$ until the critical value of the Reynolds number is detected as a bifurcation point.

Step 2: We restart the computation from $Re = Re_c$ and construct the neutral stability curve. The process is called `stab` and the three necessary files, `stab.f`, `c.stab.1` and `c.stab.2` are in the AUTO source code discussed later.

The first step is implemented with the following sequence of commands:

```
cp c.stab.1 c.stab
@r stab
@sv 1
```

During the computation, AUTO summarizes the results on the screen:

[1] The latest distribution AUTO-07P, released in 2007, has a user-friendly command line interface based on the "Python language," as well as a graphical user interface (GUI). Yet, AUTO-07P, like older versions of AUTO, can still be used effectively with the help of the standard Unix commands. Therefore, we leave to the reader the choice of using the Python and GUI interfaces or not and present only the standard Unix procedure to which most current users of AUTO are accustomed.

```
  BR    PT  TY  LAB    PAR(1)        L2-NORM       MAX U(1)
  MAX U(2)      MAX U(3)      MAX U(4)      PAR(2)        PAR(3)
   1     1  EP    1   1.00000E-01   2.42212E+00   1.00000E+00
0.00000E+00   2.00000E+00   0.00000E+00   0.00000E+00   1.00000E+00
   1    15  BP    2   1.19172E+01   2.42212E+00   1.00000E+00
0.00000E+00   2.00000E+00   0.00000E+00   0.00000E+00   1.00000E+00
   1   100  EP    3   9.69172E+01   2.42212E+00   1.00000E+00
0.00000E+00   2.00000E+00   0.00000E+00   0.00000E+00   1.00000E+00
```

The switch from the trivial solution to the neutral stability boundary is enabled by setting the constant `ISW` to -1 in `c.stab.2`. The results are stored in files `b.1`, `s.1` and `d.1`. The critical point is detected as a "branch point" (indicated by `BP` in the screen outputs) at $Re = 11.91722$, in agreement with the theoretically predicted value of the critical Reynolds number, $Re_c = 5/6\cot(4\pi/180)$. This point is labeled as 2 and gives the starting conditions for the second step. Notice that the detection of the (bifurcation) point 2 is enabled by setting the constant `ISP` to 2 in the constant file `c.stab.1`.

The second step is achieved with the following commands:

```
cp c.stab.2 c.stab
@r stab 1
@sv 2
```

The computation is stopped when Re reaches the value 70 (last row of the constant file `c.stab.2`). The results are then stored in files `b.2`, `s.2` and `d.2`, and can be visualized with the command `@p 2` using the software PLAUT which opens a Tektronix window. Next, typing the following commands in the PLAUT window

```
ax
1 8
```

select the Reynolds number and the frequency (first and eighth columns of the file `b.2`). Finally, the neutral stability curve is plotted and saved in a file `2.fig` using the commands:

```
bd0
sav
2.fig
```

To convert this file into a postscript one, we can use the command `@ps 2.fig`, which creates the file `2.fig.ps`. The result is displayed in Fig. F.1 for a particular set of parameters ($\beta = 4°$, $\nu = 2.3\,10^{-6}\mathrm{m}^2\,\mathrm{s}^{-1}$, $\sigma/\rho = 62.6 \times 10^{-6}\ \mathrm{m}^3\,\mathrm{s}^{-2}$) corresponding to an experiment by Liu et al. [170] and to Fig. 7.2. Notice that AUTO draws the neutral curve for $\omega < 0$. As the curve is symmetric around $\omega = k = 0$, its part for positive values of ω can be easily recovered through $\omega \to -\omega$, $k \to -k$.

F.1.1 AUTO *Source Code*

The files necessary for the above example on the use of the software AUTO can be downloaded from extras.springer.com (search for the book by its ISBN, you will

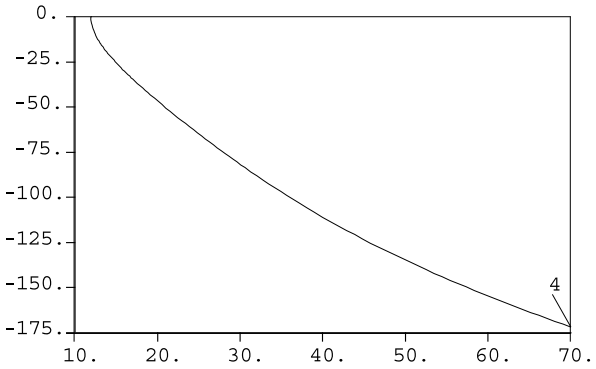

Fig. F.1 Neutral stability curve as plotted by the software `Plaut` in the (Re, ω)-plane. Notice that the second run of the computation, stored in `b.2`, `s.2` and `d.2` follows the first run stored in `b.1`, `s.1` and `d.1`. File `s.1` already contains three solutions labeled 1, 2 and 3, so that the fourth one, stored in `s.1`, is labeled 4 and corresponds to the solution at the end of the computation

then be asked to enter a password, which is given on the copyright page of this print book). They are written in the "old" Fortran style and are therefore compatible with the current release AUTO-07P (and of course with older versions). File `stab.f` contains the Orr–Sommerfeld equation (3.22a) in the format of an autonomous complex dynamical system of dimension 5 (subroutine `FUNC`), the boundary conditions (3.22c), (3.22g) and (3.22h) (subroutine `BCND`), the integral condition (F.1), and the trivial solution (F.2) (subroutine `STPNT`).

There are three "active" continuation parameters in the problem the way it is formulated: Re, k and c, corresponding to the parameters `PAR(1)`, `PAR(2)` and `PAR(3)`, respectively (subroutine `FUNC`). There are two more active parameters that are not changed in the runs, Ct and Γ, whose values are set once and for all in `STPNT`. Since the frequency ω is not a true continuation parameter in the chosen formulation based on the wavenumber k but a combination of the two parameters k and c, the dimensional frequency ω is denoted as `PAR(6)` in a separate subroutine `PVLS` that defines specific "solution measures" (non-free parameters). Of course, the value of the dimensionless frequency can be obtained as a combination of k and c, but it is useful to store the dimensional frequency in a user-defined parameter (`UZR`) in AUTO such that it explicitly appears in the output AUTO files and there is no need for additional post-processing.

F.2 Computational Search for Traveling Wave Solutions and Their Bifurcations

To investigate the behavior of the solutions of the BE, we employ bifurcation analysis using numerical *continuation* techniques [79]. Continuation is a very effective method for determining branches of stationary solutions and their bifurcations, fol-

lowing them in the parameter space using the Newton iteration method. In the context of thin films, continuation was applied in studies of traveling and solitary waves of falling films [52, 227, 228, 239], sliding drops on slightly inclined plates [268, 269], and transverse instabilities of sliding liquid ridges [266].

We seek traveling wave solutions, i.e., stationary solutions of (5.13) in a frame of reference moving downstream at constant speed c. We present the computational methodology for the BE in terms of the Nusselt scaling to illustrate how some of the figures in Chap. 5, prior to the introduction of the Shkadov scaling, are obtained. Introducing $h(x,t) = h(\xi)$ with $\xi = x - ct$, the BE (5.13), truncated at first order for simplicity and dropping ε, can be integrated once to yield

$$-ch + \frac{h^3}{3} - q_0 + \frac{2}{5}Reh^6h' + We\frac{h^3}{3}h''' - Ct\frac{h^3}{3}h' + \frac{h^2}{2}\frac{BMh'}{(1+Bh)^2} = 0, \quad \text{(F.3)}$$

where the primes denote differentiation with respect to ξ; q_0 is the integration constant and represents the flow rate in the moving frame of reference (see (5.51)). Its value is negative because the phase speed c of surface waves is generally higher than the mean velocity of the film. Assuming that no dry spots are possible, i.e., $h \neq 0$, (F.3) can be divided by $-We\,h^3/3$ to get

$$h''' = F[h,h'] = \frac{1}{We}\left[\frac{3}{h^3}(q_0 + ch) - 1 - \frac{6}{5}Reh^3h' + Cth' - \frac{3}{2}\frac{BMh'}{h(1+Bh)^2}\right]. \quad \text{(F.4)}$$

The differential equation (F.4) is recast into a *dynamical system*, as follows:

$$\begin{cases} U_1' = U_2 \\ U_2' = U_3 \\ U_3' = F[U_1, U_2], \end{cases} \quad \text{(F.5)}$$

where $U_1 = h$, $U_2 = h'$ and $U_3 = h''$. The dimension of the dynamical system ($= 3$) is fixed by the third-order surface tension term, which makes the system (F.5) applicable to the majority of the equations for the film thickness discussed in this monograph.

To determine iteratively the periodic solutions of the dynamical system (F.5), we use the continuation and bifurcation tools for ordinary differential equations in the software AUTO-07P. During the computations the periodicity of the solution is enforced, the "phase" of the wave is fixed by $U_1|_{\xi=0} = 1$ (which fixes the origin) and the total volume $\int_0^\lambda U_1\,d\xi = \langle h \rangle_\xi$—with $\lambda = 2\pi/k$—is controlled as specified by the flow condition, open or closed (see Sect. 5.3.1; both boundary conditions have been treated even though for the specific example given in the source code the closed-flow condition is enforced). This amounts to one integral and four boundary conditions, hence the continuation requires three free parameters [146]. By specifying the set of viscous-gravity parameters $\{Re, \Gamma, Ma, Bi, Ct\}$, the remaining free parameters are $\{k, c, q_0\}$. The continuation is started from the neutral mode at criticality corresponding to the *Hopf bifurcation* point with k_c from (5.18a) and

c from (5.16). The starting value of q_0 is fixed by the Nusselt flat film solution $h(\xi) = 1$ such that from (F.3), $q_0 = -2/3$.

Notice that we have avoided specifying the set of Nusselt parameters $\{Re, We, M, B, Ct\}$ (see, e.g., Appendix D.1 and Sect. 4.10). Indeed, the advantage of working with the viscous-gravity parameters is that all these parameters, apart from Re, are independent on the flow rate, which is usually the principal control parameter in experiments.

We now give the necessary steps to compute the results in Figs. 5.2, 5.4 and 5.5, namely how to follow a branch of stationary solutions from the *Hopf bifurcation* point, how to detect and follow a *period-doubling bifurcation* and, finally, how to trace the locus of *saddle-node bifurcation* points in the parameter space.

F.2.1 Hopf Bifurcation

We compute here the γ_2-family of traveling wave solutions of (F.3) using the equation file `be.f` and the constants files `c.be` that define the different constants. The command is

```
@r be
```

Once this is executed, one can visualize the results by launching the PLAUT program with the command

```
@p
```

In the PLAUT environment, entering successively the commands

```
ax
1 3
d1bd0
```

gives the γ_2 branch as plotted in Fig. 5.2a for $h_{\max}$ versus k. Now, entering successively

```
2d
a
```

gives solutions for different values of k as specified in the constants file `c.be`. The labels 2–5 correspond to the wave profiles 1–4 plotted in Fig. 5.2b. Exiting the PLAUT environment using the "quit" command, one can save the γ_2-family with the command

```
@sv g2
```

F.2.2 Period-Doubling Bifurcation

Let us now compute the γ_2-family of solutions for the first harmonic. To do so one has to set $f = 2$, the "harmonic parameter" ($\equiv n$, the number of waves in the

wavetrain required to compute the period-doubling bifurcation—see Sect. 5.3.2) in the solution subroutine STPNT() of the file `be.f`. Once changed and saved, the file must be run with another constant file, `c.be.HP2`, where the detection of the bifurcation point is enabled (ISP = 2), the number of mesh points is doubled (NTST = 100), the tolerance parameters (EP*) are slightly decreased and the initial continuation stepsize is adjusted (DS = −1.e−06). The commands then to run and save are

```
@r be HP2
@sv be
```

AUTO-07P finds several bifurcation points (BP), the first one of which corresponds to the period-doubling bifurcation point for the γ_1-family of traveling waves. We shall then compute the corresponding branch using the third constants file, `c.be.PD`, where the label of the starting bifurcation point is specified (IRS = 2), the branch switching is enabled (ISW = −1) and the direction of the continuation is changed (by changing the sign of DS). The commands then to run and save are

```
@r be PD
@sv g1
```

One can finally append the two families of solutions and plot them as follows

```
@ap g1 g12
@ap g2 g12
@p g12
```

In the PLAUT environment, entering as before the commands

```
ax
1 3
d0bd0
```

shows the two families of solution for $h_{\max}$ versus k, while entering

```
ax
1 7
d0bd0
```

shows the two families of solution for c versus k, exactly as presented in Fig. 5.2a. As an exercise, one can try to compute other bifurcating families by changing the value of the BP-starting solution in the constants file `c.be.PD`, i.e., IRS = 3–6, then following the same procedure as above to run, save, append and plot. Once finished and before going to the next section, delete the bifurcation, solution and diagnostic files, respectively `b.be`, `s.be` and `d.be`, with the following command,

```
@dl be
```

and set back to $f = 1$ the harmonic parameter in `be.f`.

F.2.3 Locus of Saddle-Node Bifurcation Points

The different branches of solutions reported in Fig. 5.4 can be reproduced by tuning the Kapitza number to $\Gamma = 2950$ in the equation file be.f and varying the value of the Reynolds number. Let us trace here the branch for $Re = 3$:

```
@r be
@sv be
```

Because the detection of fold is enabled (ILP = 1) in the file `c.be`, a turning point (see the asterisk in Fig. 5.4) is found (LP) and recorded with the label 6. We shall then track the locus of this turning point in the parameter space. The constants file `c.be.TP0`—with the turning point as initial solution (IRS = 6), the Reynolds number as an additional continuation parameter (PAR(3)), the continuation of fold enabled (ISW = 2) and the tolerance parameters (EP*) decreased—is first used to generate starting data

```
@r be TP0
@ap be
```

The fold continuation can then be performed using the constants file `c.be.TP` starting with the last solution (IRS = 11), and where the iteration parameters are increased (ITMX = 10, ITNW = 8) and the initial continuation stepsize is adjusted (DS = 0.1):

```
@r be TP
@ap be
```

Launching the PLAUT environment with `@p` and typing the commands

```
ax
7 1
d0bd0
```

shows the blow up boundary as plotted in Fig. 5.5 (dashed line).

F.2.4 AUTO *Source Code*

The Fortran files necessary for the above example on the use of the software AUTO-07P can be downloaded from extras.springer.com (search for the book by its ISBN, you will then be asked to enter a password, which is given on the copyright page of this print book). These are: `be.f` that contains subroutines `FUNC`, `STPNT`, `BCND`, `ICND` and all the constants files.

F.3 Time-Dependent Computations Using Finite Differences

We briefly present here the key points of the algorithm implemented to simulate the spatio-temporal evolution of the film based on models of reduced dimensionality,

i.e., one evolution equation for h, e.g., the BE (5.12), two coupled evolution equations for h, q, e.g., the Kapitza–Shkadov model (6.13a), (6.13b) and the regularized model (6.1), (6.92), or more than two as, e.g., the three-equation model formulated in [226]. The reader interested in more details of finite difference schemes can refer to one of the many available textbooks, e.g., [220].

In all cases, the equations to be solved can be recast in the form

$$\partial_t \mathbf{H} = \boldsymbol{\mathcal{L}}(\mathbf{H}) + \boldsymbol{\mathcal{N}}(\mathbf{H}), \tag{F.6a}$$

where $\mathbf{H}$ denotes the set of unknowns. Therefore, in the case of the Kapitza–Shkadov model or the more refined two-equation models, $\mathbf{H} = (h, q)$. $\boldsymbol{\mathcal{L}}$ is a linear matrix-differential operator and $\boldsymbol{\mathcal{N}}$ is a nonlinear functional of $\mathbf{H}$ and its spatial derivatives. The spatial evolution of the film is then determined by solving system (F.6a) in a semi-infinite domain with initial conditions

$$\mathbf{H}(x, 0) = \mathbf{H}_0(x) \tag{F.6b}$$

and boundary conditions

$$\mathbf{H}(0, t) = \mathbf{H}_f(t), \qquad \mathbf{H}(\infty, t) = \mathbf{H}_0(\infty) = \text{const.} \tag{F.6c}$$

appropriate for a semi-infinite domain, where $\mathbf{H}_f$ is a function of time corresponding to the forcing at the inlet. Notice that for a semi-infinite domain the boundary condition at infinity will not affect the spatial evolution, provided that it is compatible with the initial condition, more specifically that the limit of the initial condition at infinity coincides with the boundary condition there, as is indeed the case with (F.6a)–(F.6c).

Because boundary conditions (F.6c) are not periodic, a spectral method for the numerical integration of (F.6a)–(F.6c) cannot be used. Instead, a finite-difference scheme is employed.

The computational domain of size L is discretized into a regular grid of N points or "nodes," $x_j = j\Delta x$; $j = 1, 2, \ldots, N$, $\Delta x = L/N$. The discretized variables at the node (x_j, t_n) are denoted by $\mathbf{H}_j^{(n)} = (h_j^{(n)} \; q_j^{(n)}, \ldots)$. Notice that the necessary limitation in size of the actual semi-infinite domain demands the introduction of additional boundary conditions at the downstream limit $x = L$ that do not generate parasitic reflections upstream. We shall return to this point below.

We choose the Crank–Nicholson scheme,

$$\mathbf{H}_j^{(n+1)} - \mathbf{H}_j^{(n)} = \frac{\Delta t}{2}\left(\boldsymbol{\mathcal{L}}\left(\mathbf{H}_j^{(n+1)}\right) + \boldsymbol{\mathcal{N}}\left(\mathbf{H}_j^{(n+1)}\right) + \boldsymbol{\mathcal{L}}\left(\mathbf{H}_j^{(n)}\right) + \boldsymbol{\mathcal{N}}\left(\mathbf{H}_j^{(n)}\right)\right), \tag{F.7}$$

where $\Delta t = t_{n+1} - t_n$ is the time step. As the solution $\mathbf{H}_j^{(n)}$ is known at time step n, the inversion of (F.7) gives $\mathbf{H}_j^{(n+1)}$. This can be achieved using Newton's method. However, it might not always be easy to implement due to the nature of the nonlinearities $\boldsymbol{\mathcal{N}}(\mathbf{H}_j^{(n+1)})$ and the dimensionality of the equations to be solved. A quasi-

linearization can be employed instead which gives

$$\mathbf{H}_j^{(n+1)} - \mathbf{H}_j^{(n)} = \frac{\Delta t}{2}\big[\mathcal{L}\big(\mathbf{H}_j^{(n+1)}\big) + \mathcal{L}\big(\mathbf{H}_j^{(n)}\big) + 2\mathcal{N}\big(\mathbf{H}_j^{(n)}\big) + \mathcal{N}'\big(\mathbf{H}_j^{(n)}\big)\big(\mathbf{H}_j^{(n+1)} - \mathbf{H}_j^{(n)}\big)\big]. \tag{F.8}$$

This scheme substantially simplifies the numerical analysis, though in general the time steps must be smaller than those required for the Newton method. The scheme (F.8) is "consistent" (the solution of the numerical scheme converges to the solution of the partial differential equation (F.6a) as Δt goes to zero) and of "second-order precision" in time (the error associated with the time integration is of $\mathcal{O}(\Delta t^2)$)). Indeed, a Taylor expansion at the node $(x_j,\ t_{n+1/2} = \frac{1}{2}(t_{n+1} + t_n))$ yields

$$\begin{aligned}&\frac{\Delta t}{2}\big[\mathcal{L}\big(\mathbf{H}_j^{(n+1)}\big) + \mathcal{L}\big(\mathbf{H}_j^{(n)}\big) + 2\mathcal{N}\big(\mathbf{H}_j^{(n)}\big)\\ &+ \mathcal{N}'\big(\mathbf{H}_j^{(n)}\big)\big(\mathbf{H}_j^{(n+1)} - \mathbf{H}_j^{(n)}\big)\big] - \big(\mathbf{H}_j^{(n+1)} - \mathbf{H}_j^{(n)}\big)\\ &- \Delta t\big[\mathcal{L}\big(\mathbf{H}_j^{(n+1/2)}\big) + \mathcal{N}\big(\mathbf{H}_j^{(n+1/2)}\big) - (\partial_t \mathbf{H})_j^{(n+1/2)}\big] = \mathcal{O}\big(\Delta t^2\big).\end{aligned} \tag{F.9}$$

The spatial derivatives are approximated by central difference schemes whose precision is again of second-order:

$$(\partial_x \mathbf{H})_j = \frac{1}{2\Delta x}(\mathbf{H}_{j+1} - \mathbf{H}_{j-1}) + \mathcal{O}\big(\Delta x^2\big) \tag{F.10a}$$

$$(\partial_{x^2} \mathbf{H})_j = \frac{1}{\Delta x^2}(\mathbf{H}_{j+1} - 2\mathbf{H}_j + \mathbf{H}_{j-1}) + \mathcal{O}\big(\Delta x^2\big) \tag{F.10b}$$

$$(\partial_{x^3} \mathbf{H})_j = \frac{1}{2\Delta x^3}(\mathbf{H}_{j+2} - 2\mathbf{H}_{j+1} + 2\mathbf{H}_{j-1} - \mathbf{H}_{j-2}) + \mathcal{O}\big(\Delta x^2\big). \tag{F.10c}$$

The quasi-linearized Crank–Nicholson scheme is then formally written as

$$\mathbf{H}^{n+1} = \mathbf{L}^n \mathbf{H}^n, \tag{F.11}$$

where $\mathbf{L}^n$ corresponds to the linear operator $\mathbf{I} - (\Delta t/2)[\mathcal{L} + \mathcal{N}'(\mathbf{H}_j^{(n)})]$ and where $\mathbf{H}^n$ and $\mathbf{H}^{n+1}$ are the unknowns. Thanks to the choice of central differences, $\mathbf{L}^n$ is a diagonally dominant matrix[2] with a nonzero determinant, which then ensures the existence of the inverse of this matrix, which in turn ensures the existence and uniqueness at each time step of the solution to (F.8). $\mathbf{L}^n$ is a "banded matrix," i.e., a sparse matrix whose nonzero entries are confined to a diagonal band whose bandwidth depends on the order of the spatial derivatives. In practice, the numerical

[2] A matrix $\mathbf{A} = (a_{ij})$ is said to be "diagonally dominant" if in every row of the matrix the magnitude of the diagonal entry in that row is larger than the sum of the magnitudes of all the other (nondiagonal) entries in that row, i.e., $\forall i\ \ |a_{ii}| \geq \sum_{j \neq i} |a_{ij}|$. For the properties of diagonally dominant matrices see for example [104].

inversion of (F.11) at each time step can be achieved effectively by direct methods like "LU decomposition," for which, in the case of a banded matrix, the number of required operations is proportional to N and to the bandwidth.

Applying our equations at the first node $j = 1$ demands the values of the film height at two fictitious nodes, $x_0 = 0$ and $x_{-1} = -\Delta x$, upstream of the left end of the computational domain: The finite difference approximation for the third derivative in (F.10c) (the highest derivative for h) involves the nodes $j - 1$ and $j - 2$. For the flow rate, the highest derivative of our equation is a second one, which from (F.10b) involves the node $j - 1$ and hence we need to know the flow rate at the fictitious node $x_0 = 0$. We then impose

$$h_{-1}^{(n)} = h_0^{(n)} = h_f(t_n), \tag{F.12a}$$

$$q_0^{(n)} = q_f(t_n), \tag{F.12b}$$

so that nodes h_1 and h_0 are excited simultaneously. Hence, we have a total of three boundary conditions at the inlet.

The treatment of the outlet boundary condition is more subtle. If we had to solve a system of hyperbolic equations (where information travels from left to right) we would not need an outlet boundary condition. But the presence of surface tension makes our equations parabolic and we need boundary conditions at two points. At the same time, we wish to avoid fictitious nodes outside the right end of the computational domain, as we do not have any information about the dynamics there (we wish to keep the "flow" of information from the left to the right). Hence, if $j = N$ is the last node, we could utilize backward finite differences and use only the information at nodes $j = N - 1, N - 2, N - 3, \ldots$. Any boundary condition which would require more than three nodes would introduce more diagonals in the matrix to be inverted (and hence the bandwidth of the matrix to be inverted would be larger) and would therefore increase the number of operations needed at each time step, which in turn might generate spurious reflections of the waves at the endpoint of the domain. A simple and effective way then to deal with the right end of the domain is to impose there a set of linear hyperbolic equations, e.g.,

$$\partial_t \mathbf{H} = v_f \partial_x \mathbf{H}, \tag{F.13}$$

with $v_f > 0$, corresponding to two boundary conditions for h and q at the outlet, which together with (F.12a), (F.12b) means a total of five boundary conditions for our equations (we have a third spatial derivative for h and a second one for q). The wave equation (F.13) is an ad hoc outlet "soft" boundary condition that simulates the wavy behavior of the film, with v_f being a relaxation parameter that is empirically tuned to limit wave reflections. It has a first-order spatial derivative whose discretization in (F.14) requires only the $j = N, N - 1, N - 2$ nodes and hence it does not increase the bandwidth of the matrix to be inverted.

Equation (F.13) ensures that the information is transported downstream and limits wave reflection. It effectively "hyperbolizes" our original system of equations at the end of the domain, ensuring that the information travels from the left to the

right. The drawback of using (F.13) is the generation of some numerical errors at the outlet. However, thanks to the convective nature of the primary and secondary instabilities of falling film flows (Sect. 7.1.2), these numerical disturbances cannot invade the numerical domain and therefore affect only a few nodes at an outlet boundary layer. At the last node, the spatial derivative is discretized using an upstream second-order accurate scheme (for consistency with (F.10a)–(F.10c)):

$$(\partial_x \mathbf{H})_N = \frac{1}{2\Delta x}(\mathbf{H}_{N-2} - 4\mathbf{H}_{N-1} + 3\mathbf{H}_N) + \mathcal{O}(\Delta x^2). \tag{F.14}$$

Notice that according to the "Lax–Richtmyer equivalence theorem", for a consistent difference scheme for a linear system of equations, there is equivalence between convergence and stability [220]. For linear systems a stability analysis is therefore sufficient to determine the convergence properties of the scheme. However, in our case, a stability analysis is rather difficult, if not impossible.

As far as the Crank–Nicholson scheme is concerned, Richtmyer and Morton [220] give the following result on its stability. Consider the one-dimensional problem

$$\partial_t u + a(x)\partial_x u = 0, \tag{F.15a}$$

$$u(0,t) = 0, \qquad u(x,0) = F(x), \tag{F.15b}$$

where $a(x)$ is a positive function. The Crank–Nicholson scheme for (F.15a), (F.15b) is stable and convergent if

$$4K_L \Delta t < 1 \tag{F.16}$$

is satisfied, where K_L is a Lipschitz constant of the function $a(x)$ such that $\forall x, x',\ |a(x) - a(x')| \leq K_L|x - x'|$. Since $a(x) = -\partial_t u/\partial_x u \sim -\Delta x/\Delta t$, this result suggests that we impose a condition similar to the "Courant–Friedrichs–Lewy (CFL) condition" [5, 59]. Stated in simple terms, the CFL condition demands that the speed at which the information propagates in the numerical scheme ($\sim \Delta x/\Delta t$) must be larger than the speed of propagation of the physical phenomenon ($\sim K_L$) that is simulated, which in turn implies a constraint on the time step, $\Delta t < K'\Delta x$, where K' is a constant.

Assume for simplicity now that we are dealing with a surface equation so that $\mathbf{H}$ is a scalar, H. For our quasi-linearized Crank–Nicholson scheme (F.11) then let

$$a_j^{(n)} = \Delta t \frac{|(\partial_x H)_j^{(n)}|}{|H_j^{(n)} - H_j^{(n-1)}|}$$

be a measure of the local propagation speed of the physical phenomenon. At each time step, the maximum speed $\max_j |a_j^{(n)}|$ is computed and the time step is adjusted to verify the CFL-like condition,

$$\Delta t < \frac{C\Delta x}{\max_j |a_j^{(n)}|}, \tag{F.17}$$

where C a constant larger than unity.

F.4 Spectral Representation and Aliasing

The time-dependent simulations and the stability analysis of the traveling wave solutions shown in Sects. 8.3 and 8.4 made extensive use of the representation of periodic solutions in Fourier space. For this purpose, an efficient algorithm, the fast Fourier transform (FFT), was utilized. It enables us to go back and forth from the physical space to the Fourier space at a low computational cost. We sketch below the representation of the solutions in the Fourier space and its main limitation related to the *aliasing phenomenon* to be defined soon. Interested readers can consult the book by Press et al. as an introduction to the use of spectral and pseudo-spectral methods [213].

Real periodic solutions can be represented by Fourier series of the form

$$X(\xi) = \hat{\Xi}_0 + \sum_{j=1}^{\infty} \hat{\Xi}_{2j-1} \cos(jk_x\xi) + \hat{\Xi}_{2j} \sin(jk_x\xi), \tag{F.18}$$

where k_x again denotes the streamwise wavenumber. Equation (F.18) can be rewritten in the equivalent form

$$X(\xi) = \frac{1}{L_x} \sum_{j=-\infty}^{\infty} \hat{X}_j \exp(-ijk_x\xi). \tag{F.19}$$

Complex Fourier coefficients $\hat{X}_j$ are defined by means of a continuous Fourier transform,

$$\hat{X}_j = \int_0^{L_x} X(\xi) \exp(ijk_x\xi)\, d\xi, \tag{F.20}$$

where $i = \sqrt{-1}$ denotes the imaginary unit. As X is a real function, the complex coefficients $\hat{X}_j$ satisfy $\hat{X}^{\star}_{-j} = \hat{X}_j = L_x(\hat{\Xi}_{2j-1} - i\hat{\Xi}_{2j})$, where the star denotes complex conjugation.

An approximation to X can be obtained by truncating the Fourier series (F.18) at N coefficients,

$$X \simeq \hat{\Xi}_0 + \hat{\Xi}_{N-1} \cos\big[(N/2)k_x\xi\big] + \sum_{j=1}^{N/2-1} \hat{\Xi}_{2j-1} \cos(jk_x\xi) + \hat{\Xi}_{2k} \sin(jk_x\xi), \tag{F.21}$$

where N is an even integer; this is equivalent to canceling the coefficients of all frequencies that are not in the interval $[-f_c,\ f_c]$ with $f_c = N/(2L_x)$, the "Nyquist cut-off frequency." This truncation is acceptable only when the neglected part of the spectrum has a sufficiently small norm, which can be easily controlled by looking at the coefficient $\hat{\Xi}_{N-1}$ of the cut-off frequency.

Whenever the condition $\hat{\Xi}_{N-1} \ll 1$ is satisfied, one can replace the continuous Fourier transform with a discrete one,

$$\hat{X}_j^N = \sum_{p=0}^{N-1} X(\xi_p) \exp(ijk_x\xi_p), \tag{F.22}$$

where the nodes $\xi_p = pL_x/N$ are evenly distributed over a period. We note that $\hat{X}_{N/2}^N = \hat{X}_{-N/2}^N$ are real coefficients. The exponent N here is reserved for the discrete Fourier transform and is introduced to distinguish discrete and continuous Fourier transforms. For periodic signals the two transforms converge to the same result after rescaling:

$$\lim_{N\to\infty} \frac{L_x \hat{X}_j^N}{N} \to \hat{X}_j. \tag{F.23}$$

The bad news about the discrete Fourier transform is that it "confuses" harmonics:

$$\begin{aligned}
\hat{X}_j^N &= \sum_{p=0}^{N-1} \frac{1}{L_x} \sum_{q=-\infty}^{\infty} \hat{X}_q \exp(-iqk_x\xi_p) \exp(ijk_x\xi_p) \\
&= \frac{1}{L_x} \sum_{q=-\infty}^{\infty} \hat{X}_q \sum_{p=0}^{N-1} \exp\big[i2\pi p(j-q)/N\big] \\
&= \frac{N}{L_x} \sum_{q=-\infty}^{\infty} \hat{X}_{j+qN}.
\end{aligned} \tag{F.24}$$

As a result, the part of the power spectrum density that does not lie in the frequency range $[-f_c,\ f_c]$ is moved into that range. This phenomenon is called *aliasing*. Any frequency coefficient outside this range is aliased, that is falsely displaced. Aliasing errors can be limited by ensuring that the norm $\|\hat{X}_{N/2}^N\|$ corresponding to the Nyquist frequency is sufficiently small.

In any algorithm based on pseudo-spectral methods, derivatives are computed in the Fourier space, as a differentiation there corresponds to a simple product,

$$\hat{X'}_j^N = -ijk_x \hat{X}_j^N, \tag{F.25}$$

whereas nonlinearities are computed in the physical space as they correspond to convolutions in the Fourier space. Unfortunately, convolutions in the Fourier space widen the spectrum.

Consider an order σ_{NL} nonlinearity $X^{\sigma_{\mathrm{NL}}}$ with σ_{NL} an integer. We have

$$\begin{aligned}
\big[X(\xi_p)\big]^{\sigma_{\mathrm{NL}}} &= \left(\frac{1}{N} \sum_{j=1-N/2}^{N/2} \hat{X}_j^N \exp^{-ijk_x\xi_p} \right)^{\sigma_{\mathrm{NL}}} \\
&= \frac{1}{N^{\sigma_{\mathrm{NL}}}} \sum_{j=\sigma_{\mathrm{NL}}-\sigma_{\mathrm{NL}}N/2}^{\sigma_{\mathrm{NL}}N/2} \sum_{D_j^N} \left(\prod_{l=1}^{\sigma_{\mathrm{NL}}} \hat{X}_{j_l}^N \right) \exp(-ijk_x\xi_p),
\end{aligned} \tag{F.26}$$

where D_j^N is the set defined by

$$D_j^N = \left\{ (j_1, j_2, \ldots, j_{\sigma_{\mathrm{NL}}}) \Big/ \sum_{l=1}^{\sigma_{\mathrm{NL}}} j_l = j;\ -N/2+1 \le j_l \le N/2 \right\}. \tag{F.27}$$

Let us assume that σ_{NL} is even (only the details of the proof are modified in the odd case) and let us "aliase" the frequencies outside the interval $[-f_{\mathrm{c}},\ f_{\mathrm{c}}]$, first by use of the periodicity $\exp(-ijk_x\xi_p) = \exp[-ip(j+N)k_xL_x/N] = \exp[-i(j+N)k_x\xi_p]$,

$$\begin{aligned}
\left[X(\xi_p)\right]^{\sigma_{\mathrm{NL}}} = \frac{1}{N_{\mathrm{NL}}^{\sigma}} \Bigg[& \sum_{j=\sigma_{\mathrm{NL}}-\sigma_{\mathrm{NL}}N/2}^{-(\sigma_{\mathrm{NL}}-1)N/2} \sum_{D_j^N} \left(\prod_{l=1}^{\sigma_{\mathrm{NL}}} \hat{X}_{j_l}^N \right) e^{-i(j+\sigma_{\mathrm{NL}}N/2)k_x\xi_p} \\
& + \sum_{j=-(\sigma_{\mathrm{NL}}-1)N/2+1}^{-(\sigma_{\mathrm{NL}}-2)N/2} \sum_{D_j^N} \left(\prod_{l=1}^{\sigma_{\mathrm{NL}}} \hat{X}_{j_l}^N \right) e^{-i(j+(\sigma_{\mathrm{NL}}-2)N/2)k_x\xi_p} \\
& + \cdots + \sum_{j=(\sigma_{\mathrm{NL}}-1)N/2+1}^{\sigma_{\mathrm{NL}}N/2} \sum_{D_j^N} \left(\prod_{l=1}^{\sigma_{\mathrm{NL}}} \hat{X}_{j_l}^N \right) e^{-i(j-\sigma_{\mathrm{NL}}N/2)k_x\xi_p} \Bigg],
\end{aligned} \tag{F.28}$$

and then through a change of variables,

$$\begin{aligned}
\left[X(\xi_p)\right]^{\sigma_{\mathrm{NL}}} = \frac{1}{N_{\mathrm{NL}}^{\sigma}} \Bigg[& \sum_{j=\sigma_{\mathrm{NL}}}^{N/2} \sum_{D^N_{j-\sigma_{\mathrm{NL}}N/2}} \left(\prod_{l=1}^{\sigma_{\mathrm{NL}}} \hat{X}_{j_l}^N \right) e^{-ijk_x\xi_p} \\
& + \sum_{j=-N/2+1}^{0} \sum_{D^N_{j-(\sigma_{\mathrm{NL}}-2)N/2}} \left(\prod_{l=1}^{\sigma_{\mathrm{NL}}} \hat{X}_{j_l}^N \right) e^{-ijk_x\xi_p} \\
& + \cdots + \sum_{j=-N/2+1}^{N/2} \sum_{D_j^N} \left(\prod_{l=1}^{\sigma_{\mathrm{NL}}} \hat{X}_{j_l}^N \right) e^{-ijk_x\xi_p} \\
& + \cdots + \sum_{j=-N/2+1}^{0} \sum_{D^N_{j+\sigma_{\mathrm{NL}}N/2}} \left(\prod_{l=1}^{\sigma_{\mathrm{NL}}} \hat{X}_{j_l}^N \right) e^{-ijk_x\xi_p} \Bigg].
\end{aligned} \tag{F.29}$$

In (F.29) the result of the convolution of the frequencies that lie inside the interval $[-f_{\mathrm{c}},\ f_{\mathrm{c}}]$ is the sum $\sum_{j=-N/2+1}^{N/2} \sum_{D_j^N} (\prod_{l=1}^{\sigma_{\mathrm{NL}}} \hat{X}_{j_l}^N) e^{-ijk_x\xi_p}$. All other terms in (F.29) arise from the aliasing of frequencies outside this interval.

The Fourier coefficients of X^{σ}_{NL} for $j<0$ are thus given by

$$\frac{1}{N}\big(\hat{X}^{\sigma}_{\mathrm{NL}}\big)^N_j=\frac{1}{N^{\sigma}_{\mathrm{NL}}}\Bigg[\sum_{m\in[0,\ (\sigma_{\mathrm{NL}}-2)/4[\cap\mathbb{N}}\ \sum_{D^N_{j-(\sigma_{\mathrm{NL}}-2-4m)N/2}}\left(\prod_{l=1}^{\sigma_{\mathrm{NL}}}\hat{X}^N_{j_l}\right)$$
$$+\sum_{m\in[0,\ \sigma_{\mathrm{NL}}/4[\cap\mathbb{N}}\ \sum_{D^N_{j+(\sigma_{\mathrm{NL}}-4m)N/2}}\left(\prod_{l=1}^{\sigma_{\mathrm{NL}}}\hat{X}^N_{j_l}\right)+\sum_{D^N_j}\left(\prod_{l=1}^{\sigma_{\mathrm{NL}}}\hat{X}^N_{j_l}\right)\Bigg].\quad\text{(F.30)}$$

Similar expressions are obtained for $j>0$.

One solution to limit aliasing is to truncate the Fourier spectrum of the function X. Let M be an integer that divides N and $f_{\mathrm{trunc}}=M/(2L_x)=Mf_{\mathrm{c}}/N$, a truncation frequency. If the coefficients of all frequencies outside the range $[f_{\mathrm{trunc}},\ f_{\mathrm{trunc}}]$ are set to zero, expression (F.30) is modified by the substitution of the sets D^M_j for D^N_j. It is therefore sufficient to chose M so that the set

$$\left(\bigcup_{m\in[0,\ (\sigma_{\mathrm{NL}}-2)/4[\cap\mathbb{N}}D^M_{j-(\sigma_{\mathrm{NL}}-2-4m)N/2}\right)\cup\left(\bigcup_{m\in[0,\ \sigma_{\mathrm{NL}}/4[\cap\mathbb{N}}D^M_{j+(\sigma_{\mathrm{NL}}-4m)N/2}\right)$$

is empty. A sufficient condition is that the sets $D^M_{j\pm N}$ be empty, which reads

$$j-N<\sum_{l=1}^{\sigma_{\mathrm{NL}}}j_l<j+N;\quad j,j_l\in\{-M/2+1,M/2\},\qquad\text{(F.31)}$$

or, equivalently,

$$-N<\left(\sum_{l=1}^{\sigma_{\mathrm{NL}}}j_l\right)-j<N;\quad j,j_l\in\{-M/2+1,M/2\}.\qquad\text{(F.32)}$$

Since, $\sigma_{\mathrm{NL}}-(\sigma_{\mathrm{NL}}+1)M/2\le(\sum_{l=1}^{\sigma_{\mathrm{NL}}}j_l)-j\le(\sigma_{\mathrm{NL}}+1)M/2-1$, we finally obtain the sufficient condition

$$M\le\frac{2}{\sigma_{\mathrm{NL}}+1}N.\qquad\text{(F.33)}$$

For quadratic nonlinearities ($\sigma_{\mathrm{NL}}=2$), as in the case of the Navier–Stokes equations, condition (F.33) is known as the "two-third rule." Inequality (F.33) is a constraining condition. As the price to pay for the elimination of the cross-stream coordinate y in our modeling strategy is the emergence of high-order nonlinearities, the treatment of the aliasing phenomenon imposes shutting down a significant number of Fourier coefficients.

References

1. Adomeit, P., Renz, U.: Hydrodynamics of three-dimensional waves in laminar falling films. Int. J. Multiph. Flow **26**, 1183–1208 (2000)
2. Adrian, R.J., Meinhart, C.D., Tumkins, A.: Vortex organization in the outer region of the turbulent boundary layer. J. Fluid Mech. **422**, 1–54 (2000)
3. Alekseenko, S.V., Nakoryakov, V.E., Pokusaev, B.G.: Wave Flow in Liquid Films, 3rd edn. Begell House, New York (1994)
4. Alekseenko, S.V., Nakoryakov, V.E., Pokusaev, B.G.: Wave formation on a vertical falling liquid film. AIChE J. **31**, 1446–1460 (1985)
5. Allaire, G., Craig, A.: An Introduction to Mathematical Modelling and Numerical Simulation. Oxford University Press, London (2007)
6. Alleborn, N.: Progress in coating theory. Therm. Sci. **5**(1), 131–152 (2001)
7. Alleborn, N., Durst, F., Lienhart, H.: Use of curtain coating for surface treatment of concrete construction parts. Chem. Ing. Tech. **77**, 84–89 (1996). (In German)
8. Allgower, E.L., Georg, K.: Numerical Continuation Methods. Springer, New York (1990)
9. Amaouche, M., Mehidi, N., Amataousse, N.: An accurate modeling of thin film flows down an incline for inertia dominated regimes. Eur. J. Mech. B, Fluids **24**, 49–70 (2004)
10. Anshus, B.E., Goren, S.L.: A method of getting approximate solutions to the Orr–Sommerfeld equation for flow on a vertical wall. AIChE J. **12**(5), 1004–1008 (1966)
11. Argyriadi, K., Vlachogiannis, M., Bontozoglou, V.: Experimental study of inclined film flow along periodic corrugations: the effect of wall steepness. Phys. Fluids **18**, 012102 (2006)
12. Aris, R.: Vectors, Tensors, and the Basic Equations of Fluid Mechanics. Dover, New York (1962)
13. Bach, P., Villadsen, J.: Simulation of the vertical flow of a thin, wavy film using a finite-element method. Int. J. Heat Mass Transf. **27**, 815–827 (1984)
14. Balmforth, N.J., Liu, J.J.: Roll waves in mud. J. Fluid Mech. **519**, 33–54 (2004)
15. Balmforth, N.J., Ierley, G.R., Spiegel, E.A.: Chaotic pulse trains. SIAM J. Appl. Math. **54**(5), 1291–1334 (1994)
16. Bamforth, J.R., Kalliadasis, S., Merkin, J.H., Scott, S.K.: Modelling flow-distributing oscillations in the CDIMA reaction. Phys. Chem. Chem. Phys. **2**, 4013–4021 (2000)
17. Bejan, A.: Convection Heat Transfer. Wiley-VCH, New York (1995)
18. Bender, C.M., Orszag, S.A.: Advanced Mathematical Methods for Scientists and Engineers. McGraw-Hill, New York (1978)
19. Benjamin, T.B.: Wave formation in laminar flow down an inclined plane. J. Fluid Mech. **2**, 554–574 (1957). Corrigendum in J. Fluid Mech. **3**, 657
20. Benjamin, T.B.: The development of three-dimensional disturbances in an unstable film of liquid flowing down an inclined plane. J. Fluid Mech. **10**, 401–419 (1961)
21. Benney, D.J.: Long waves on liquid films. J. Math. Phys. **45**, 150–155 (1966)

S. Kalliadasis et al., *Falling Liquid Films*, Applied Mathematical Sciences 176,
DOI 10.1007/978-1-84882-367-9, © Springer-Verlag London Limited 2012

22. Bertozzi, A.L., Pugh, M.: Long-wave instabilities and saturation in thin film equations. Commun. Pure Appl. Math. **51**, 625–661 (1998)
23. Bertschy, J.R., Chin, R.W., Abernathy, F.H.: High-strain-rate free-surface boundary layer flows. J. Fluid Mech. **126**, 443–461 (1983)
24. Bestehorn, M., Pototsky, A., Thiele, U.: 3D large scale Marangoni convection in liquid films. Eur. Phys. J. B **33**, 457–467 (2003)
25. Binnie, A.M.: Experiments on the onset of wave formation on a film of water flowing down a vertical plane. J. Fluid Mech. **2**, 551–553 (1957)
26. Bird, R.B., Stewart, W.E., Lightfoot, E.N.: Transport Phenomena. Wiley, New York (1960)
27. Birikh, R.V., Brisman, V.A., Velarde, M.G., Legros, J.C.: Liquid Interfacial Systems. Oscillations and Instability. Dekker, New York (2003)
28. Boag, J.W., Rubinin, P.E., Shoenberg, D.: Kapitza in Cambridge and Moscow. Life and Letters of a Russian Physicist. North-Holland, Amsterdam (1990)
29. Boos, W., Thess, A.: Cascade of structures in long-wavelength Marangoni instability. Phys. Fluids **11**, 1484–1494 (1999)
30. Boussinesq, J.V.: Essai sur la theorie des eaux courantes. Memoires presentes par divers savants a l'Academie des Sciences, Institute de France (Paris) **23**, 1–680 (1877)
31. Brevdo, L., Laure, P., Dias, F., Bridges, T.J.: Linear pulse structure and signaling in a film flow on an inclined plane. J. Fluid Mech. **396**, 37–71 (1999)
32. Briggs, R.J.: Electron-Stream Interaction with Plasmas. MIT Press, Cambridge (1964)
33. Brock, R.R.: Periodic permanent roll waves. J. Hydrol. Eng. **96**(12), 2565–2580 (1970)
34. Bunov, A.V., Demekhin, E.A., Shkadov, V. Ya.: On the non uniqueness of nonlinear waves on a falling film. J. Appl. Math. Mech. **48**(4), 691–696 (1984)
35. Burns, J.C.: Long waves in running water. Proc. Camb. Philol. Soc. **49**, 695–706 (1953)
36. Cachile, M., Schneemilch, M., Hamraoui, A., Cazabat, A.M.: Films driven by surface tension gradients. Adv. Colloid Interface Sci. **96**, 59–74 (2002)
37. Carbone, F., Aubry, N., Liu, J., Gollub, J.P., Lima, R.: Space-time description of the splitting and coalescence of wave fronts in film flows. Physica D **96**, 182–199 (1996)
38. Carr, J.: Applications of Centre Manifold Theory. Springer, New York (1981)
39. Champneys, A.R., Kuznetsov, Y.A.: Numerical detection and continuation of codimension-two homoclinic bifurcations. Int. J. Bifurc. Chaos **4**, 785–822 (1994)
40. Chan, B., Balmforth, N.J., Hosoi, A.E.: Building a better snail: lubrication and adhesive locomotion. Phys. Fluids **17**, 113101 (2005)
41. Chang, H.-C.: Onset of nonlinear waves on falling films. Phys. Fluids A, Fluid Dyn. **1**, 1314–1327 (1989)
42. Chang, H.-C.: Wave evolution on a falling film. Annu. Rev. Fluid Mech. **26**, 103–136 (1994)
43. Chang, H.-C., Demekhin, E.A.: Coherent structures, self similarity, and universal roll-wave coarsening dynamics. Phys. Fluids **12**(9), 2268–2278 (2000)
44. Chang, H.-C., Demekhin, E.A.: Complex Wave Dynamics on Thin Films. D. Möbius and R. Miller. Elsevier, Amsterdam (2002)
45. Chang, H.-C., Demekhin, E., Kalaidin, E.: Interaction dynamics of solitary waves on a falling film. J. Fluid Mech. **294**, 123–154 (1995)
46. Chang, H.-C., Demekhin, E.A., Kalaidin, E.: Simulation of noise-driven wave dynamics on a falling film. AIChE J. **42**, 1553–1568 (1996)
47. Chang, H.-C., Demekhin, E.A., Kalaidin, E.: Generation and suppression of radiation by solitary pulses. SIAM J. Appl. Math. **58**(4), 1246–1277 (1998)
48. Chang, H.-C., Demekhin, E.A., Kopelevitch, D.I.: Construction of stationary waves on a falling film. Comput. Mech. **11**, 313–322 (1993)
49. Chang, H.-C., Demekhin, E.A., Kopelevitch, D.I.: Laminarizing effects of dispersion in an active-dissipative nonlinear medium. Physica D **63**, 299–320 (1993)
50. Chang, H.-C., Demekhin, E.A., Kopelevitch, D.I.: Nonlinear evolution of waves on a vertically falling film. J. Fluid Mech. **250**, 433–480 (1993)
51. Chang, H.-C., Demekhin, E.A., Kopelevitch, D.I.: Local stability theory of solitary pulses in an active medium. Physica D **97**, 353–375 (1996)

52. Chang, H.-C., Cheng, M., Demekhin, E.A., Kopelevitch, D.I.: Secondary and tertiary excitation of three-dimensional patterns on a falling film. J. Fluid Mech. **270**, 251–275 (1994)
53. Cheng, M., Chang, H.-C.: A generalized sideband stability theory via center manifold projection. Phys. Fluids **2**, 1364–1379 (1990)
54. Chicone, C.: Ordinary Differential Equations and Applications. Springer, New York (1999)
55. Christov, C.I., Velarde, M.G.: Dissipative solitons. Physica D **86**, 323–347 (1995)
56. Chu, K.J., Dukler, A.E.: Statistical characteristics of thin, wavy films. Part 2. Studies of the substrate and its wave structure. AIChE J. **20**, 695–706 (1974)
57. Chu, K.J., Dukler, A.E.: Statistical characteristics of thin, wavy films. Part 3. Structure of the large waves and their resistance of gas flow. AIChE J. **21**, 583–593 (1975)
58. Colinet, P., Legros, J.C., Velarde, M.G.: Nonlinear Dynamics of Surface-Tension-Driven Instabilities, p. 512. Wiley-VCH, New York (2001)
59. Courant, R., Friedrichs, K., Lewy, H.: On the partial difference equations of mathematical physics. IBM J. 215–234 (1967)
60. Craster, R.V., Matar, O.K.: On viscous beads flowing down a vertical fibre. J. Fluid Mech. **553**, 85–105 (2006)
61. Craster, R.V., Matar, O.K.: Dynamics and stability of thin liquid films. Rev. Mod. Phys. **81**, 1131–1198 (2009)
62. Cross, M.C., Hohenberg, P.C.: Pattern formation outside of equilibrium. Rev. Mod. Phys. **65**, 851–1112 (1993)
63. Dávalos-Orozco, L.A.: Nonlinear instability of a thin film flowing down a smoothly deformed surface. Phys. Fluids **19**, 074103 (2007)
64. Dávalos-Orozco, L.A., Busse, F.H.: Instability of a thin film flowing on a rotating horizontal or inclined plane. Phys. Rev. E **65**, 026312 (2002)
65. Dávalos-Orozco, L.A., Ruiz-Chavarria, G.: Hydrodynamic stability of a fluid layer flowing down a rotating inclined plane. Phys. Fluids A, Fluid Dyn. **4**(8), 1651–1665 (1992)
66. Dávalos-Orozco, L.A., Ruiz-Chavarria, G.: Hydrodynamic instability of a fluid layer flowing down a rotating cylinder. Phys. Fluids A, Fluid Dyn. **5**(10), 2390–2404 (1993)
67. Davey, A.: A simple numerical method for solving Orr–Sommerfeld problems. Q. J. Mech. Appl. Math. **26**, 401–411 (1973)
68. de Gennes, P.G., Brochard-Wyart, F., Quéré, D.: Capillarity and Wetting Phenomena: Drops, Bubbles, Pearls, Waves. Springer, New York (2004)
69. de Groot, S.R., Mazur, P.: Nonequilibrium Thermodynamics. North-Holland, Amsterdam (1962)
70. Demekhin, E.A., Kaplan, M.A.: Construction of exact numerical solutions of the stationary traveling type for viscous thin films. Izv. Akad. Nauk SSSR, Meh. židk. Gaza **6**, 73–81 (1989)
71. Demekhin, E.A., Shkadov, V.Ya.: Three-dimensional waves in a liquid flowing down a wall. Izv. Akad. Nauk SSSR, Meh. židk. Gaza **5**, 21–27 (1984)
72. Demekhin, E.A., Kaplan, M.A., Shkadov, V.Ya.: Mathematical models of the theory of viscous liquid films. Izv. Akad. Nauk SSSR, Meh. židk. Gaza **6**, 73–81 (1987)
73. Demekhin, E.A., Tokarev, G.Yu., Shkadov, V.Ya.: Hierarchy of bifurcations of space-periodic structures in a nonlinear model of active dissipative media. Physica D **52**, 338–361 (1991)
74. Demekhin, E.A., Tokarev, G.Yu., Shkadov, V.Ya.: Numerical modeling of three-dimensional wave evolution in a falling layer of viscous fluid. Vestn. Mosk. Univ., Ser. 1: Mat., Mekh. **2**, 50–54 (1988)
75. Demekhin, E.A., Kalaidin, E.N., Kalliadasis, S., Vlaskin, S.Yu.: Three-dimensional localized coherent structures of surface turbulence: I. Scenarios of two-dimensional three-dimensional transitions. Phys. Fluids **19**, 114103 (2007)
76. Demekhin, E.A., Kalaidin, E.N., Kalliadasis, S., Vlaskin, S.Yu.: Three-dimensional localized coherent structures of surface turbulence: II. Λ solitons. Phys. Fluids **19**, 114104 (2007)
77. De Wit, A.: Fingering of chemical fronts in porous media. Phys. Rev. Lett. **87**, 054502 (2002)
78. Diez, J.A., Kondic, L., Bertozzi, A.: Global models for moving contact lines. Phys. Rev. E **63**, 011208 (2000)

79. Doedel, E.J.: AUTO07P continuation and bifurcation software for ordinary differential equations. Montreal Concordia University (2008)
80. Doedel, E.J., Keller, H.B., Kernévez, J.P.: Numerical analysis and control of bifurcation problems: (I) Bifurcation in finite dimensions. Int. J. Bifurc. Chaos **1**(3), 493–520 (1991)
81. Doedel, E.J., Keller, H.B., Kernevez, J.P.: Numerical analysis and control of bifurcation problems: (II) Bifurcation in infinite dimensions. Int. J. Bifurc. Chaos **1**(4), 745–772 (1991)
82. Drazin, P.G., Johnson, R.S.: Solitons: an Introduction. Cambridge University Press, London (1989)
83. Drazin, P.G., Reid, W.H.: Hydrodynamic Instability. Cambridge University Press, London (1981)
84. Dressler, R.F.: Mathematical solution of the problem of roll-waves in inclined open channels. Commun. Pure Appl. Math. **2**, 149–194 (1949)
85. Duprat, C., Ruyer-Quil, C., Giorgiutti-Dauphiné, F.: Spatial evolution of a film flowing down a fiber. Phys. Fluids **21**, 042109 (2009)
86. Duprat, C., Ruyer-Quil, C., Kalliadasis, S., Giorgiutti-Dauphiné, F.: Absolute and convective instabilities of a film flowing down a vertical fiber. Phys. Rev. Lett. **98**, 244502 (2007)
87. Duprat, C., Giorgiutti-Dauphiné, F., Tseluiko, D., Saprykin, S., Kalliadasis, S.: Liquid film coating a fiber as a model system for the formation of bound states in active dispersive-dissipative nonlinear media. Phys. Rev. Lett. **103**, 234501 (2009)
88. Dussan, E.B., Davis, S.H.: On the motion of a fluid-fluid interface along a solid surface. J. Fluid Mech. **65**, 71–95 (1974)
89. Dussan, E.B.: On the spreading of liquids on solid surfaces: static and dynamic contact lines. Annu. Rev. Fluid Mech. **11**, 371–400 (1979)
90. Elphick, C., Ierley, G.R., Regev, O., Spiegel, E.A.: Interacting localized structures with Galilean invariance. Phys. Rev. A **44**, 1110–1123 (1991)
91. Émery, H., Brosse, O.: Écoulement d'un film le long d'un plan incliné: développement spatio-temporel des instabilités. PhD thesis, École Polytechnique, Rapport d'option X92 (1995)
92. Finlayson, B.A.: The Method of Weighted Residuals and Variational Principles, with Application in Fluid Mechanics, Heat and Mass Transfer. Academic Press, San Diego (1972)
93. Floquet, G.: Sur les équations différentielles linéaires à coefficients périodiques. Ann. Ec. Norm. Supér. **12**, 47–88 (1883)
94. Floryan, J.M., Davis, S.H., Kelly, R.E.: Instabilities of a liquid film flowing down a slightly inclined plane. Phys. Fluids **30**, 983–989 (1987)
95. Frenkel, A.L.: Nonlinear theory of strongly undulating thin films flowing down vertical cylinders. Europhys. Lett. **18**, 583–588 (1992)
96. Friedman, B.: Principles and Techniques of Applied Mathematics. Wiley, New York (1956)
97. Frisk, D.P., Davis, E.J.: The enhancement of heat transfer by waves in stratified gas–liquid flow. Int. J. Heat Mass Transf. **15**, 1537–1552 (1972)
98. Gallay, T.: A center-stable manifold theorem for differential equations in Banach spaces. Commun. Math. Phys. **152**, 249–268 (1993)
99. Gao, D., Morley, N.B., Dhir, V.: Numerical simulation of wavy falling film flow using VOF method. J. Comput. Phys. **192**, 624–642 (2003)
100. Garazo, A.N., Velarde, M.G.: Dissipative Korteweg–de Vries description of Marangoni–Bénard oscillatory convection. Phys. Fluids **3**, 2295–2300 (1991)
101. Gaspard, P.: Local birth of homoclinic chaos. Physica D **62**, 94–122 (1993)
102. Gjevik, B.: Occurrence of finite-amplitude surface waves on falling liquid films. Phys. Fluids **13**, 1918–1925 (1970)
103. Glendinning, P., Sparrow, C.: Local and global behavior near homoclinic orbits. J. Stat. Phys. **35**, 645–696 (1984)
104. Golub, G.H., Loan, F.V.: Matrix Computations, 3rd edn. John Hopkins University Press, Baltimore (1996)
105. Gondret, P., Rabaud, M.: Shear instability of two-fluid parallel flow in a Hele–Shaw cell. Phys. Fluids **9**(11), 3267–3274 (1997)

106. Goren, S.L., Mani, P.V.S.: Mass transfer through horizontal liquid films in wavy motion. AIChE J. **14**, 57–61 (1968)
107. Goussis, D.A., Kelly, R.E.: Surface wave and thermocapillary instabilities in a liquid film flow. J. Fluid Mech. **223**, 25 (1991). Corrigendum in J. Fluid Mech. **226**, 663
108. Greenberg, M.D.: Foundations of Applied Mathematics. Prentice-Hall, New York (1978)
109. Greenberg, M.D.: Advanced Engineering Mathematics, 2nd edn. Prentice-Hall, New York (1998)
110. Grotberg, J.B.: Pulmonary flow and transport phenomena. Annu. Rev. Fluid Mech. **26**, 529–571 (1994)
111. Guckenheimer, J., Holmes, P.: Nonlinear Oscillations, Dynamical Systems and Bifurcations of Vector Fields. Springer, New York (1983)
112. Häcker, T., Uecker, H.: An integral boundary layer equation for film flow over inclined wavy bottoms. Phys. Fluids **21**, 092105 (2009)
113. Herbert, T.: Secondary instability of boundary layers. Annu. Rev. Fluid Mech. **20**, 487–526 (1988)
114. Hinch, E.J.: A note on the mechanism of the instability at the interface between two shearing fluids. J. Fluid Mech. **144**, 463–465 (1984)
115. Hinch, E.J.: Perturbation Methods. Cambridge University Press, London (1991)
116. Ho, L.W., Patera, A.T.: A Legendre spectral element method for simulation of unsteady incompressible viscous free-surface flows. Comput. Methods Appl. Mech. Eng. **80**, 355–366 (1990)
117. Hocherman, T., Rosenau, P.: On KS-type equations describing the evolution and rupture of a liquid interface. Physica D **67**, 113 (1993)
118. Homsy, G.M.: Model equations for wavy viscous film flow. Lect. Appl. Math. **15**, 191 (1974)
119. Homsy, G.M.: Model equations for wavy viscous film flow, in nonlinear wave motion. In: Newell, A. (Ed.) Lectures in Applied Mathematics, vol. 15, pp. 191–194. American Mathematical Society, Providence (1974)
120. Huerre, P., Monkewitz, P.: Local and global instabilities in spatially developing flows. Annu. Rev. Fluid Mech. **22**, 473–537 (1990)
121. Huerre, P., Rossi, M.: Hydrodynamic instabilities in open flows. In: Godrèche, C., Manneville, P. (Eds.) Hydrodynamic and Nonlinear Instabilities, pp. 81–294. Cambridge University Press, London (1998). Especially §8, 9
122. Huh, C., Scriven, L.E.: Hydrodynamic model of steady movement of solid/liquid/fluid contact line. J. Colloid Interface Sci. **35**, 85–101 (1971)
123. Iooss, G., Joseph, D.D.: Elementary Stability and Bifurcation Theory. Springer, New York (1980)
124. Ito, A., Masunaga, N., Baba, K.: Marangoni effects on wave structure and liquid film breakdown along heated vertical tube. In: Serizawa, A., Fukano, T., Bataille, J. (Eds.) Advances in Multiphase Flow, pp. 255–265. Elsevier, New York (1995)
125. Johnson, R.S.: Shallow water waves on a viscous fluid—the undular bore. Phys. Fluids **15**(10), 1693–1699 (1972)
126. Johnson, R.S.: A Modern Introduction to the Mathematical Theory of Water Waves, 1st edn. Cambridge Texts in Applied Mathematics (No. 19), p. 445. Cambridge University Press, Cambridge (1997)
127. Joo, S.W., Davis, S.H.: Instabilities of three-dimensional viscous falling films. J. Fluid Mech. **242**, 529–547 (1992)
128. Joo, S.W., Davis, S.H., Bankoff, S.G.: Long-wave instabilities of heated falling films: two-dimensional theory of uniform layers. J. Fluid Mech. **230**, 117–146 (1991)
129. Joo, S.W., Davis, S.H., Bankoff, S.G.: A mechanism for rivulet formation in heated falling films. J. Fluid Mech. **321**, 279–298 (1996)
130. Joseph, D.D., Bai, R., Chen, K.P., Renardy, Y.Y.: Core-annular flows. Annu. Rev. Fluid Mech. **29**, 65–90 (1997)
131. Kabov, O.A.: Heat transfer from a small heater to a falling liquid film. Heat Transf. Res. **27**, 221 (1996)

132. Kabov, O.A., Chinnov, E.A.: Heat transfer from a local heat source to a subcooled falling liquid film evaporating in a vapor–gas medium. Russ. J. Eng. Thermophys. **7**, 1–34 (1997)
133. Kabov, O.A., Chinnov, E.A., Legros, J.C.: Three-dimensional deformations in non-uniformly heated falling liquid film at small and moderate Reynolds numbers. In: Proceedings of the Conference on Transport Phenomena with Moving Boundaries, 11–12 October, Berlin, Germany (2003)
134. Kabov, O.A., Marchuk, I.V., Muzykantov, A.V., Legros, J.C., Istasse, E., Dewandel, J.-L.: Regular structures in locally heated falling liquid films. In: Celata, G.P., Di Marco, P., Shah, R.K. (Eds.) 2nd Intern. Symp. on Two-Phase Flow Modelling and Experimentation, May, Pisa (Italy), vol. 2, pp. 1225–1233 (1999)
135. Kalliadasis, S.: Nonlinear instability of a contact line driven by gravity. J. Fluid Mech. **413**, 355–378 (2000)
136. Kalliadasis, S., Chang, H.-C.: Drop formation during coating of vertical fibres. J. Fluid Mech. **261**, 135–168 (1994)
137. Kalliadasis, S., Thiele, U. (Eds.): Thin Films of Soft Matter. Springer-Wien, New York (2007)
138. Kalliadasis, S., Kiyashko, A., Demekhin, E.A.: Marangoni instability of a thin liquid film heated from below by a local heat source. J. Fluid Mech. **475**, 377–408 (2003)
139. Kalliadasis, S., Demekhin, E.A., Ruyer-Quil, C., Velarde, M.G.: Thermocapillary instability and wave formation on a film flowing down a uniformly heated plane. J. Fluid Mech. **492**, 303–338 (2003)
140. Kapitza, P.L.: Wave flow of thin layers of a viscous fluid: I. Free flow. II. Fluid flow in the presence of continuous gas flow and heat transfer. In: ter Haar, D. (Ed.) Collected Papers of P.L. Kapitza (1965), pp. 662–689. Pergamon, Oxford (1948). (Original paper in Russian: Zh. Eksp. Teor. Fiz. **18**, I. 3–18, II. 19–28)
141. Kapitza, P.L., Kapitza, S.P.: Wave flow of thin layers of a viscous fluid: III. Experimental study of undulatory flow conditions. In: ter Haar, D. (Ed.) Collected Papers of P.L. Kapitza (1965), pp. 690–709. Pergamon, Oxford (1949). (Original paper in Russian: Zh. Eksp. Teor. Fiz. **19**, 105–120)
142. Kargupta, K., Sharma, A.: Dewetting of thin films on periodic physically and chemically patterned surfaces. Langmuir **18**, 1893–1903 (2002)
143. Kataoka, D.E., Troian, S.M.: Patterning liquid flow on the microscopic scale. Nature **402**, 794–797 (1999)
144. Kawahara, T.: Formation of saturated solitons in a nonlinear dispersive system with instability and dissipation. Phys. Rev. Lett. **51**, 381–383 (1983)
145. Kawahara, T., Toh, S.: Pulse interactions in an unstable dissipative-dispersive nonlinear system. Phys. Fluids **31**, 2103–2111 (1988)
146. Keller, H.B.: Numerical solution of bifurcation and nonlinear eigenvalue problems. In: Rabinowitz, P.H. (Ed.) Applications of Bifurcation Theory, 3rd edn., pp. 359–384. Academic Press, New York (1977)
147. Kelly, R.E., Goussis, D.A., Lin, S.P., Hsu, F.K.: The mechanism for surface wave instability in film flow down an inclined plane. Phys. Fluids A, Fluid Dyn. **1**, 819–828 (1989)
148. Kistler, S.F., Schweitzer, P.M.: Liquid Film Coating: Scientific Principles and Their Technological Implications. Chapman & Hall, London (1997)
149. Kliakhandler, I.L., Davis, S.H., Bankoff, S.G.: Viscous beads on vertical fibre. J. Fluid Mech. **429**, 381–390 (2001)
150. Kliakhandler, I.L., Porubov, A.V., Velarde, M.G.: Localized finite-amplitude disturbances and selection of solitary waves. Phys. Rev. E **62**(4), 4959–4962 (2000)
151. Kondic, L.: Instabilities in gravity driven flow of thin fluid films. SIAM Rev. **45**(1), 95–115 (2003)
152. Kondic, L., Diez, J.: Flow of thin films on patterned surfaces: controlling the instability. Phys. Rev. E **45**, 045301 (2002)
153. Kondic, L., Palffy-Muhoray, P., Shelley, M.J.: Models of non-Newtonian Hele–Shaw flow. Phys. Rev. E **54**(5), 4536–4539 (1996)

154. Krantz, W.B., Goren, S.L.: Finite-amplitude, long waves on liquid films flowing down a plane. Ind. Eng. Chem. Res. **9**, 107–113 (1970)
155. Krantz, W.B., Goren, S.L.: Stability of thin liquid films flowing down a plane. Ind. Eng. Chem. Res. **10**, 91–101 (1971)
156. Krishnamoorthy, S., Ramaswamy, B.: Spontaneous rupture of thin liquid films due to thermocapillarity: a full-scale direct numerical simulation. Phys. Fluids **7**, 2291 (1995)
157. Lamger, J.S.: Instabilities and pattern formation in crystal growth. Rev. Mod. Phys. **52**(1), 1–28 (1980)
158. Landau, L.D., Lifsitz, E.M.: Fluid Mechanics. Pergamon, Oxford (1959)
159. Leal, L.G.: Laminar Flow and Convective Transport Processes. Butterworth-Heinemann, Stoneham (1992)
160. Leal, L.G.: Fluid Mechanics and Convective Transport Processes. Cambridge University Press, Cambridge (2007)
161. Lee, J.-J., Mei, C.C.: Stationary waves on an inclined sheet of viscous fluid at high Reynolds and moderate Weber numbers. J. Fluid Mech. **307**, 191–229 (1996)
162. Lienhard, J.H. IV, Leinhard, J.H. V: A Heat Transfer Textbook, 3rd edn. Phlogiston Press, Lexington (2004)
163. Levich, V.G.: Physico-Chemical Hydrodynamics. Prentice-Hall, Englewood Cliffs (1962)
164. Lin, S.P.: Finite amplitude side-band stability of a viscous fluid. J. Fluid Mech. **63**, 417–429 (1974)
165. Lin, S.P., Jiang, W.Y.: The mechanism of suppression or enhancement of three-dimensional surface waves in film flow down a vertical plane. Phys. Fluids **14**(2), 4088 (2002)
166. Lin, S.P., Chen, J.N., Woods, D.R.: Suppression of instability in a liquid film flow. Phys. Fluids **8**(12), 3247–3252 (1996)
167. Liu, J., Gollub, J.P.: Onset of spatially chaotic waves on flowing films. Phys. Rev. Lett. **70**, 2289–2292 (1993)
168. Liu, J., Gollub, J.P.: Solitary wave dynamics of film flows. Phys. Fluids **6**, 1702–1712 (1994)
169. Liu, J., Paul, J.D., Gollub, J.P.: Measurements of the primary instabilities of film flows. J. Fluid Mech. **250**, 69–101 (1993)
170. Liu, J., Schneider, J.B., Gollub, J.P.: Three-dimensional instabilities of film flows. Phys. Fluids **7**, 55–67 (1995)
171. Liu, K., Mei, C.C.: Roll waves on a layer of a muddy fluid flowing down a gentle slope—a Bingham model. Phys. Fluids **6**(8), 2577–2589 (1994)
172. Liu, Q.Q., Chen, L., Li, J.C., Singh, V.P.: Roll waves in overland flow. J. Hydrol. Eng. **10**(2), 110–117 (2005)
173. Loglio, G.: Carlo Marangoni and the Laboratory of Physics at the High School "Liceo Classico Dante" in Firenze (Italy). In: Gade, M., Huhnerfuss, H., Korenowski, G.M. (Eds.) Marine Surface Films. Chemical Characteristics, Influence on Air–Sea Interactions and Remote Sensing, pp. 13–15. Springer, Berlin (2006)
174. Lopez, P.G., Miksis, M.J., Bankoff, S.G.: Inertial effects on contact line instability in the coating of a dry inclined plane. Phys. Fluids **9**, 2177–2183 (1997)
175. Malamataris, N.A., Papanastasiou, T.C.: Unsteady free surface flows on truncated domains. Ind. Eng. Chem. Res. **30**, 2211–2219 (1991)
176. Malamataris, N.A., Vlachogiannis, M., Bontozoglou, V.: Solitary waves on inclined films: Flow structure and binary interactions. Phys. Fluids **14**(3), 1082–1094 (2002)
177. Manneville, P.: Dissipative Structures and Weak Turbulence. Academic Press, New York (1990)
178. Marangoni, C.: Sull' Espansione delle Gocce di Un Liquido Galleggiante Sulla Superficie di Altro Liquido. Pavia, Tipographic Fusi (1865)
179. Marangoni, C.: Sul principio della viscosita superficiale dei liquidi stabilito dal Sig. J. Plateau. Part 1. Nuovo Cim., Ser. II **2**(5/6), 238–266 (1872)
180. Marangoni, C.: Sul principio della viscosita superficiale dei liquidi stabilito dal Sig. J. Plateau. Part 2. Nuovo Cim., Ser. II **2**(5/6), 266–273 (1872), p. 268 §14. Abbonacciamento delle onde (pp. 268–270)

181. Meron, E.: Pattern formation in excitable media. Phys. Rep. **218**, 1–66 (1992)
182. Miklavcic, M., Williams, M.: Stability of mean flows over an infinite flat plate. Arch. Ration. Mech. Anal. **80**, 57–69 (1982)
183. Moffatt, H.K.: Viscous and resistive eddies near a sharp corner. J. Fluid Mech. **18**, 1 (1964)
184. Moldavsky, L., Frichman, M., Oron, A.: Dynamics of thin films falling on vertical cylindrical Durfaces subjected to ultrasound forcing. Phys. Rev. E **76**, 045301 (2007)
185. Nakaya, C.: Long waves on a viscous fluid down a vertical wall. Phys. Fluids A, Fluid Dyn. **18**, 1407–1412 (1975)
186. Nakaya, C.: Waves on a viscous fluid down a vertical wall. Phys. Fluids A, Fluid Dyn. **1**, 1143 (1989)
187. Nakoryakov, V.E., Pokusaev, B.G., Alekseenko, S.V., Orlov, V.V.: Instataneous velocity profile in a wavy liquid film. Inzh.-Fiz Zh. **33**, 399–405 (1977). (In Russian)
188. Nepomnyashchy, A.A.: Three-dimensional spatially periodic motions in liquid films flowing down a vertical plane. Hydrodynam. Perm **7**, 43–52 (1974). (In Russian)
189. Nepomnyashchy, A.A., Velarde, M.G., Colinet, P.: Interfacial Phenomena and Convection. Chapman & Hall/CRC, London (2002)
190. Nguyen, L.T., Balakotaiah, V.: Modeling and experimental studies of wave evolution on free falling viscous films. Phys. Fluids **12**, 2236–2256 (2000)
191. Normand, C., Pomeau, Y., Velarde, M.G.: Convective instability: a physicist's approach. Rev. Mod. Phys. **49**, 581–624 (1977)
192. Nosoko, T., Miyara, A.: The evolution and subsequent dynamics of waves on a vertically falling liquid film. Phys. Fluids **16**(4), 1118–1126 (2004)
193. Nosoko, T., Yoshimura, P.N., Nagata, T., Okawa, K.: Characteristics of two-dimensional waves on a falling liquid film. Chem. Eng. Sci. **51**, 725–732 (1996)
194. Nusselt, W.: Die oberflachenkondensation des wasserdampfes. Z. VDI **50**, 541–546 (1916)
195. Oldeman, B.E., Champneys, A.R., Krauskopf, B.: Homoclinic branch switching: a numerical implementation of Lin's method. Int. J. Bifurc. Chaos **13**, 2977–2999 (2003)
196. Ooshida, T.: Surface equation of falling film flows with moderate Reynolds number and large but finite Weber number. Phys. Fluids **11**, 3247–3269 (1999)
197. Oron, A.: Nonlinear dynamics of three-dimensional long-wave Marangoni instability in thin liquid films. Phys. Fluids **12**, 1633 (2000)
198. Oron, A., Gottlieb, O.: Nonlinear dynamics of temporally excited falling liquid films. Phys. Fluids **14**, 2622–2636 (2002)
199. Oron, A., Gottlieb, O.: Subcritical and supercritical bifurcations of the first- and second-order Benney equations. J. Eng. Math. **50**, 121–140 (2004)
200. Oron, A., Rosenau, P.: Evolution and formation of dispersive-dissipative patterns. Phys. Rev. E **55**, 1267–1270 (1997)
201. Oron, A., Davis, S.H., Bankoff, S.G.: Long-scale evolution of thin liquid films. Rev. Mod. Phys. **69**, 931–980 (1997)
202. Orszag, S.A.: Accurate solution of the Oss–Sommerfeld stability equation. J. Fluid Mech. **50**, 689–703 (1971)
203. Park, C.D., Nosoko, T.: Three-dimensional wave dynamics on a falling film and associated mass transfer. AIChE J. **49**, 2715–2727 (2003)
204. Pascal, J.P.: Linear stability of fluid flow down a porous inclined plane. J. Phys. D, Appl. Phys. **32**, 417–422 (1999)
205. Pascal, J.P.: Instability of power-law fluid flow down a porous incline. J. Non-Newton. Fluid Mech. **133**, 109–120 (2006)
206. Pearson, J.R.A.: On convection cells induced by surface tension. J. Fluid Mech. **4**, 489–500 (1958)
207. Pereira, A., Kalliadasis, S.: Dynamics of a falling film with solutal Marangoni effect. Phys. Rev. E **78**, 036312 (2008)
208. Pereira, A., Trevelyan, P.M.J., Thiele, U., Kalliadasis, S.: Dynamics of a horizontal thin liquid film in the presence of reactive surfactants. Phys. Fluids **19**, 112102 (2007)
209. Pereira, A., Trevelyan, P.M.J., Thiele, U., Kalliadasis, S.: Interfacial hydrodynamic waves driven by chemical reactions. J. Eng. Math. **59**, 207–220 (2007)

210. Petviashvili, V.I., Tsvelodub, O.Yu.: Horse-shoe shaped solitons on an inclined viscous liquid film. Dokl. Akad. Nauk SSSR **238**, 1321–1324 (1978)
211. Pierson, F.W., Whitaker, S.: Some theoretical and experimental observations of the wave structure of falling liquid films. Ind. Eng. Chem. Res. **16**, 401–408 (1977)
212. Pradas, M., Tseluiko, D., Kalliadasis, S.: Rigorous coherent-structure theory for falling liquid films: Viscous dispersion effects on bound-state formation and self-organization. Phys. Fluids **23**, 044104 (2011)
213. Press, W.H., Teukolsky, S.A., Vetterling, W.T., Flannery, B.P.: Numerical Recipes in C—The Art of Scientific Computing, 2nd edn. Cambridge University Press, New York (1992)
214. Prokopiou, T., Cheng, M., Chang, H.-C.: Long waves on inclined films at high Reynolds number. J. Fluid Mech. **222**, 665–691 (1991)
215. de Saint-Venant, A.J.C.: Théorie du mouvement non-permanent des eaux, avec applications aux crues des rivières et à l'introduction des marées dans leur lit. C. R. Acad. Sci. Paris **73**, 147–154 (1871)
216. Pumir, A., Manneville, P., Pomeau, Y.: On solitary waves running down an inclined plane. J. Fluid Mech. **135**, 27–50 (1983)
217. Quéré, D.: Fluid coating on a fiber. Annu. Rev. Fluid Mech. **31**, 347–384 (1999)
218. Ramaswamy, B., Chippada, S., Joo, S.W.: A full-scale numerical study of interfacial instabilities in thin-film flows. J. Fluid Mech. **325**, 163–194 (1996)
219. Ramaswamy, B., Krishnamoorthy, S., Joo, S.W.: Three-dimensional simulation of instabilities and rivulet formation in heated falling films. J. Comput. Phys. **131**, 70–88 (1997)
220. Richtmyer, R.D., Morton, K.W.: Difference Methods for Initial-Value Problems. Interscience, New York (1967)
221. Roberts, A.J.: Low-dimensional models of thin film fluid dynamics. Phys. Lett. A **212**, 63–71 (1996)
222. Roberts, A.J.: Low-dimensional modelling of dynamics via computer algebra. Comput. Phys. Commun. **100**, 215–230 (1997)
223. Roberts, A.J., Li, Z.-Q.: An accurate and comprehensive model of thin fluid flows with inertia on curved substrates. J. Fluid Mech. **553**, 33–73 (2006)
224. Roy, R.V., Roberts, A.J., Simpson, M.E.: A lubrication model of coating flows over a curved substrate in space. J. Fluid Mech. **454**, 235–261 (2002)
225. Ruyer-Quil, C.: Inertial corrections to the Darcy law in a Hele–Shaw cell. C. R. Acad. Sci. Sér. IIb **329**, 337–342 (2001)
226. Ruyer-Quil, C., Manneville, P.: Modeling film flows down inclined planes. Eur. Phys. J. B **6**, 277–292 (1998)
227. Ruyer-Quil, C., Manneville, P.: Improved modeling of flows down inclined planes. Eur. Phys. J. B **15**, 357–369 (2000)
228. Ruyer-Quil, C., Manneville, P.: Further accuracy and convergence results on the modeling of flows down inclined planes by weighted-residual approximations. Phys. Fluids **14**, 170–183 (2002)
229. Ruyer-Quil, C., Manneville, P.: On the speed of solitary waves running down a vertical wall. J. Fluid Mech. **531**, 181–190 (2005)
230. Ruyer-Quil, C., Scheid, B., Kalliadasis, S., Velarde, M.G., Zeytounian, R. Kh.: Thermocapillary long waves in a liquid film flow. Part 1. Low dimensional formulation. J. Fluid Mech. **538**, 199–222 (2005)
231. Ruyer-Quil, C., Treveleyan, P., Giorgiutti-Dauphiné, F., Duprat, C., Kalliadasis, S.: Modelling film flows down a fibre. J. Fluid Mech. **603**, 431–462 (2008)
232. Salamon, T.R., Armstrong, R.C., Brown, R.A.: Traveling waves on vertical films: Numerical analysis using the finite element method. Phys. Fluids **6**, 2202 (1994)
233. Saprykin, S., Demekhin, E.A., Kalliadasis, S.: Self-organization of two-dimensional waves in an active dispersive-dissipative nonlinear medium. Phys. Rev. Lett. **94**, 224101 (2005)
234. Saprykin, S., Demekhin, E.A., Kalliadasis, S.: Two-dimensional wave dynamics in thin films. I. Stationary solitary pulses. Phys. Fluids **17**, 117105 (2005)

235. Saprykin, S., Demekhin, E.A., Kalliadasis, S.: Two-dimensional wave dynamics in thin films. II. Formation of lattices of interacting stationary solitary pulses. Phys. Fluids **17**, 117106 (2005)
236. Saprykin, S., Koopmans, R.J., Kalliadasis, S.: Free-surface thin-film flows over topography: influence of inertia and viscoelasticity. J. Fluid Mech. **578**, 271–293 (2007)
237. Saprykin, S., Trevelyan, P.M.J., Koopmans, R.J., Kalliadasis, S.: Free-surface thin-film flows over uniformly heated topography. Phys. Rev. E **75**, 026306 (2007)
238. Scheid, B., Ruyer-Quil, C., Manneville, P.: Wave patterns in film flows: modelling and three-dimensional waves. J. Fluid Mech. **562**, 183–222 (2006)
239. Scheid, B., Oron, A., Colinet, P., Thiele, U., Legros, J.C.: Nonlinear evolution of non-uniformly heated falling liquid films. Phys. Fluids **14**, 4130–4151 (2002). Erratum: Phys. Fluids **15**, 583 (2003)
240. Scheid, B., Ruyer-Quil, C., Kalliadasis, S., Velarde, M.G., Zeytounian, R. Kh.: Thermocapillary long waves in a liquid film flow. Part 2. Linear stability and nonlinear waves. J. Fluid Mech. **538**, 223–244 (2005)
241. Scheid, B., Ruyer-Quil, C., Thiele, U., Kabov, O.A., Legros, J.C., Colinet, P.: Validity domain of the Benney equation including the Marangoni effect for closed and open flows. J. Fluid Mech. **527**, 303–335 (2005)
242. Scheid, B., Kalliadasis, S., Ruyer-Quil, C., Colinet, P.: Interaction of three-dimensional hydrodynamic and thermocapillary instabilities in film flows. Phys. Rev. E **78**, 066311 (2008)
243. Schlichting, H.: Boundary-Layer Theory, 7th edn. McGraw-Hill, New York (1979)
244. Schmid, P.J., Henningson, D.S.: Stability and Transition in Shear Flows. Springer, Berlin (2001)
245. Scott, S.K.: Chemical Chaos. Oxford University Press, London (1993)
246. Scriven, L.E., Sterling, C.V.: On cellular convection driven surface tension gradients: effects of mean surface tension and surface viscosity. J. Fluid Mech. **19**, 321–340 (1964)
247. Shankar, V., Sharma, A.: Instability of the interface between thin fluid films subjected to electric fields. Langmuir **21**, 3710–3721 (2005)
248. Shkadov, V.Ya.: Wave flow regimes of a thin layer of viscous fluid subject to gravity. Izv. Akad. Nauk SSSR, Meh. židk. Gaza **1**, 43–51 (1967). (English translation in Fluid Dynamics **2**, 29–34 (Faraday Press, New York, 1970))
249. Shkadov, V.Ya.: Solitary waves in a layer of viscous liquid. Izv. Akad. Nauk SSSR, Meh. židk. Gaza **1**, 63–66 (1977)
250. Shkadov, V.Ya., Sisoev, G.M.: Waves induced by instability in falling films of finite thickness. Fluid Dyn. Res. **35**, 357–389 (2004)
251. Shkadov, V.Ya., Velarde, M.G., Shkadova, V.P.: Falling films and the Marangoni effect. Phys. Rev. E **69**, 056310 (2004)
252. Shraiman, B.I.: Diffusive transport in a Rayleigh–Bénard convection cell. Phys. Rev. A **36**, 261–267 (1987)
253. Sisoev, G.M., Shkadov, V.Ya.: A two-parameter manifold of wave solutions to an equation for a falling film of viscous fluid. Dokl. Phys. **44**, 454–459 (1999)
254. Skotheim, J.M., Thiele, U., Scheid, B.: On the instability of a falling film due to localized heating. J. Fluid Mech. **475**, 1–19 (2003)
255. Smith, K.A.: On convective instability induced by surface-tension gradients. J. Fluid Mech. **24**, 401–414 (1966)
256. Smith, M.K.: The mechanism for the long-wave instability in thin liquid films. J. Fluid Mech. **217**, 469–485 (1990)
257. Smith, M.K., Davis, S.H.: Instabilities of dynamic thermocapillary liquid layers. Part 1. Convective instabilities. J. Fluid Mech. **132**, 119–144 (1983)
258. Smith, M.K., Davis, S.H.: Instabilities of dynamic thermocapillary liquid layers. Part 2. Surface-wave instabilities. J. Fluid Mech. **132**, 145–162 (1983)
259. Solorio, F.J., Sen, M.: Linear stability of a cylindrical falling film. J. Fluid Mech. **183**, 365–377 (1987)
260. Spindler, B.: Linear stability of liquid films with interfacial phase change. Int. J. Heat Mass Transf. **25**(2), 161–173 (1982)

261. Sreenivasan, S., Lin, S.P.: Surface tension driven instability of a liquid film flow down a heated incline. Int. J. Heat Mass Transf. **21**, 1517 (1978)
262. Stainthorp, F.P., Allen, J.M.: The development of ripples on the inside of a liquid film moving inside a vertical tube. Trans. Inst. Chem. Eng. **43**, 85–91 (1965)
263. Stuart, J.T.: Nonlinear stability theory. Annu. Rev. Fluid Mech. **3**, 347–370 (1971)
264. Tailby, S.R., Portalski, S.: The hydrodynamics of liquid films flowing on vertical surfaces. Trans. Inst. Chem. Eng. **38**, 324–330 (1960)
265. Thess, A., Orszag, S.A.: Surface-tension-driven Bénard convection at infinite Prandtl number. J. Fluid Mech. **283**, 201–230 (1995)
266. Thiele, U., Knobloch, E.: Front and back instability of a liquid film on a slightly inclined plate. Phys. Fluids **15**, 892–907 (2003)
267. Thiele, U., Goyeau, B., Velarde, M.G.: Stability analysis of thin film flow along a heated porous substrate. Phys. Fluids **21**, 014103 (2009)
268. Thiele, U., Velarde, M.G., Neuffer, K.: Dewetting: film rupture by nucleation in the spinodal regime. Phys. Rev. Lett. **87**(2), 1–4 (2001)
269. Thiele, U., Neuffer, K., Bestehorn, M., Pomeau, Y., Velarde, M.G.: Sliding drops on an inclined plane. Colloids Surf. A **206**, 87–104 (2002)
270. Thomas, H.A.: The propagation of waves in steep prismatic conduits. In: Proc. Hydraulics Conf., pp. 214–229. Univ. of Iowa, Iowa City (1939)
271. Thompson, J.: On certain curious motions observable on the surfaces of wine and other alcoholic liquours. Philos. Mag. **10**, 330–335 (1855)
272. Tiffany, J.M.: The viscosity of human tears. Int. Ophthalmol. **15**, 371–376 (1991)
273. Tihon, J., Serifi, K., Argyiriadi, K., Bontozoglou, V.: Solitary waves on inclined films: their characteristics and the effects on wall shear stress. Exp. Fluids **41**, 79–89 (2006)
274. Trevelyan, P.M.J., Kalliadasis, S.: Dynamics of a reactive falling film at large Péclet numbers. I. Long-wave approximation. Phys. Fluids **16**, 3191–3208 (2004)
275. Trevelyan, P.M.J., Kalliadasis, S.: Dynamics of a reactive falling film at large Péclet numbers. II. Nonlinear waves far from criticality: Integral-boundary-layer approximation. Phys. Fluids **16**, 3209–3226 (2004)
276. Trevelyan, P.M.J., Kalliadasis, S.: Dynamics of a thin-liquid film falling down a heated wall. J. Eng. Math. **50**, 177–208 (2004)
277. Trevelyan, P.M.J., Kalliadasis, S., Merkin, J.H., Scott, S.K.: Dynamics of a vertically falling film in the presence of a first-order chemical reaction. Phys. Fluids **14**, 2402–2121 (2002)
278. Trevelyan, P.M.J., Kalliadasis, S., Merkin, J.H., Scott, S.K.: Mass transport enhancement in regions bounded by rigid walls. J. Eng. Math. **42**, 45–64 (2002)
279. Trevelyan, P.M.J., Scheid, B., Ruyer-Quil, C., Kalliadasis, S.: Heated falling films. J. Fluid Mech. **592**, 295–334 (2007)
280. Trifonov, Yu.Ya.: Steady-state travelling waves on the surface of a viscous liquid film falling down vertucal wires and tubes. AIChE J. **38**, 821–834 (1992)
281. Trifonov, Yu.Ya., Tsvelodub, O.Yu.: Nonlinear waves on the surface of a falling liquid film. Part 1. Waves of the first family and their stability. J. Fluid Mech. **229**, 531–554 (1991)
282. Trifonov, Yu.Ya.: Bifurcations of two-dimensional into three-dimensional wave regimes for a vertically flowing liquid film. Izv. Akad. Nauk SSSR, Meh. židk. Gaza **5**, 109–114 (1989)
283. Tseluiko, D., Kalliadasis, S.: Coherent-structure theory for 3d active dispersive-dissipative nonlinear media (2011, in preparation)
284. Tseluiko, D., Saprykin, S., Kalliadasis, S.: Interaction of solitary pulses in active dispersive-dissipative media. Proc. Est. Acad. Sci. **59**, 139–144 (2010)
285. Tseluiko, D., Blyth, M.G., Papageorgiou, D.T., Vanden-Broeck, J.-M.: Electrified viscous thin film flow over topography. J. Fluid Mech. **597**, 449–475 (2008)
286. Tseluiko, D., Saprykin, S., Duprat, C., Giorgiutti-Dauphiné, F., Kalliadasis, S.: Pulse dynamics in low-Reynolds-number interfacial hydrodynamics: Experiments and theory. Physica D **239**, 2000–2010 (2010)
287. Tsvelodub, O.Yu., Trifonov, Yu.Ya.: Nonlinear waves on the surface of a falling liquid film. Part 2. Bifurcations of the first-family waves and other types of nonlinear waves. J. Fluid Mech. **244**, 149–169 (1992)

288. Usha, R., Uma, B.: Modeling of stationary waves on a thin viscous film down an inclined plane at high Reynolds numbers and moderate Weber numbers using energy integral method. Phys. Fluids **16**(7), 2679–2696 (2004)
289. Van Hook, S.J., Schatz, M.F., Swift, J.B., McCormick, W.D., Swinney, H.L.: Long wavelength surface-tension-driven Bénard convection: experiment and theory. J. Fluid Mech. **345**, 45–78 (1997)
290. Velarde, M.G., Zeytounian, R. Kh. (Eds.): Interfacial Phenomena and the Marangoni Effect. Springer-Wien, New York (2002)
291. Velarde, M.G., Nepomnyashchy, A.A., Hennenberg, M.: Onset of oscillatory interfacial instability and wave motions in Bénard layers. Adv. Appl. Mech. **37**, 167–238 (2000)
292. Verhulst, F.: Nonlinear Differential Equations and Dynamical Systems. Springer, Berlin (1990)
293. Verma, R., Sharma, A., Kargupta, K., Bhaumik, J.: Electric field induced instability and pattern formation in thin liquid films. Langmuir **21**, 3710–3721 (2005)
294. Vlachogiannis, M., Bontozoglou, V.: Observations of solitary wave dynamics of film flows. J. Fluid Mech. **435**, 191–215 (2001)
295. Wasden, F.K., Dukler, A.E.: Insights into the hydrodynamics of free falling wavy films. AIChE J. **35**, 187–195 (1989)
296. Weast, R.W., Selby, S.M.: Handbook of Chemistry and Physics, 63rd edn. CRC, Cleveland (1966)
297. Weinstein, S.J., Ruschak, K.J.: Coating flows. Annu. Rev. Fluid Mech. **36**, 29–53 (2004)
298. Whitaker, S.: Effect of surface active agents on the stability of falling liquid films. Ind. Eng. Chem. Res. **3**, 132–142 (1964)
299. Whitham, G.B.: Linear and Nonlinear Waves. Wiley, New York (1974)
300. Wierschem, A., Linde, H., Velarde, M.G.: Properties of surface wave trains excited by mass transfer through a liquid surface. Phys. Rev. E **64**, 022601 (2001)
301. Wiggins, S.: Introduction to Applied Nonlinear Dynamical Systems and Chaos. Springer, New York (1990)
302. Yang, J., D'Onofrio, A., Kalliadasis, S., De Wit, A.: Rayleigh–Taylor instability of reaction-diffusion acidity fronts. J. Chem. Phys. **117**, 9395–9408 (2002)
303. Yih, C.-S.: Stability of two-dimensional parallel flows for three dimensional disturbances. Quart. Appl. Math. **12**, 434–435 (1955)
304. Yih, C.-S.: Stability of liquid flow down an inclined plane. Phys. Fluids **6**, 321–334 (1963)
305. Yoshimura, P.N., Nosoko, T., Nagata, T.: Enhancement of mass transfer into a falling laminar liquid film by two-dimensional surface waves—some experimental observations and modeling. Chem. Eng. Sci. **51**(8), 1231–1240 (1996)
306. Yu, L.-Q., Wasden, F.K., Dukler, A.E., Balakotaiah, V.: Nonlinear evolution of waves on falling films at high Reynolds numbers. Phys. Fluids **7**, 1886–1902 (1995)

Index

S. Kalliadasis et al., *Falling Liquid Films*, Applied Mathematical Sciences 176,
DOI 10.1007/978-1-84882-367-9, © Springer-Verlag London Limited 2012